Sugar mill gears
Crack detection;

JCU2S

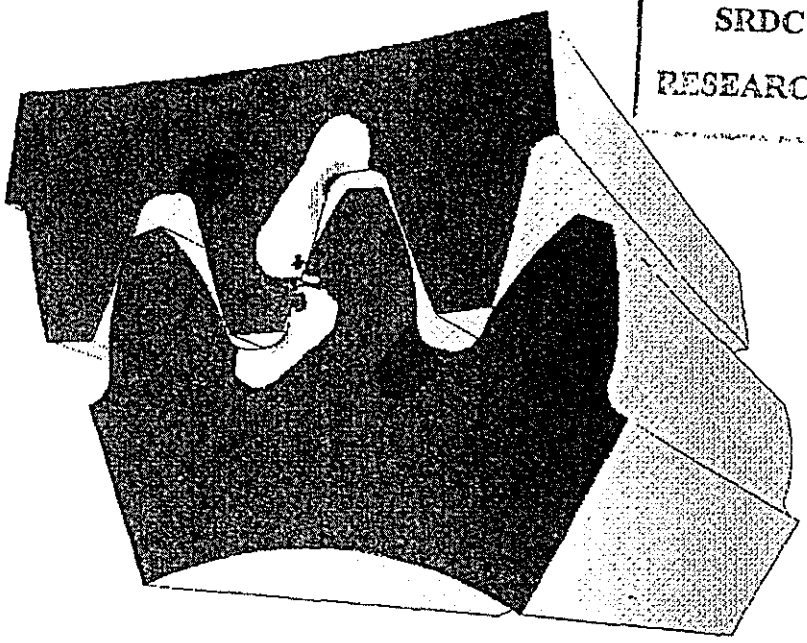

"Crack Detection and Durability Assessment of Low Speed Gears."

(Section B)

by

S.I.Anderson and J.G.Loughran
Department of Mechanical Engineering
James Cook University of North Queensland

December 1995

Funding for this project (JCU2S) was received from the Sugar Research and Development Corporation.

CONTENTS

1.0 SUMMARY - 1-1

2.0 INTRODUCTION / LITERATURE REVIEW 2-1

2.1 Project introduction 2-1
2.2 Gear nomenclature 2-2
2.3 Review of Industry , AGMA , ISO and BS standards 2-8
2.4 Basic fracture mechanics and crack propagation prediction theory 2-9

3.0 PROCEDURE 3-1

3.1 Use of computer codes : PATRAN, PFATIGUE, ABAQUS (Standard) and NSOFT 3-1
3.2 General procedure 3-4

4.0 TARGET GEARS : GEOMETRY, LOAD AND CRACK DATA 4-1

4.1 Non-destructive testing records 4-1
4.2 Relevant gear dimensions, materials and properties 4-4
4.3 Torque history details and accuracy 4-5

5.0 INITIAL 2D FINITE ELEMENT MODELLING OF SPUR AND PINION GEAR INTERACTION 5-1

5.1 Geometry modelling of candidate teeth 5-1
5.2 Analysis of single pair of meshing teeth 5-3
5.3 Analysis of multiple of meshing teeth 5-9
5.3.1 Effect of mesh refinement on tooth stresses 5-11
5.3.2 Effect of friction coefficient on tooth stresses 5-18

6.0 STRESS INTENSITY ANALYSIS (PLANE STRAIN APPROACH). 6-1

6.1 Procedure for producing a geometry function for the candidate spur tooth. 6-1
6.2 Validation for using plane strain theory and the J-Integral solutions. 6-3
6.3 Reference stress for uncracked tooth. 6-7
6.4 Stress analysis with varying length cracks in root region. 6-9
6.5 Calculation of geometry function and feasibility. 6-14

.... continued ....

7.0 PREDICTION OF CRACK PROPAGATING RATES. 7-1

7.1 Crack propagation analysis and results under nominal loading conditions. 7-2
7.2 Sensitivity analysis. 7-6
7.2.1 Effect of varying material properties and behaviour. 7-6
7.2.2 Effect of varying torque transmission loads. 7-8
7.2.3 Effect of non-uniform loading across the spur tooth face. 7-10

8.0 PROJECT LIMITATIONS. 8-1

8.1 Insufficient fracture properties and surface / heat treatment details for spur gear material. 8-1
8.2 Accuracy of torque measurements, tooth profile and possible gear misalignment details. 8-2

9.0 PROJECT OUTCOMES AND RECOMMENDATIONS. 9-1

9.1 General results and conclusions. 9-1
9.2 Future research possibilities. 9-3
9.2.1 Obtaining accurate material and fracture properties from gear samples. 9-3
9.2.2 Creating methods for back-calculating properties from crack histories. 9-3
9.2.3 Producing a rapid method for analysing cracked gears of varying geometry. 9-4
9.2.4 Modelling misalignment and 3Dcrack shapes using ABAQUS (Explicit). 9-4

REFERENCES / RECCOMENDED READING rr-1

References. rr-1
Reccomended Reading. rr-2

APPENDICES app-1

- A1 Several typical non-destructive testing reports. app-1
- A2 Candidate gear drawings fax from gear manufacturer. app-10
- A3 Summarized input deck and status file for fine mesh triple teeth model. app-15
- A4 Summarized input deck and results file for 50 mm crack model. app-20
- A5 Fax showing typical graphs used to calculate torque loads. app-23

1.0 Summary

Heavy low speed gearing used by the Australian Sugar Industry is manufactured according to code specifications. These gears fail in several ways with the most common failure modes being the gradual surface fatigue of the contacting teeth due to poor lubrication and sudden tooth fracture resulting from the presence of cracks. Over the last decade, sudden gear failures have cost the industry millions of dollars. The problem is exacerbated by the unexpected lost production time and cost of gear replacements.

The general goal of this project was to apply fracture mechanics technology to predict the life of cracked gearing under routine operating conditions and to answer questions such as:

- What size crack can be tolerated under existing and alternative loading conditions?
- Approximately how long would it take for a crack to reach the critical crack length?
- How often should a cracked gear be inspected?

Fundamental to this investigation was the development of a geometry function for the gear tooth profile. This has been achieved for a candidate spur wheel (Victoria Mill, Gear-train 4B) and utilised during crack propagation modelling. This investigation describes a methodology for handling gears whose teeth contain root region cracks. However, the application of this technology is hindered by a lack of fracture properties for gear steels. Without having the exact fracture properties, sensitivity analysis can be done to account for this shortfall.

Acquiring fracture properties for gears currently in use, especially those that have been in service for over twenty years, would be difficult. As a result, it may be advisable that fracture properties now be provided with every new gear installed. This would be beneficial for assessing possible future cracks so that the frequency of unexpected gear failures, hence unscheduled shutdowns and lost production time, is reduced.

2.0 Introduction / Literature Review

2.1 Project introduction

This report is concerned with the second part of the project JCU2S which was funded by Sugar Research and Development Corporation. The funding commenced in July 1994. The general objective for this project was to apply finite element methods and durability analysis to predict the life of cracked gearing under routine operating conditions.

The Australian raw sugar industry has conservatively over $70 million of low speed sugar mill gearing with a single replacement bull wheel costing upwards of $200 000. These gears operate under arduous conditions. Milling units are set generally according to the allowable torque that can be transmitted through the gearing. If gear teeth exhibit cracks then the mill settings should be reviewed to enable the gear to at least survive until a replacement can be sought (typically 12-20 weeks for a large gear). No rapid technique is currently used in the sugar industry to access the onset of cracks in gear teeth even though several factories have sophisticated condition monitoring equipment. Further, no one in Australia has attempted to apply state-of-the-art durability techniques to predict an acceptable torque setting for a cracked heavy gearing to enable survival until a replacement gear can be sought.

In short, finite element and durability analysis will be applied to predict the life of cracked sugar mill gears under a range of loading regimes. It was initially envisaged that a specialised computer code could be written to interface with existing PATRAN finite element modules thus enabling cracks in arbitrary gear geometry to be quickly assessed for life. As the project was being conducted it was realised that such a task was not achievable within the given time frame. Efforts were concentrated on refining a method for analysing cracked gears and predicting the remaining life of cracked gearing under various loading conditions. As a rapid response to gear failure problems is particularly important, the feasibility of a specialised computer code mentioned above should be investigated in the future.

2.2 Gear nomenclature

This section is necessary for the understanding of gear related terminology which is used throughout the report. As this research project was based on a candidate gear, a large spur gear currently in use at Victoria Mill, the descriptions below will be biased towards spur gear geometries. This is justified as the majority of large low speed gears used in the sugar industry are spur gears. The following information is a short summary covering the major aspects of spur gear characteristics. More detailed information on spur or other gear types can be found in specific gear related texts (see References / Recommended Reading).

Spur gears are used to transmit rotary motion between parallel shafts and are usually cylindrical in shape, with straight teeth that are parallel to the axis of rotation. For a mating pair of gears, the gear with the smallest number of teeth is referred to as the 'pinion', whilst the larger is referred to as the 'gear'. To transmit motion at a constant angular velocity between mating gears, the teeth profiles are to be theoretically of an involute form. Previously, gear manufacturers unable to machine involute teeth, used circular forms of approximate shape. This is the case with a portion of the low speed gearing still in use in the Australian raw sugar industry.

The terminology for spur gears is shown in Figures 2.1 and 2.2.

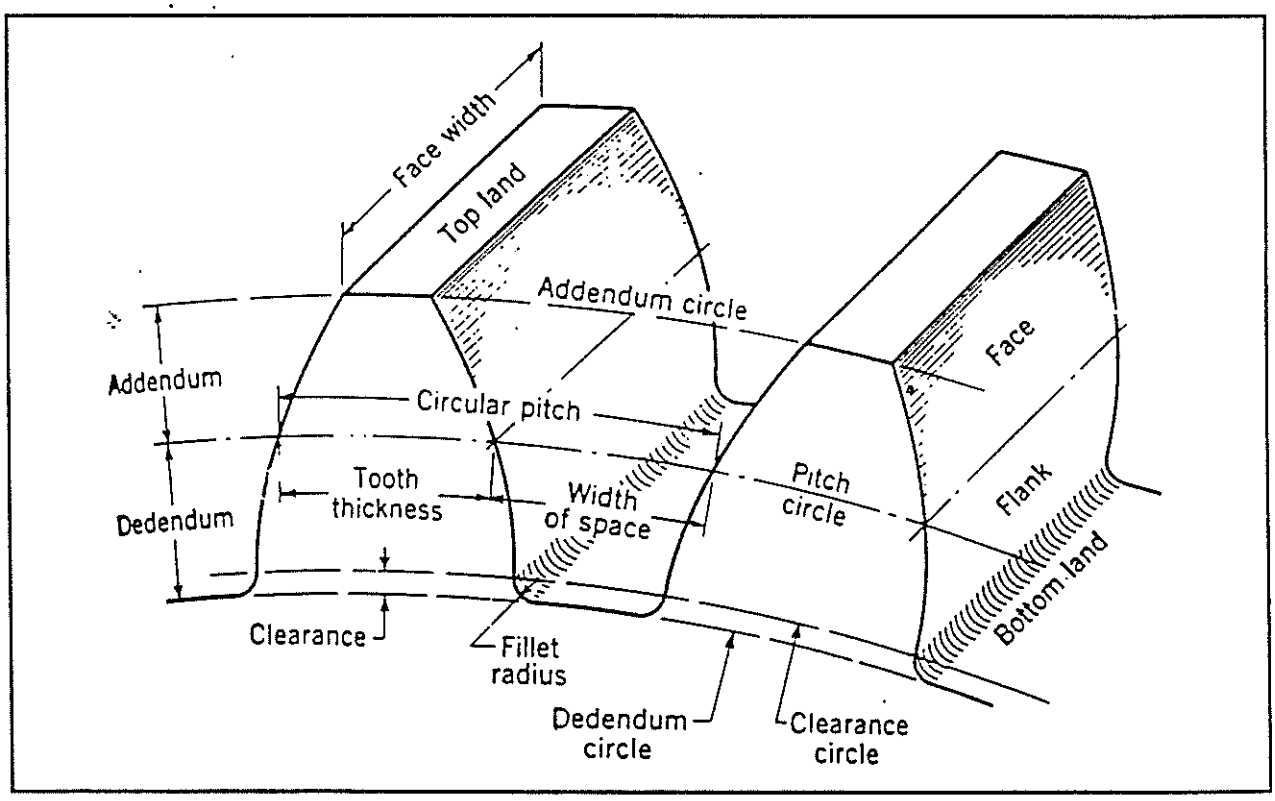

Figure 2.1 Common gear nomenclature [1].

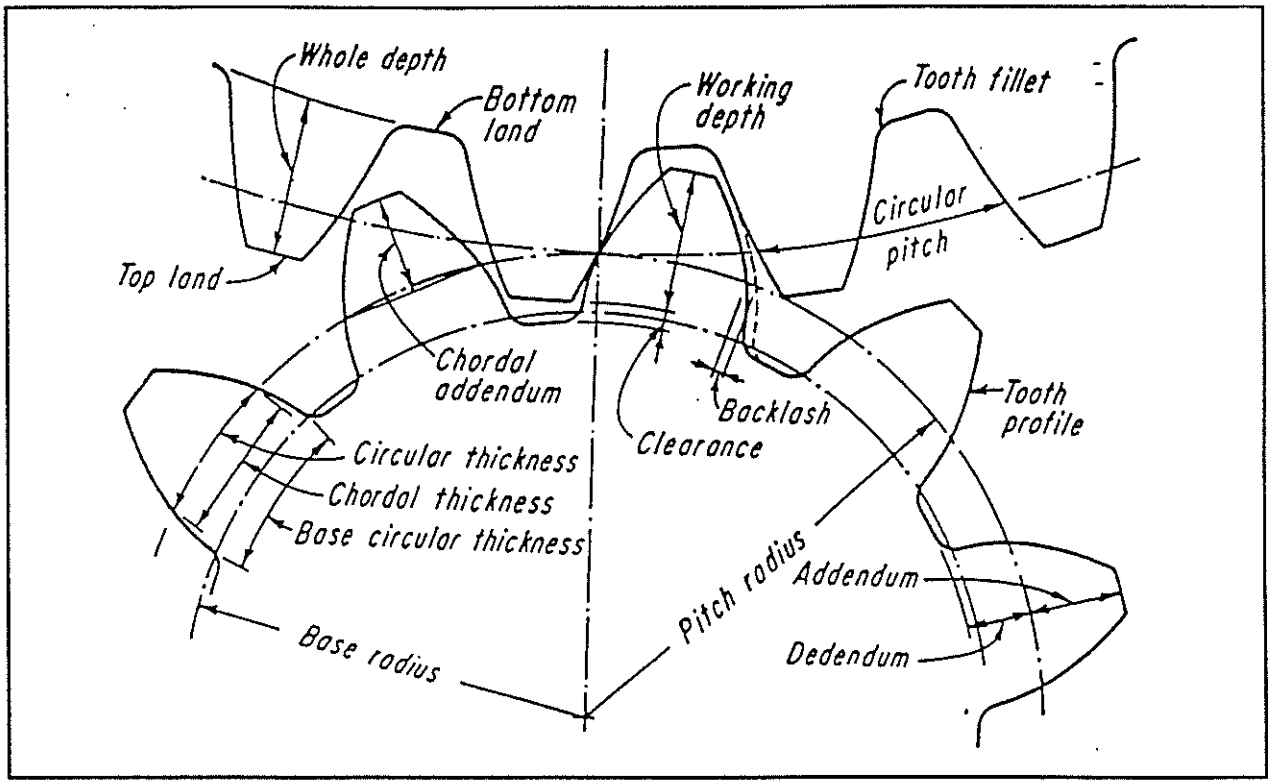

Figure 2.2 Additional gear nomenclature [2].

The pitch circles of a pair of mating gears are tangent to each other [2]. The circular pitch (p), is the distance measured along the pitch circle, from a point on one tooth to a corresponding point on an adjacent tooth.

The module (m) is the ratio of the pitch diameter to the number of teeth. A pair of meshing spur gears must have exactly the same module, if they are to mesh properly. Backlash, in general is the maximum length of arc of the pitch circle through which a gear can be rotated to bring its non-working flanks into contact with those of the mating gear, when the mating gear is held rigid. Other important and interrelated gear terms are the base circle, pressure angle and the line of action.

Reference is made to Figures 2.3 through 2.5 to aid with the following definitions. The base circle for an involute cylindrical gear, is the circle from which the tooth flank involute is formed. The base circle radius (r_B) can be directly calculated if the pitch circle radius (r) and pressure angle (ϕ) are known. The pitch point (P) is the point of contact between the two meshing gears' pitch circles. The pressure angle defines the slope of the pressure line which passes through the pitch point. Referring to Figure 2.5, it can be seen that contact between gears occurs along the pressure line. The initial contact between mating teeth will take place when the flank of the pinion (driver) comes into contact with the tip of the gear (driven). This occurs at point (a), where the addendum circle of the driven gear crosses the pressure line. The final point of contact occurs at point (b),

where the dedendum circle of the driven gear crosses the pressure line. The line segment (ab) which lies on the pressure line is referred to as the line of action. This line of action is the locus of successive points of contact made by two mating tooth profiles during rotation.

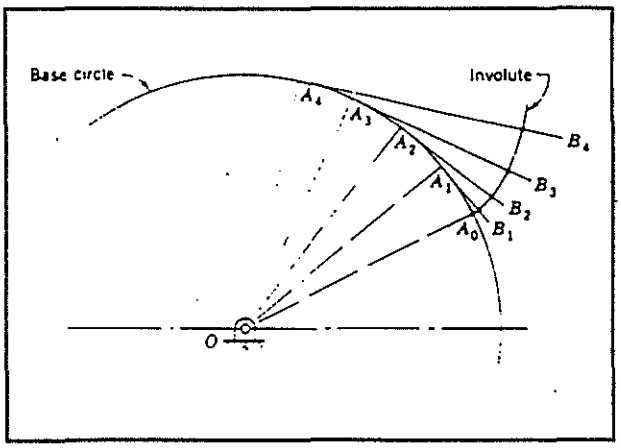

Figure 2.3 Involute curve [1].

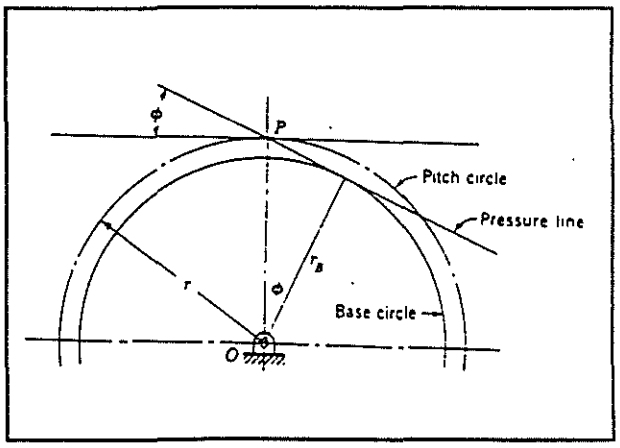

Figure 2.4 Base circle [1].

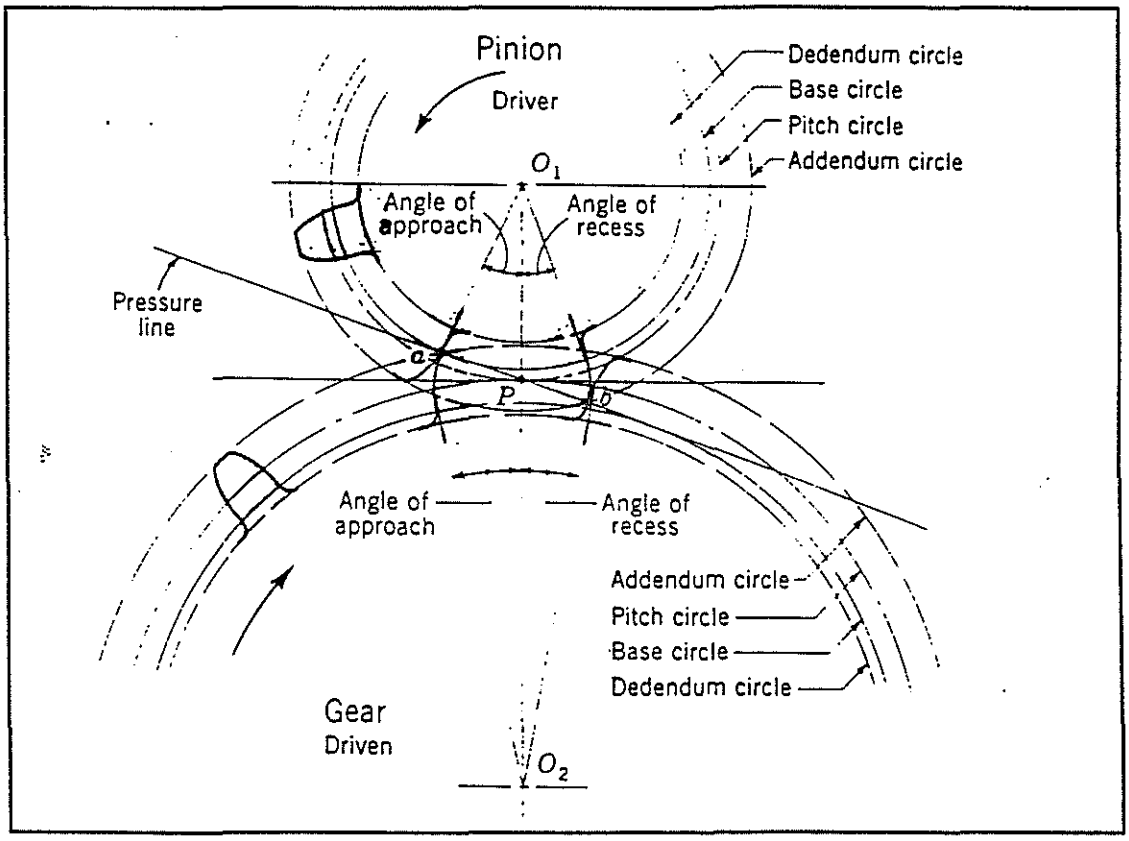

Figure 2.5 Tooth interaction [1].

The gear terminology discussed so far relates to the design and theoretical interaction of mating gears. Errors in manufacture, deflections of mountings under load and deflections of the teeth under load all contribute to losing the desired true involute contact in gear meshes. As a result, the teeth do not perform as they are supposed to (by theory). Hence, gears designed without considering the above mentioned effects may experience non-uniform angular motion and high dynamic loads due to meshing irregularities. In order to reduce these effects, tooth profile modifications are used. The major profile modification type of relevance to this project was tip relief as its impact to the successful computer modelling of contacting gear teeth (Chapter 5) was crucial. Tip relief (see Figure 2.6), is the intentional modification of the form of the tooth profile by removal of material at the tip to smooth contact of a flank with its mating flank [3].

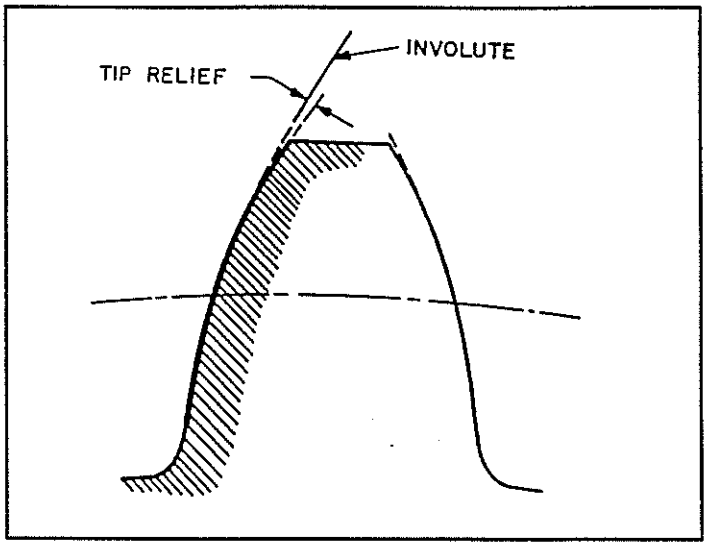

Figure 2.6 Tip relief [3].

Apart from understanding the basic nomenclature related to the gear design and operation, it is useful to have an appreciation of the failure modes for gears. A gear has failed when it can no longer efficiently do the job for which it was designed [4]. The more common modes of gear failure are wear, surface fatigue, plastic flow and breakage. Generally each type of failure mode has a distinguishable cause and a possible remedy. This project is only concerned with tooth breakages resulting from cracks in the root region of the tooth profile. Breakage is a failure caused by the fracture of a whole tooth or a substantial portion of a tooth. This can result from overload or more commonly by cyclic stressing of the gear tooth beyond the endurance limit of the material.

'Bending Fatigue Breakage', the focus point of this project, generally results from a crack originating in the root section of the tooth (see Figure 2.7). These cracks continue to propagate under repeated tooth loading cycles until the remaining section of tooth is insufficient to withstand the load, whereupon the section of tooth fractures (see Figures 2.8 and 2.9).

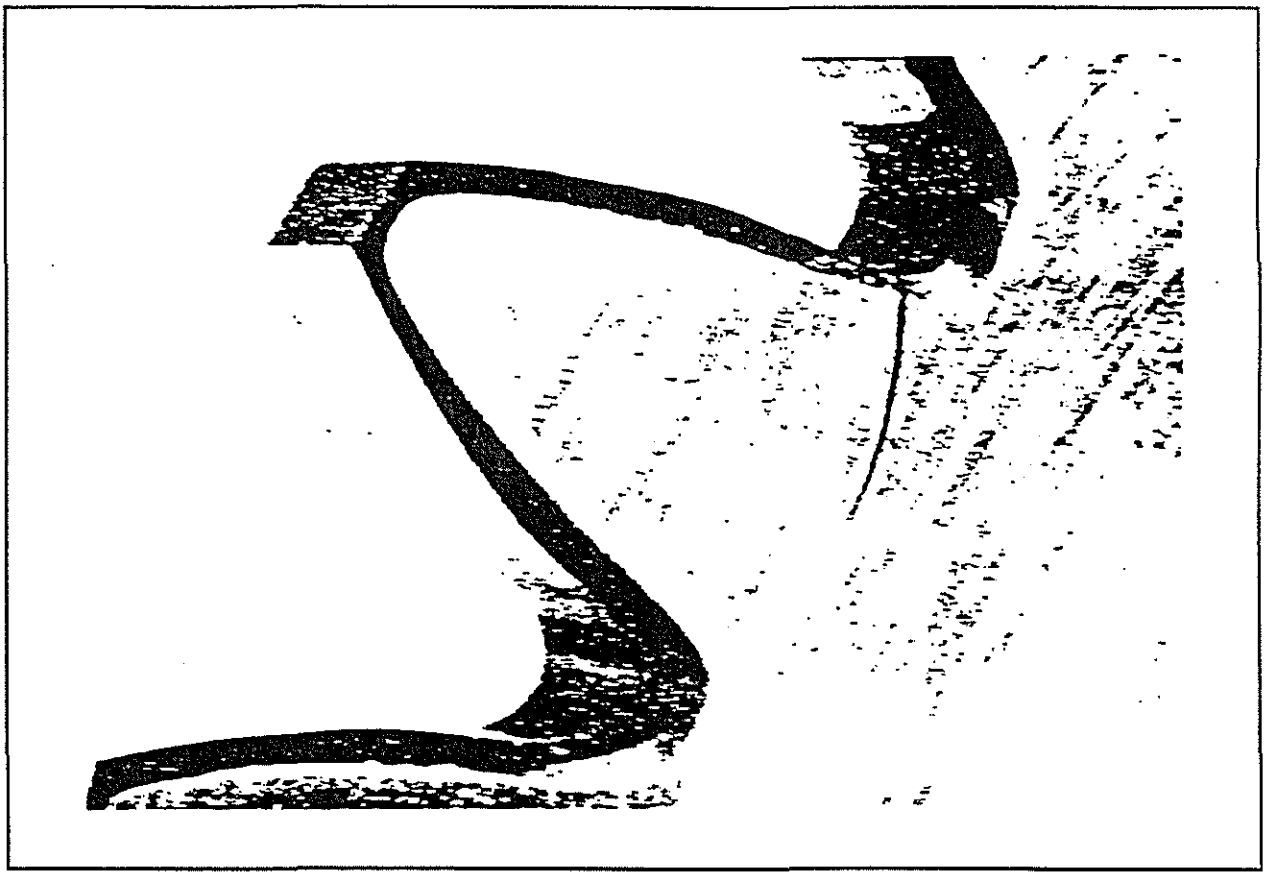

Figure 2.7 Root region crack due to beam bending fatigue [4].

As seen in Figures 2.8 and 2.9, the fracture surfaces consist of two major sections. The smooth elliptical pattern on the fracture surface highlights the region of slow stable crack propagation. The remainder of the fracture surface, rough in appearance, is the region of the tooth which experienced rapid unstable fracture resulting in a piece breaking off the gear.

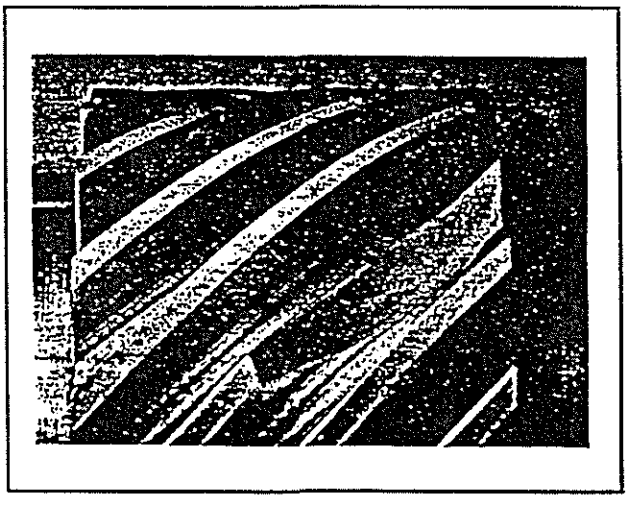

Figure 2.8 Partial tooth fracture [4].

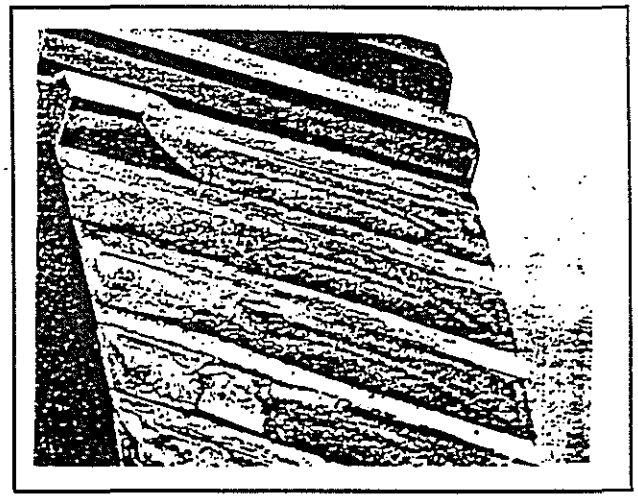

Figure 2.9 Complete tooth failures [4].

Occasionally stress concentrations aid in initiating and propagating these cracks, subjecting the gear to higher root stress levels than allowed for during design [4]. Typical stress concentrations are caused by notches in the root fillet, machining marks, particle inclusions, small heat-treatment cracks, grinding burns or residual stresses. Poor installation (gear alignment), poor lubrication, and inadequate design can all contribute to unexpected stress levels in the root region of the tooth profile.

Unfortunately, prevention is better than a cure when dealing with fatigue cracks. Several manufacturing solutions can be utilised to reduce the possibility of fatigue cracks forming in the critical root region. These solutions include redesigning the fillet region of the tooth, polishing and shot peening the root region, using higher strength material and/or care during the heat treatment stage of the gear's construction to minimise the chance of any harmful residual stresses.

Although breakage is most predominant in the root region, failure can occur in other regions of the gear tooth. Figure 2.10 displays some typical random fatigue breaks. Failures of this kind are often caused by deficiencies in the gear tooth, which result in high local stress concentrations. These deficiencies (flaws) or minute cracks propagate under repeated stress cycling, often resulting in fracture. Unfortunately it is difficult to prevent failures of this type except by good design and manufacturing practices. Modelling such cracks on the contact surfaces of the tooth flank is not practical due to the complexity of the triaxial stress state in this region. In this project, effort was directed towards modelling root region cracks so as to predict their propagation characteristics.

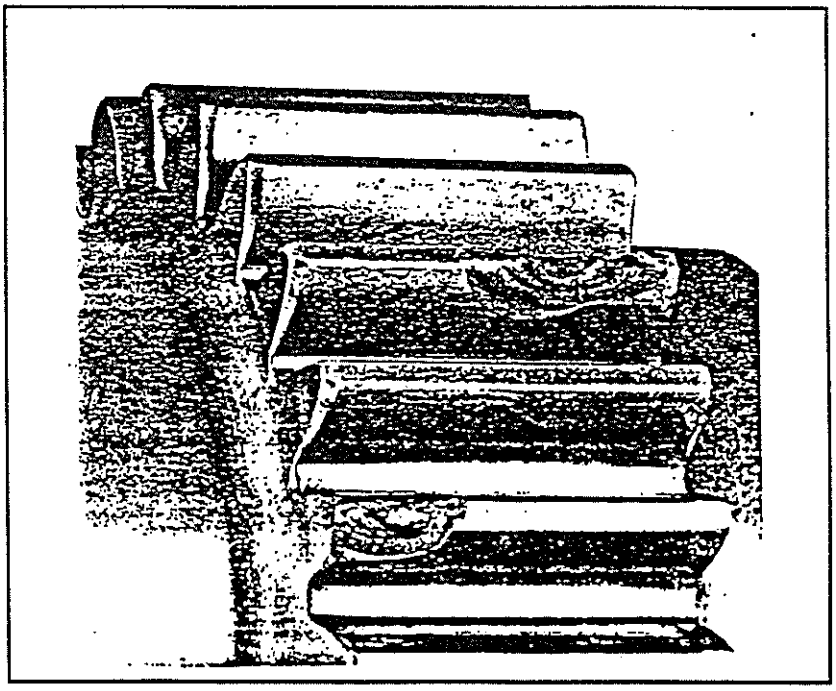

Figure 2.10 Random fatigue breaks [4].

2.3 Review of Industry, AGMA, ISO and BS standards

Historically [5], manufacturers of gears for both the Australian mining and sugar industries used the British Standard 'BS 436 - 1940' for the design and specification of gears. Currently, the Australian Gear Industry utilises any one or a combination of the major standards for gear design. They include such standards as BS (British Standards), AGMA (American Gear Manufacturers Association) [6] and DIN (German Standards). The current Australian Standard '2938 - 1987' [7], based largely on the AGMA 2001, is used throughout the sugar industry for gear specification.

From the sugar industry's viewpoint, it is important to understand the contrasts and similarities of the standards so that they may be used when specifying and evaluating gears. Fortunately, ISO (International Standardisation Organisation) has developed gearing standards [8] which encompass all the major standards to minimise the shortfalls and maximise the effective characteristics of the separate standards used internationally. These ISO standards seem to resemble the German standards and are expected to have a larger impact on Australian gear manufacture in the future.

Two standards were reviewed to assess their possible application for this research project.

- AS 2938 - 1987, "Gears - Spur and Helical - Guide to Specification and Rating"
- AGMA 2001 - B88, "Fundamental Rating Factors and Calculation Methods for Involute Spur and Helical Gear Teeth".

These standards cover calculations of allowable stresses, pitting resistance and tooth breakage factors as well as life and reliability factors. Effects of misalignment, material selection and treatment and overloads are incorporated for use in gear design through safety factors. Unfortunately, these standards do not cover the effects of crack like defects on the remaining useful life of a gear. Standards concentrate on the effects of pitting on the life of gearing and also the use of 'endurance limit' related fatigue methods to ascertain the anticipated life of gearing.

Cracks can appear in well designed gears, and hence there is a need to understand the effect of defects on the remaining life of gears. As the current gear standards are unable to assess the effects and characteristics of cracks, a method for determining crack propagation rates is necessary. This project will employ linear elastic fracture mechanics to predict crack propagation in slow speed gears used in the sugar industry.

2.4 Basic fracture mechanics and crack propagation prediction theory

Cracks are present in some degree in all structures [9]. Their presence increases the time and effort spent on maintenance and repair. Cracks may be present as small flaws in the material at the manufacturing stage, introduced during fabrication or they may be a result of corrosion or fatigue damage to the structure. These cracks may lead to component fracture and hence structural failure. Since cracks cannot be eliminated, procedures have been developed to quantify and predict the behaviour of cracked structures under service conditions. This field of engineering is known as 'Fracture Mechanics'.

The basic requirement of fracture mechanics theory is a means of assessing the stability of cracks. Therefore the most significant advance has been the introduction of the 'Stress Intensity Factor' as a single parameter for categorising the onset of crack propagation. The simplistic relationship between the stress intensity factor (K) and a material's toughness makes this approach attractive. However, the use of the stress intensity factor in investigating crack stability requires an accurate knowledge of the stress field in the vicinity of the crack tip. Analytical solutions only exist for simple cases, but recent improvements in numerical techniques such as finite elements and boundary integral methods have made the determination of the stress and displacement fields for complex situations possible. The past twenty years has seen a steady refinement in finite element techniques to the point where it has become a well established tool and an ideal method for numerical solutions involving the study of crack behaviour in materials.

Life prediction for a cracked component can only be achieved in two ways, laboratory testing under simulated service conditions of geometry, loading and environment or by numerical methods of crack growth processes. Laboratory testing is very expensive and time consuming as time dependent corrosion effects prohibit test acceleration. However, computer based estimation methodologies can perform similar validations with equal accuracy to laboratory testing in a fraction of the time and cost. As it would be impractical to physically test a large spur gear, computer based analysis techniques to study cracked gearing were used for this project.

Following will be a brief and simplified discussion on the theory used in analysing cracks and their growth rates via computer aided techniques. Under repeated loads a crack in a structure will grow in time [9]. The longer the crack, the higher the stress concentration at the crack tip. As a result of the increased stresses at the crack tip, one could expect the crack propagation rate to increase with time. This relationship can be seen in Figure 2.11. The presence of this crack reduces the strength of the structure. The residual (remaining) strength of the structure decreases progressively as the crack size increases as simulated in Figure 2.12. The residual strength of the structure may decrease to a level at which the structure would fail from an unexpected high service load. If such a load was not experienced, the crack would continue to grow whilst reducing the residual strength until it became so low that failure (fracture) would occur under normal service

loading. In general, design engineers should account for the possibility of fatigue in structures. To ensure safety, prediction of how fast cracks propagate (ie. how fast the residual strength decreases) needs to be made. Such predictions can be made by applying the theory of fracture mechanics.

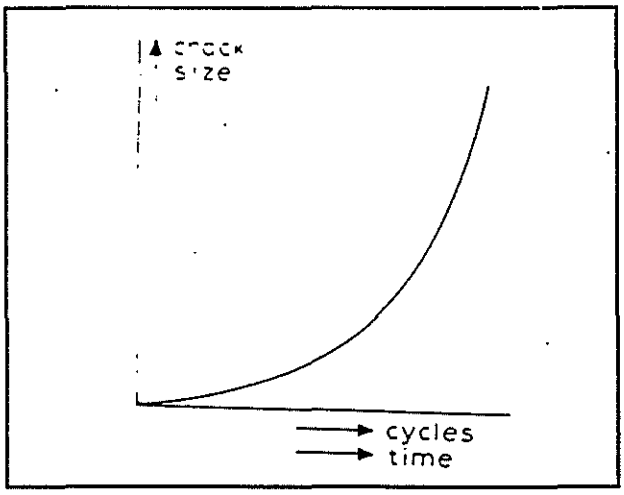

Figure 2.11 Crack growth curve [9].

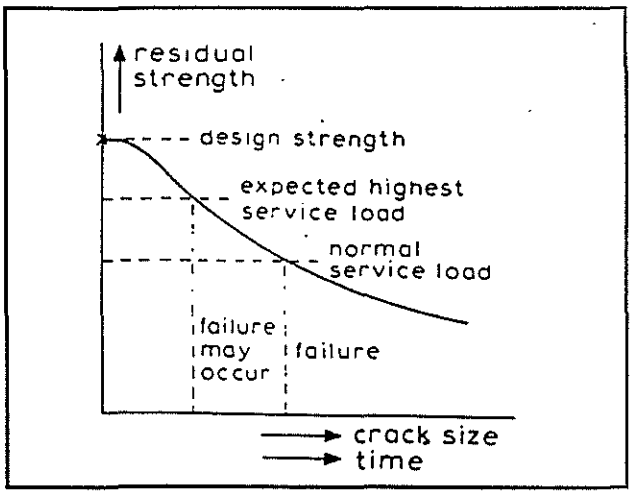

Figure 2.12 Residual strength curve [9].

A crack in a solid can be stressed in one or a combination of three different modes as seen in Figure 2.13. The most common of these modes is the opening mode (Mode I).

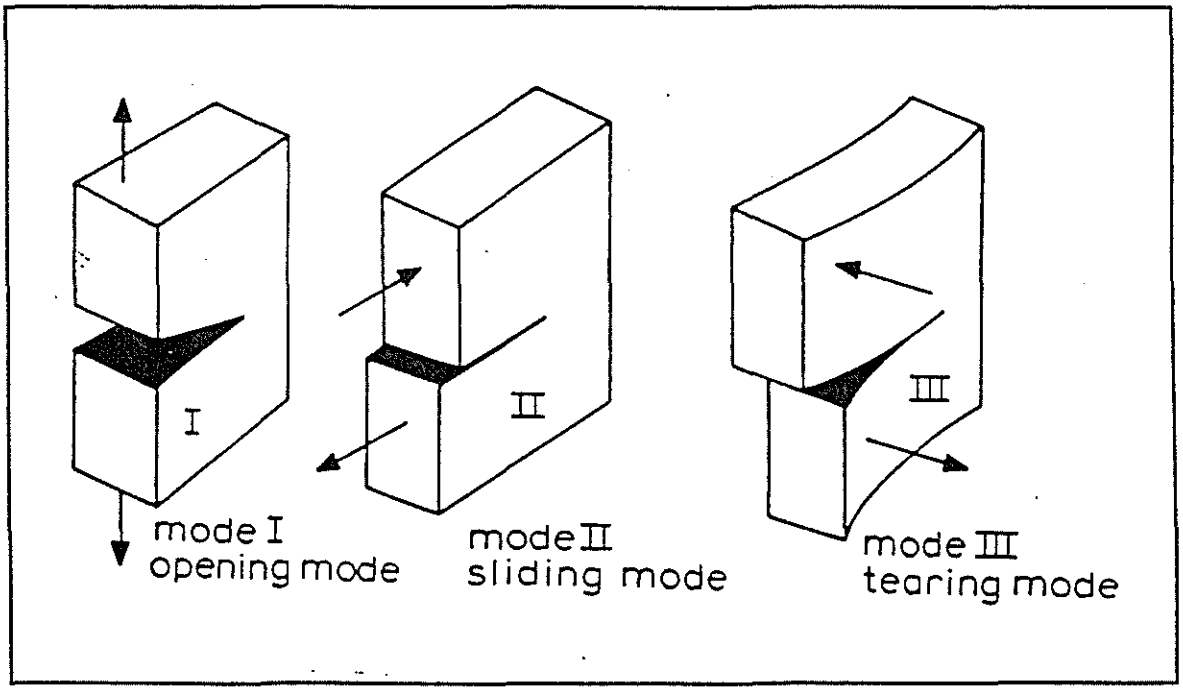

Figure 2.13 The three modes of loading [9].

The elastic stress field of a 'through the thickness' crack in an arbitrary body experiencing a mode I loading (as seen in Figure 2.14) can be expressed as:

$$\sigma_{ij} = \frac{K_I}{\sqrt{2\pi r}} f_{ij}(\theta) \qquad (2.1)$$

where $f_{ij}(\theta)$ are known functions of θ. K_I (stress intensity factor for mode I loading) describes the crack tip stresses. Similar solutions are obtained for the other modes but with differing θ functions.

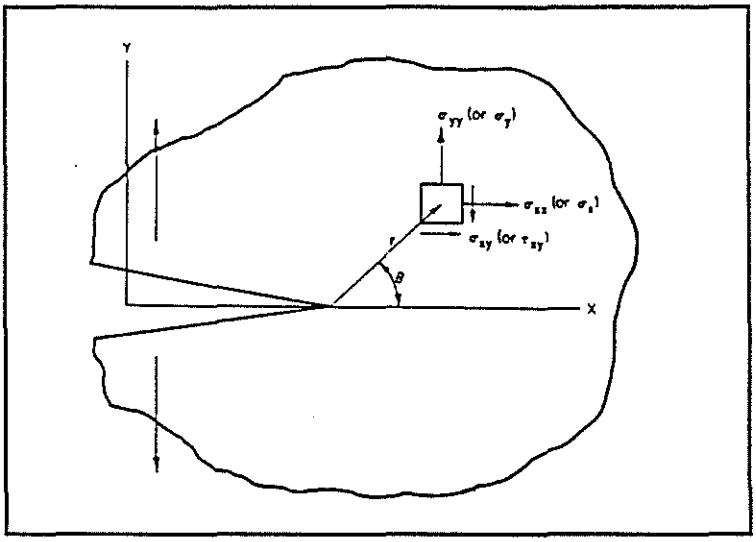

Figure 2.14 Crack in arbitrary body [9].

Combining the situation of an infinite plate under constant load or stress σ, (Figure 2.15) containing a central crack (effectively two cracks of length a) and applying equation 2.1 gives:

$$K_I = \beta\sigma\sqrt{a} \qquad (2.2)$$

If the width of the plate shown in Figure 2.15 is not infinite but of width W, the crack tip stresses would increase from the case of the infinite plate. This suggests that K_I must increase with a decrease in W. Therefore equation 2.2 should be modified to include a function of crack length divided by the width W for the case of the finite plate. Usually the stress intensity factors are expressed in relation to the stress intensity of the infinite plate mentioned previously, and therefore equation 2.2 becomes:

$$K_I = \beta\left(a/L\right)\sigma\sqrt{\pi a} \qquad (2.3)$$

where L is a generalised size parameter and $\beta\left(a/L\right)$ is a geometry function.

The entire crack tip stress field can be described once the function $\beta\left(a/L\right)$ is known. Note that the stress quoted in equation 2.3 is always the remote stress, not the stress in the cracked section. The fact that the net section stress increases with decreasing W is accounted for in β.

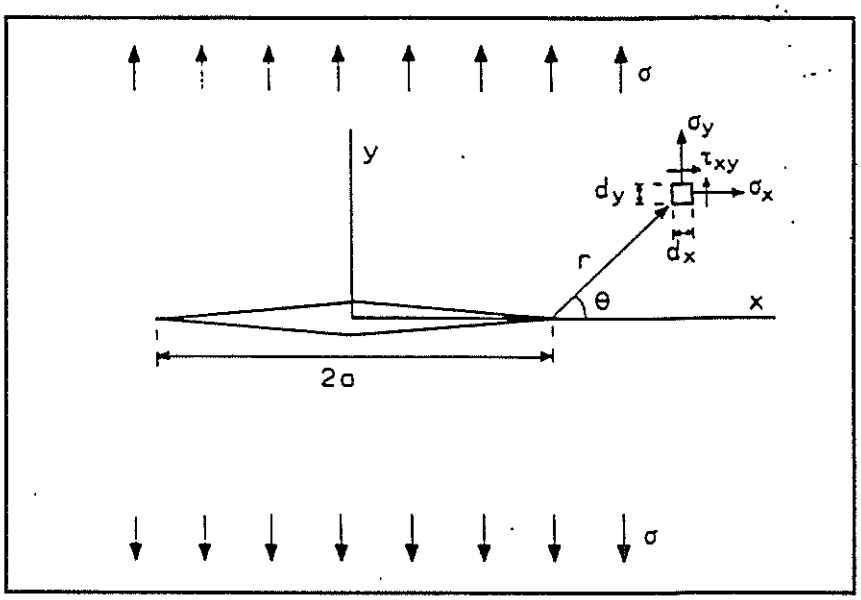

Figure 2.15 Crack in an infinite plate [9].

The function β (geometry function) has been estimated for many geometries. Unfortunately, none have been found in the literature to suit involute gear teeth geometries with root region cracks. As a result, one major task for this project was to produce a geometry function for a gear tooth of known dimensions. Geometry functions are generally written as high order polynomials such as:

$$\beta \cong C_1 + C_2\left(a/L\right) + C_3\left(a/L\right)^2 + C_4\left(a/L\right)^3 + C_5\left(a/L\right)^4. \qquad (2.4)$$

For example, the pre-calculated compliance function for the geometry shown in Figure 2.16 is

$$\beta = 1.99 - 0.41\left(a/W\right) + 18.7\left(a/W\right)^2 - 38.48\left(a/W\right)^3 + 53.85\left(a/W\right)^4$$

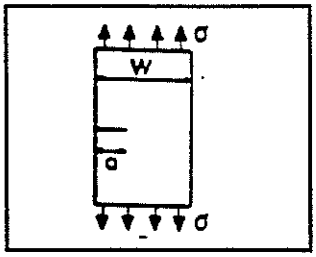

Figure 2.16 Crack in an infinite plate of width W [9].

Fundamental to fracture mechanics is that when the stress intensity of a crack reaches a certain value for that particular material, it will rapidly propagate causing component failure. Similarly, if the stress intensities for two cracked bodies (different physical size and crack size but of the same material) are equal then there is exact similitude. So one could expect the two cracks to respond in the same manner. In other words, an equal stress intensity signifies similitude in stress at the crack tip.

The stress intensity at which a cracked component made of a certain material fails is known as the fracture toughness for that material. Although, the fracture toughness of a material varies with temperature and other environmental conditions, these are secondary to component thickness. Basically, the thickness of a component effects the fracture toughness value as the out of plane stresses (dependent on the thickness) determine the final size of the plastic zone at the crack tip (Figures 2.17 and 2.18).

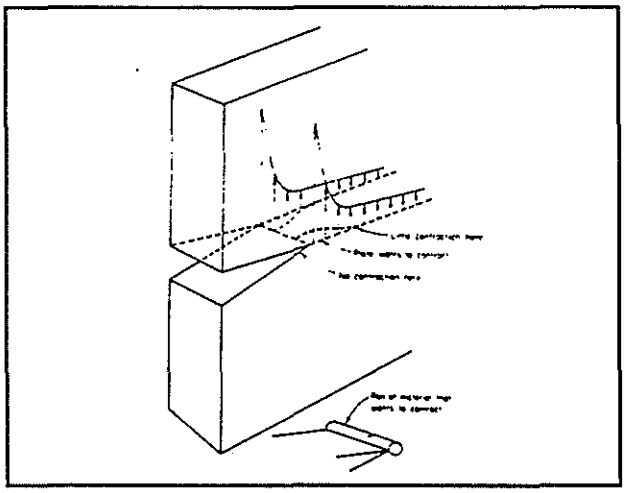

Figure 2.17 Contraction at crack tip [9].

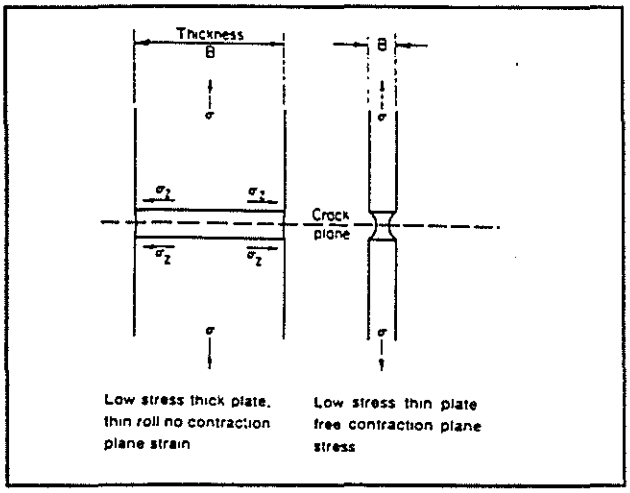

Figure 2.18 Plane strain and stress [9].

As displayed in Figure 2.17, the thin roll of material (experiencing plastic deformation due to the high in plane crack tip stresses mentioned previously) wants to contract due to a Poisson effect. The thickness of the component determines whether the surrounding material will allow contraction or not. If the thickness is sufficient to reduce the contraction of the plastic zone at the crack tip then stresses in the out of plane direction will be induced as shown in Figure 2.18. The presence of this additional stress at the crack tip effects the size of the plastic zone and stress field in front of the crack tip. Hence the behaviour of the crack changes depending on the thickness of the component. For cracks in thin section plates there is no restriction of the contraction of the crack tip plastic zone and this is referred to as 'plane stress'. In contrast where there is restriction of the crack tip plastic zone (eg cracks in thick section plate), this is referred to as 'plane strain'. The plane strain plastic zone is markedly smaller than the plane stress plastic zone. Research has shown that the effective yield stress in plane strain can be as high three times the uniaxial yield stress [9].

The approximate stress distribution for the plane stress and plane strain cases are shown in Figure 2.19. Note the relative size of the plastic zones (r_p).

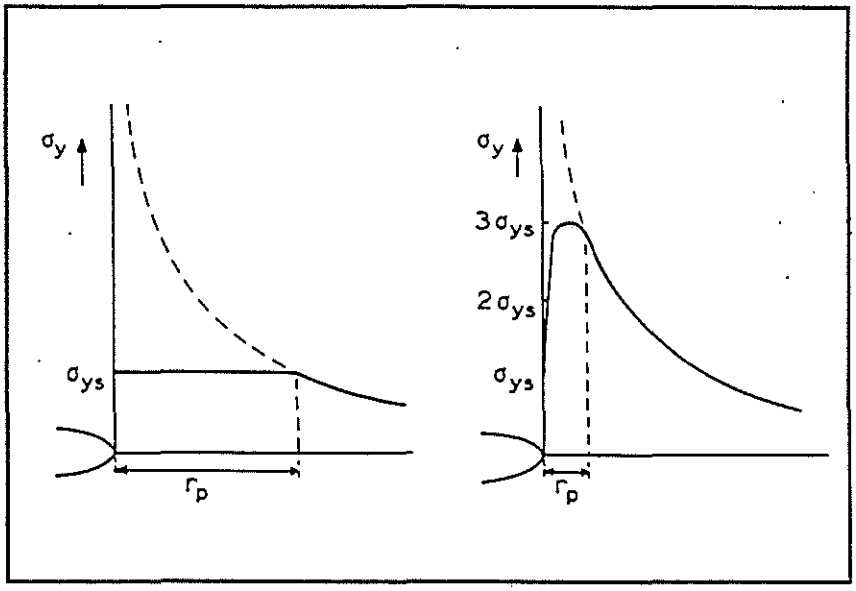

Figure 2.19 Typical stress distributions for plane stress (left) and plane strain (right) [9].

For plane strain to exist along the majority of a crack tip front, the plate thickness must be adequately large. The thickness of a plate (B_s) to ensure the condition of plane strain is :

$$Bs \geq 2.5\left(K_I/\sigma_{ys}\right)^2 \qquad (2.5)$$

where K_I is the applied stress intensity and σ_{ys} is the material's yield stress value. The fracture toughness (or critical stress intensity) is given the notation of K_{IC} to represent mode I cracking. The dependence of K_{IC} and similarly residual strength, upon thickness is shown in Figures 2.20 and 2.21. It can be seen that K_{IC} reaches a constant level after a certain thickness is obtained. The lower value for K_{IC} will be utilised in this project to ensure conservative results when predicting the behaviour of cracks found in the gearing.

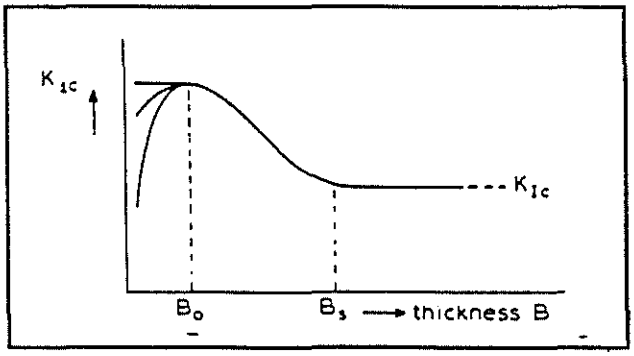

Figure 2.20 K_{IC} vs. thickness [9].

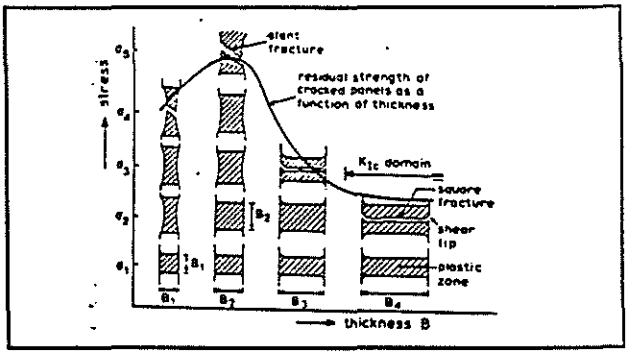

Figure 2.21 Residual strength vs. thickness [9].

So far discussions have centred around the importance of the stress intensity and its effect on stress at a crack tip and the stability of the crack. Calculating the stress intensity using equation 2.3 .requires a prior knowledge of the geometry function. Unfortunately the geometry function is not known for involute gears and needs to be determined by appropriate methods. Several methods [9] exist (numerical methods and mathematical hypothesises) with numerical methods being most appropriate for this project. The non-linear analysis computer code 'ABAQUS (standard)' employs crack tip finite elements enabling almost any two dimensional geometry and crack to be analysed. ABAQUS utilises the energy release theory for propagating cracks to calculate stress intensity values and hence geometry functions can be obtained for specific geometries. Following Broek [9], if a crack length is increased by a small amount, the energy released per unit area of the crack extension, G, is given by :

$$G_I = \left(\partial U / B\partial a\right) \qquad (2.6)$$

where B is the thickness of the component and U is the potential energy. Research [9] has shown that the stress intensity and the energy release rate have the following relationship :

$$G_I = \frac{K_I^2}{E} \quad \text{(plane stress)} \quad \underline{\text{or}} \quad G_I = \frac{K_I^2(1-\nu^2)}{E} \quad \text{(plane strain)} \qquad (2.7)$$

ABAQUS calculates a J-Integral value (contour integral surrounding the crack tip) to determine the energy release rate G_I (J-Integral value = G_I). This J-Integral calculation is an accurate method for evaluating stress intensities. Further discussions on the use of the J-Integral method will be made in Chapter 6.

From equation 2.3 it would be possible to predict the crack length for which a certain load that would cause component failure, if the material's fracture toughness was known or vice versa. The time it takes for a crack to reach a critical length for a known loading history is also of importance to a designer. Computer codes (PFATIGUE, NSOFT) can be used to assess the propagation of a crack in a structure. These codes utilise the relationship between the increase in crack length per loading cycle and the change in the stress intensity per loading cycle. The basic form of this relationship as proposed by Paris in 1966 evolved from experimental work involving pre-cracked materials. The Paris Law (equation 2.8) in simplistic form, is obtained from the straight line section shown in Figure 2.22 which is representative of a steady state crack growth region.

$$da/dN = C(\Delta K)^m \qquad (2.8)$$

where C and m are proposed material constants and N is the number of repeated load cycles. Equation 2.8 is based on the case where the repeated loads are tensile (positive).

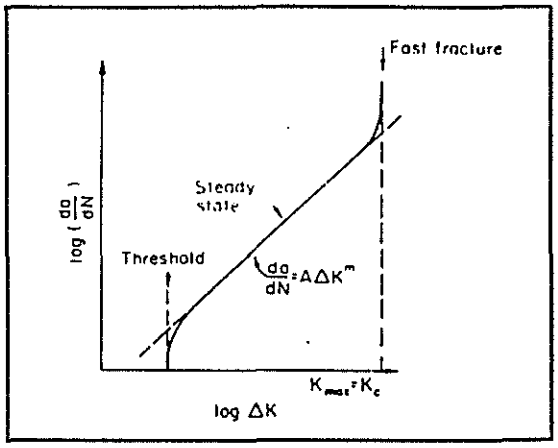

Figure 2.22 Common fatigue crack-growth rates [10].

From Figure 2.22, it can be seen that the crack growth rate remains at zero (no crack growth) until the change in stress intensity for a load cycle surpasses a threshold level. This threshold stress intensity level varies for different materials. Also of interest is the rapid increase in crack growth rate when the maximum stress intensity during a load cycle approaches or equals the fracture toughness value for a given material. At this point rapid failure occurs. Figure 2.23 illustrates the steady state growth of a crack and the increase in stress intensity for a cracked component under constant positive load cycling.

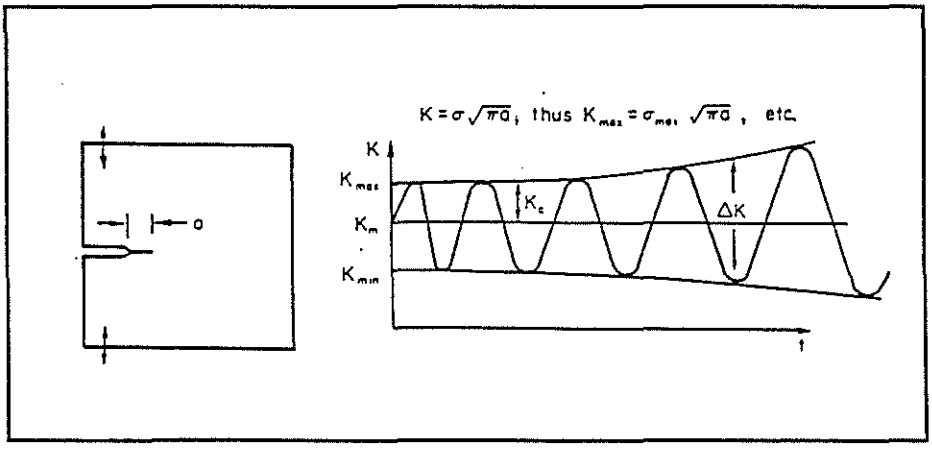

Figure 2.23 Example of fatigue crack growth [10].

In Figure 2.23 , the cyclic stress intensity increases with time as one would expect as the crack length and hence the geometry function value have increased. Hence, for a cracked specimen undergoing repeated constant load cycles, the rate of crack growth would continually accelerate until the crack reaches the critical crack length at which point the maximum stress intensity equals the fracture toughness for that material whereupon rapid failure would occur. Prediction of the growth characteristics of a known crack in a gear tooth root region to failure is made easier with the use of a specialised computer code such as 'PFATIGUE'.

A cycle by cycle fatigue crack propagation prediction code such as PFATIGUE calculates the crack extension for each load cycle in a load history and adds it to the current crack size. This process is repeated until the crack reaches the critical crack length. As previously mentioned, the driving force for crack propagation is the stress intensity range (ΔK). For each load cycle the ΔK calculated from the stress range, crack size and geometry function value for the cracked component is known as the 'apparent or applied ΔK'. To improve accuracy when using the Paris Law [11], this 'applied ΔK' is modified to obtain an 'effective ΔK' which accounts for the possible occurrence of crack closure, residual stresses, notch and environmental effects and negative loading ratios during each load cycle. Crack propagation life can therefore be accurately modelled but only on a cycle by cycle basis.

3.0 Procedure

3.1 Use of Computer Codes : PATRAN, PFATIGUE, ABAQUS (Standard) and NSOFT

Figure 3.1 shows schematically the software chosen for this investigation.

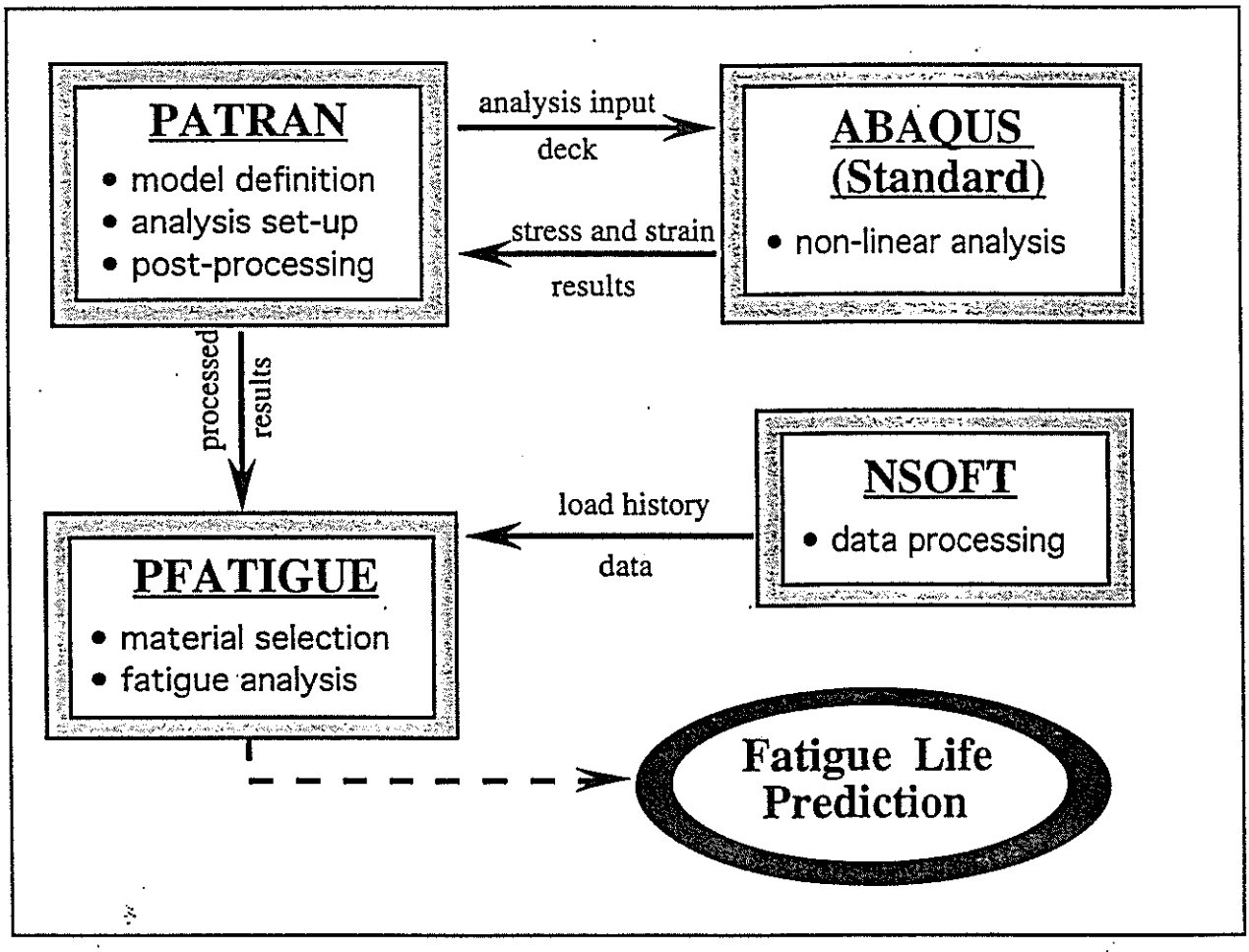

Figure 3.1 Interaction of software packages.

PATRAN (P3) is a finite element modeller [12] with an excellent pre- and post-processor. Models of involute gear teeth can be constructed and loads, boundary conditions and material properties easily assigned. Possibly of more importance is the transparent interface to the ABAQUS (standard) non-linear finite element solver and the PFATIGUE durability modeller. Such transparency aids in model building and solution and greatly speeds up the numerical analysis.

ABAQUS (standard) [13] was chosen as the general solver for this investigation. The code is extremely versatile and robust with the capability of modelling two dimensional contact between deformable bodies undergoing large motion. In addition, the code has an advanced fracture

modelling capability with built-in line spring elements for exploring the plastic zone at the crack tip as well as prediction of the J-Integral.

Factory data was processed using NSOFT. NSOFT [14] was chosen for the following reasons:

- the code's ability to display, prepare, analyse and characterise measured data.
- the ease of pre- and post-processing data and transferral of data over for use in fatigue analysis.
- the option of displaying and classifying data in both the time and frequency domains or filtering the raw data for further use.

PFATIGUE is a module of the PATRAN modelling package [15]. For the purposes of this project, PFATIGUE has been used as the fatigue life analysis code. PFATIGUE supports total life, crack initiation and crack growth estimation techniques. The ability to analyse crack growth rates for models created in PATRAN using stress results from ABAQUS and load histories prepared by NSOFT, made PFATIGUE the obvious choice for the crack growth section of this project. PFATIGUE solves crack growth problems via the utilisation of linear elastic fracture mechanics theory. Cycle-by-cycle modelling of crack closure by overloads, environmental effects, loading and history rates is included. A materials database of standard US and British fatigue data sets is available for the use of editing, creating, searching and displaying. The major attraction of PFATIGUE is the ease and speed at which sensitivity analyses can be done. The effects of changing material properties, loading values and combinations of the two can be rapidly solved and decisions can then be made towards extending the life of cracked gearing.

3.2 General Procedure

The following procedure was adopted:

1. Visits were made to Victoria mill to view the candidate gear with cracks in the root region.

2. Non destructive testing records were collected for the candidate gear.

3. Gear geometry and material property data were obtained from Walkers Limited.

4. Measurement and analysis of torque and speed data to form a duty cycle.

5. Finite element models of uncracked gearing under constant load and speed were built to determine methodologies for accurate analyses.

6. Determined a compliance function for a propagating crack in the root region under plane strain.

7. Crack propagation study was undertaken.

8. A sensitivity analysis to assess the effect of varying material properties and loads was undertaken.

9. Assessed effect of non-uniform flank loading.

4.0 Target Gears : Geometry, Load and Crack History

4.1 Non-destructive testing records

To check the validity of crack propagation models, it is useful to have records of actual crack growth rates for comparison. Reports / records from 'Intico Monitoring Services' concerning the non-destructive testing of low speed gears at Victoria Mill date back to 1985. These reports, approximately one every two years, outline the position and length of any cracks found on the bull wheel gear teeth. Copies of all the relevant non-destructive testing records relating to the candidate bull gear in 'Mill 4B' gearbox were obtained during the first of two visits to Victoria Mill. Typical reports can be found in Appendix A1.

The testing procedure used by Intico [16] involves scanning the end profile and across the entire root area of each tooth with a hand held probe (part of the EMD) rotated close to the surface in small circular motions. If a tooth exhibits any surface crack discontinuities, the lubrication is removed using kerosene so the crack can be visually examined. At this stage the crack is inspected using a supplementary 'Magnetic Particle Examination' (AS 1171-1971 AC Sustained Colour Contrast) to determine the exact length of the cracks detected earlier by the EMD equipment. Teeth numbers are stamped on the top land of each tooth to help with future identification during testing.

To gain an appreciation of the entire gear train '4B' arrangement and the cracks listed in the reports from Intico, a second visit was made to Victoria Mill in August, 1994 to view the bull wheel during a shutdown period. During this inspection, the crack positions and sizes for a select number of bull wheel teeth detailed in the most recent Intico report were cross checked. It was found that the majority of cracks had advanced only a few millimetres lengthwise, at most, since the most recent report in March, 1994. Figure 4.1 shows a mill employee removing the lubricant from the candidate gear in preparation for the magnetic particle examination. Figure 4.2 shows a close up view of two root regions on the gear covered in developer.

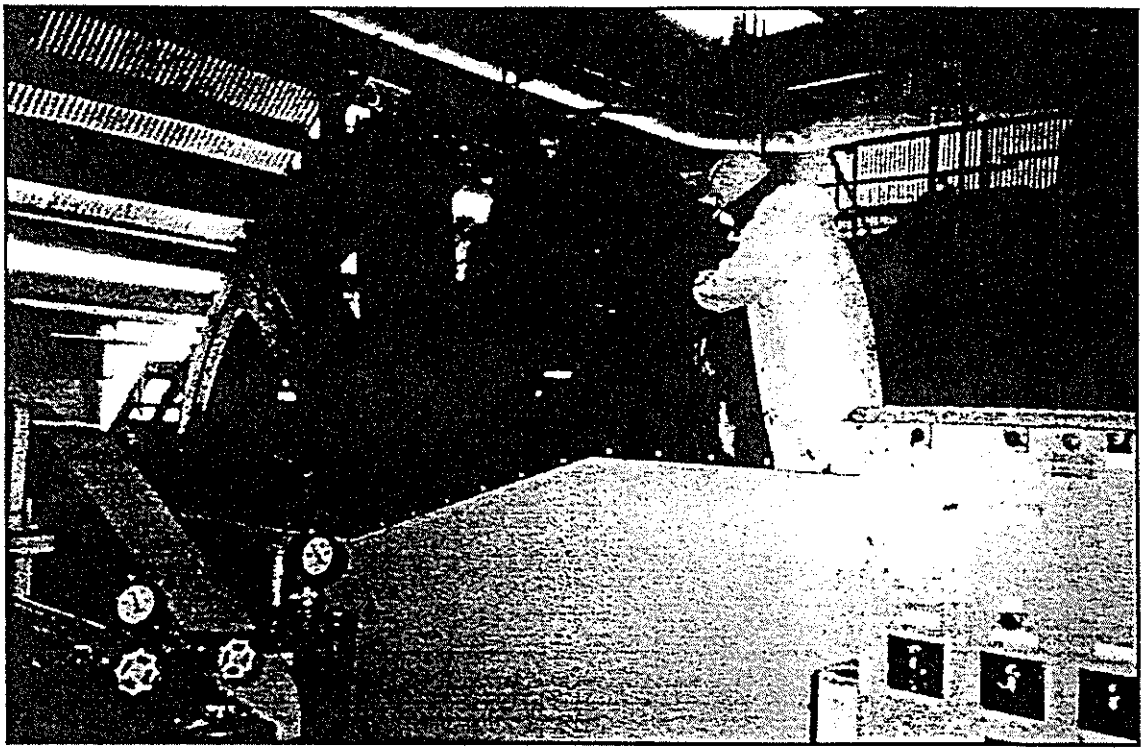

Figure 4.1 Mill employee preparing candidate gear (Mill 4B) for inspection.

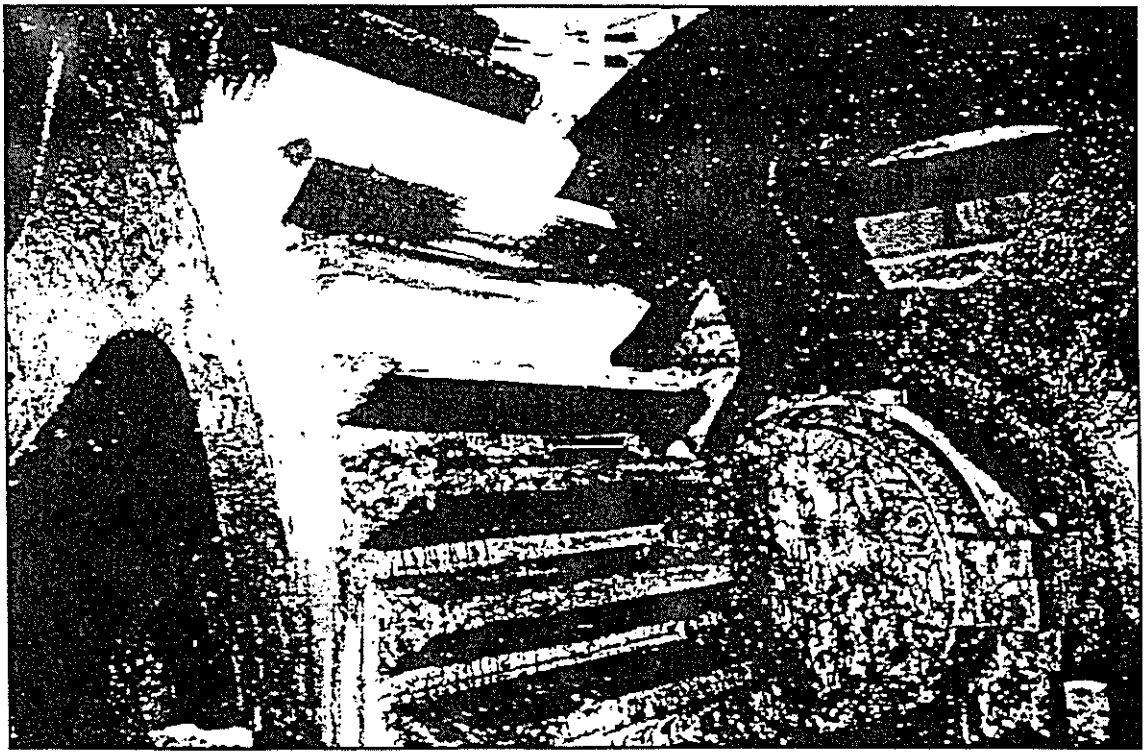

Figure 4.2 Close-up of candidate gear teeth during magnetic particle inspection.

Table 4.1 exhibits the history of several known cracks on the candidate gear over the period February, 1989 through to December, 1991. Note the crack lengths refer to the surface length of the cracks and not the depth of the cracks normal to the tooth surface.

Table 4.1 Dominant cracks and their propagation over three year period.
(Gear face width = 535 mm)

Root regions (Tooth no's between)	Crack Length (mm)			Total crack growth over period Feb-89 to Dec-91 (mm)
	Feb '89	Feb '91	Dec '91	
9 - 10	195	195	205	10
12 - 13	100	100	100	0
14 - 15	25	25	25	0
15 - 16	185	185	195	10
16 - 17	215	215	no record	-
17 - 18	150	150	180	30
18 - 19	175	195	200	25
19 - 20	120	120	no record	-
20 - 21	220	220	220	0
31 - 32	0	25	25	25

The crack monitoring reports were reviewed to gain a better understanding of the crack propagation trends and rates associated with the bull wheel gear used in the gear train '4B'. In general, the existing surface cracks grew intermittently if at all. This growth behaviour made it virtually impossible to extract any reliable crack propagation rates which would benefit the numerical modelling of crack growth. In addition, the crack growths and trends obtained from the inspections were only for crack extensions along the surface. The increase in crack depth is fundamentally of more importance. However, recent reports did suggest that crack depths were typically 5 mm. This knowledge of crack depth was of use when numerical modelling of the root region cracks commenced.

In conclusion, the inspection of the gears did prove valuable although useful crack propagation rates were not obtained. Inspection of the gear teeth highlighted the location of defects and the general wear patterns which indicated there was some degree of misalignment in the gear arrangement. This misalignment was investigated during modelling.

4.2 Relevant gear dimensions, materials and properties

To successfully attempt fatigue life estimations, several inputs must be known with some confidence. These are the geometry of the component, a representative loading history and adequate material properties.

In this case, the gear geometry was readily available on engineering drawings supplied by Walkers, the manufacturer's of the candidate gear (manufactured in 1975). These gear drawings (Appendix A2), include tooth profiles taken from the tool shop and fully dimensioned construction plans of both the pinion and bull gear. Complete as these drawings are, it must be remembered that gears are not always manufactured to specification and over time the geometry changes due to wear. The method employed in this project is based on the theoretical geometry and consequently it is recognised that a geometric error (believed to be small) will be present. However, it is possible to explore the effect of this error numerically.

In predicting crack propagation rates in low speed sugar mill gears, the most difficult aspect is the sourcing of adequate fatigue or fracture property data. Generally gear manufacturers have never been required to test gear materials. Consequently, little data other than the ultimate tensile strength, hardness and chemical composition are available. In this case, Walkers were unable to locate any metallurgical records (heat treatment and composition). Walker's reply letter stating the lack of data available for the gear's material properties is included in Appendix A2. The only material data obtained was the note on the bull gear construction drawing stating the rim was made of cast steel (Grade C, BS592-1967) with an ultimate tensile strength of 530 MPa.

To enable this project to progress, use was made of the material's database available in PFATIGUE. Although this database is extensive it applies primarily to US and British steels. Project outcomes, in terms of predictions, are therefore indications rather than absolute for the candidate gear.

4.3 Torque history details and accuracy

As mentioned previously, successful fatigue life estimations for a component using crack propagation theory requires an adequate loading history for that component. Loading on gears is a function of the torque, misalignment and lubrication. Nowadays, most sugar factories have computer based supervisory control systems available and as a result torque histories can be obtained. Misalignment under load can be assessed approximately using infrared thermometry techniques. The tractive surface loads induced inpart by boundary lubrication are not accurately known but their effect can be explored numerically.

Victoria mill has a 'Bailey' supervisory control system in operation. Two separate 24 hour periods of torque and associated mill rotation speed data (sampled once a minute) was obtained from the Bailey system. The rotational speed data for the candidate gear has little error involved. However, as the torque data is calculated empirically from turbine curves and chest pressures, the absolute error in the data would be significant. A mill engineer quoted the possible error as high as 20 per cent.

The torque and speed data provided by Victoria mill were processed using the package NSOFT described in Section 3.1. The final data as displayed in Figures 4.3 through 4.6 were later manipulated for use during the final crack gearing life predictions. In total there was two torque and speed data sets analysed. The time of these data recordings is as below :

Test 1. 6th Sept. 1994, 5:50 a.m. -------> 7th Sept. 1994, 5:50 a.m.
Test 2. 8th Sept. 1994, 7:45 a.m. -------> 9th Sept. 1994, 7:45 a.m.

Table 4.3.1 Summary of torque and gear speed data.

Data Description	Mean Value	Minimum Value	Maximum Value	Related Figure
Torque Test1 (TOR1)	0.957 MNm	0.164 MNm	1.202 MNm	4.3
Gear Speed Test1 (RPM1)	3.693 rpm	2.493 rpm	5.293 rpm	4.4
Torque Test2 (TOR2)	0.944 MNm	0.200 MNm	1.262 MNm	4.5
Gear Speed Test2 (RPM2)	2.859 rpm	1.727 rpm	3.842 rpm	4.6

Figures 4.3 through 4.6 show summary statistics in graphical form. The data are presented as a history plot of recorded data over the 24 hour period (top), a probability density function of the data (bottom left) and a frequency - amplitude spectrum of the data (bottom right). The history plot and associated statistical information highlight the fluctuation of the data for the candidate gear. The probability density function plot characterises the spread and grouping of data values over the 24 hour period. The spectrum plot, although not suited for this data with low sampling rates, is often used to expose operating and/or natural frequencies for components.

In general, the data provided proved adequate for use in the fatigue modelling stage of this project. However more data from other periods of the crushing season would reduce the effects of the variations in cane varieties, fibre and moisture content which may have biased the data processed for this project. Figures 4.3 through 4.6 can be found overleaf.

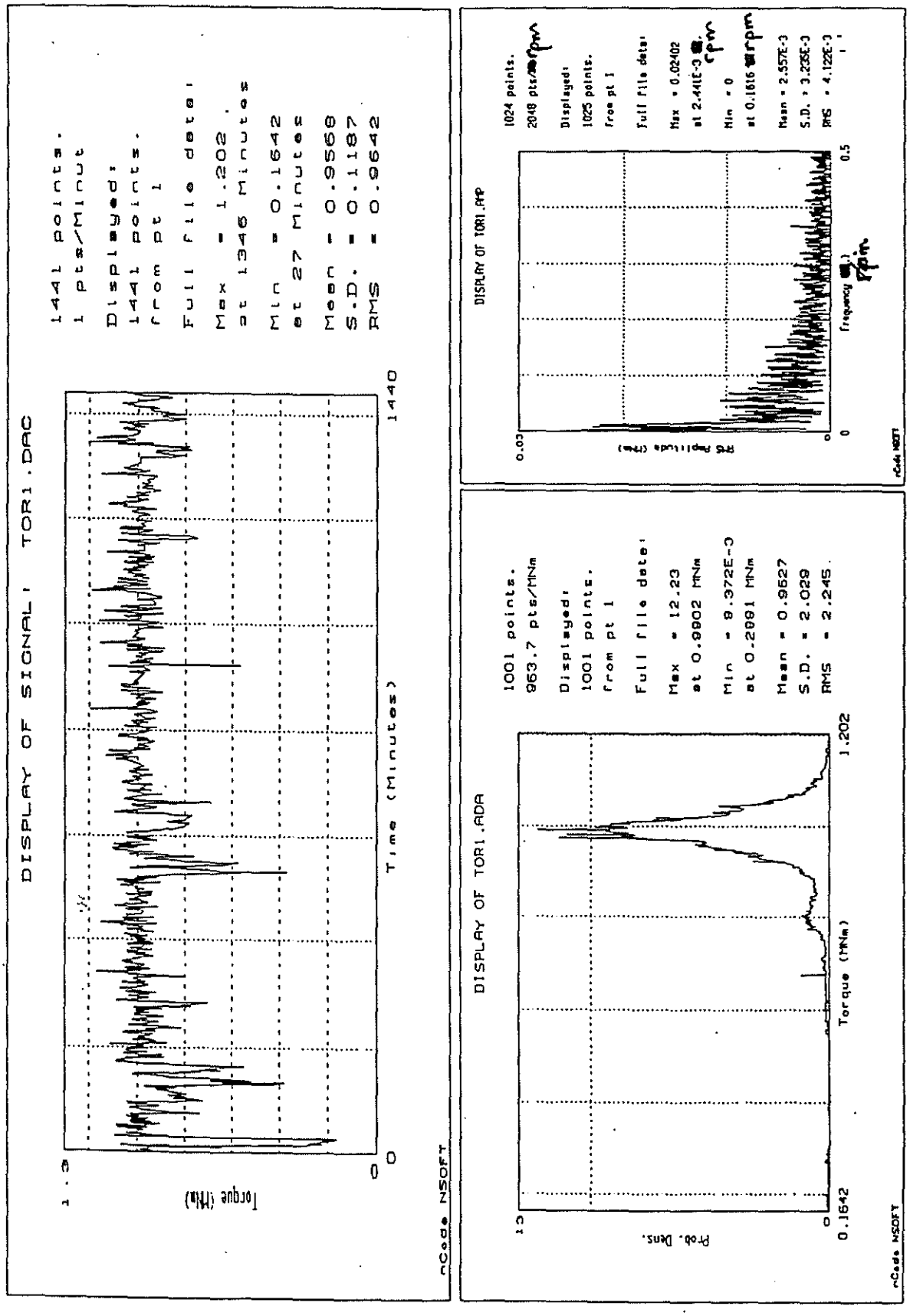

Figure 4.3 History, probability density and frequency spectrum plots for TOR1.

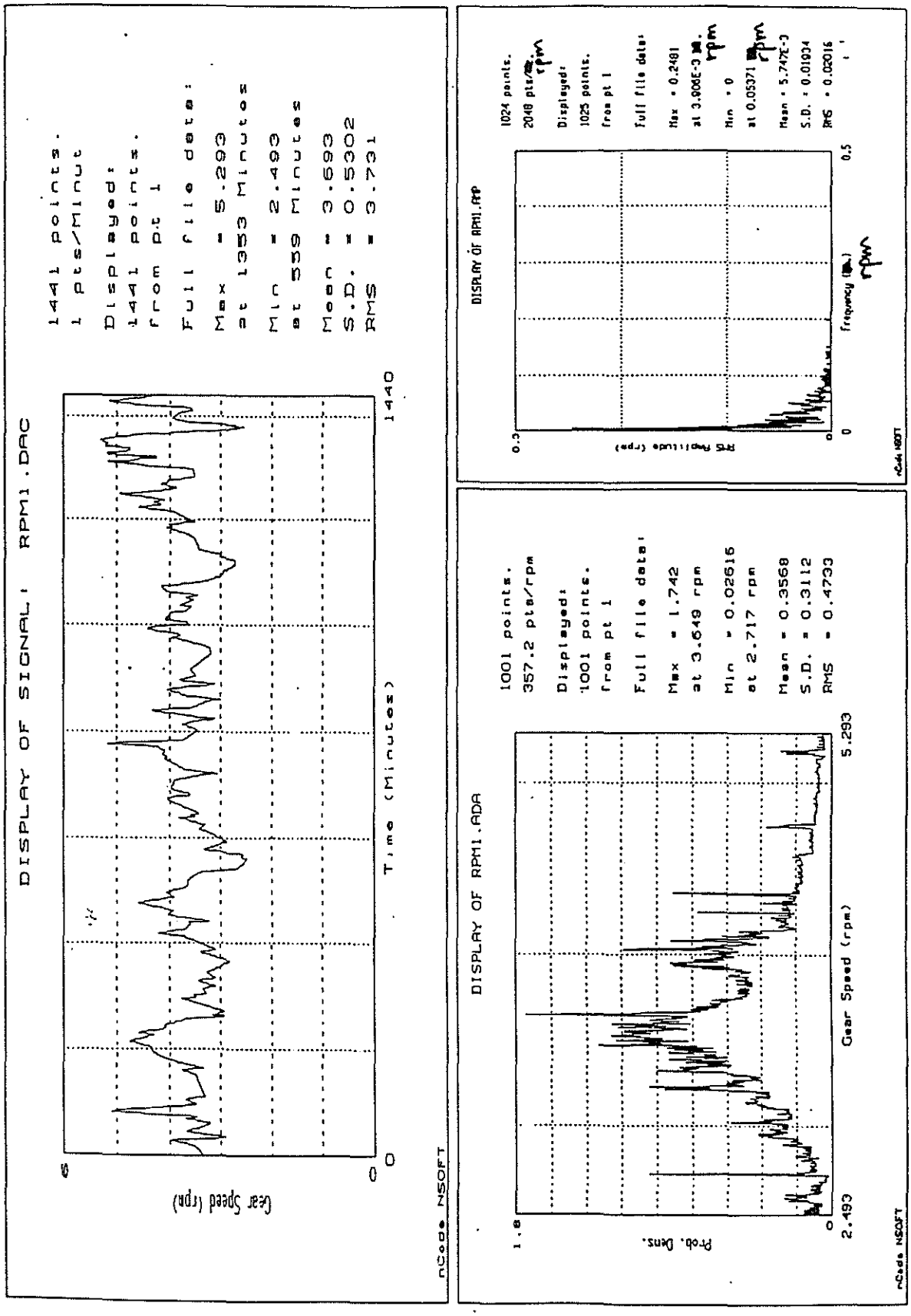

Figure 4.4 History, probability density and frequency spectrum plots for RPM1.

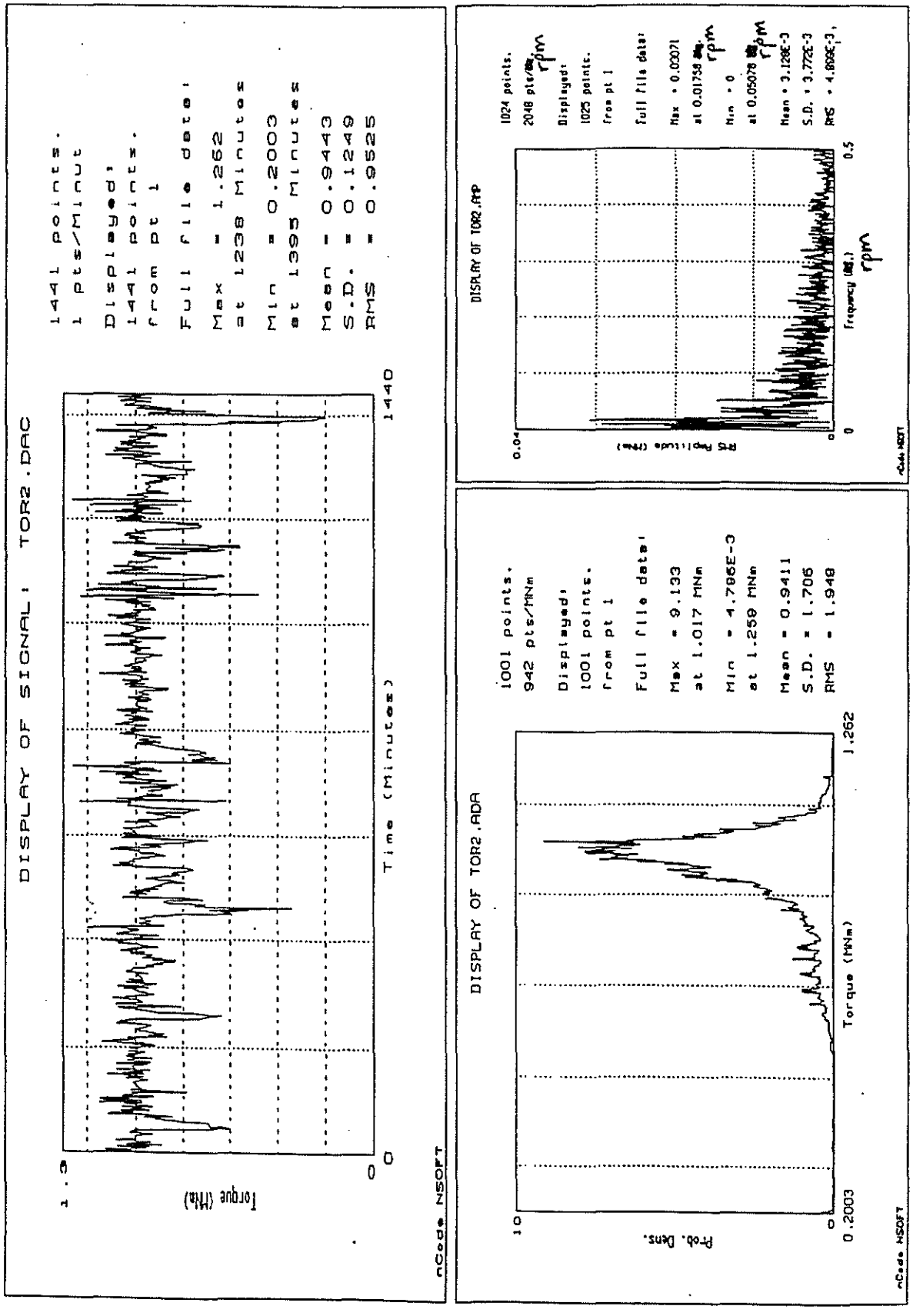

Figure 4.5 History, probability density and frequency spectrum plots for TOR2.

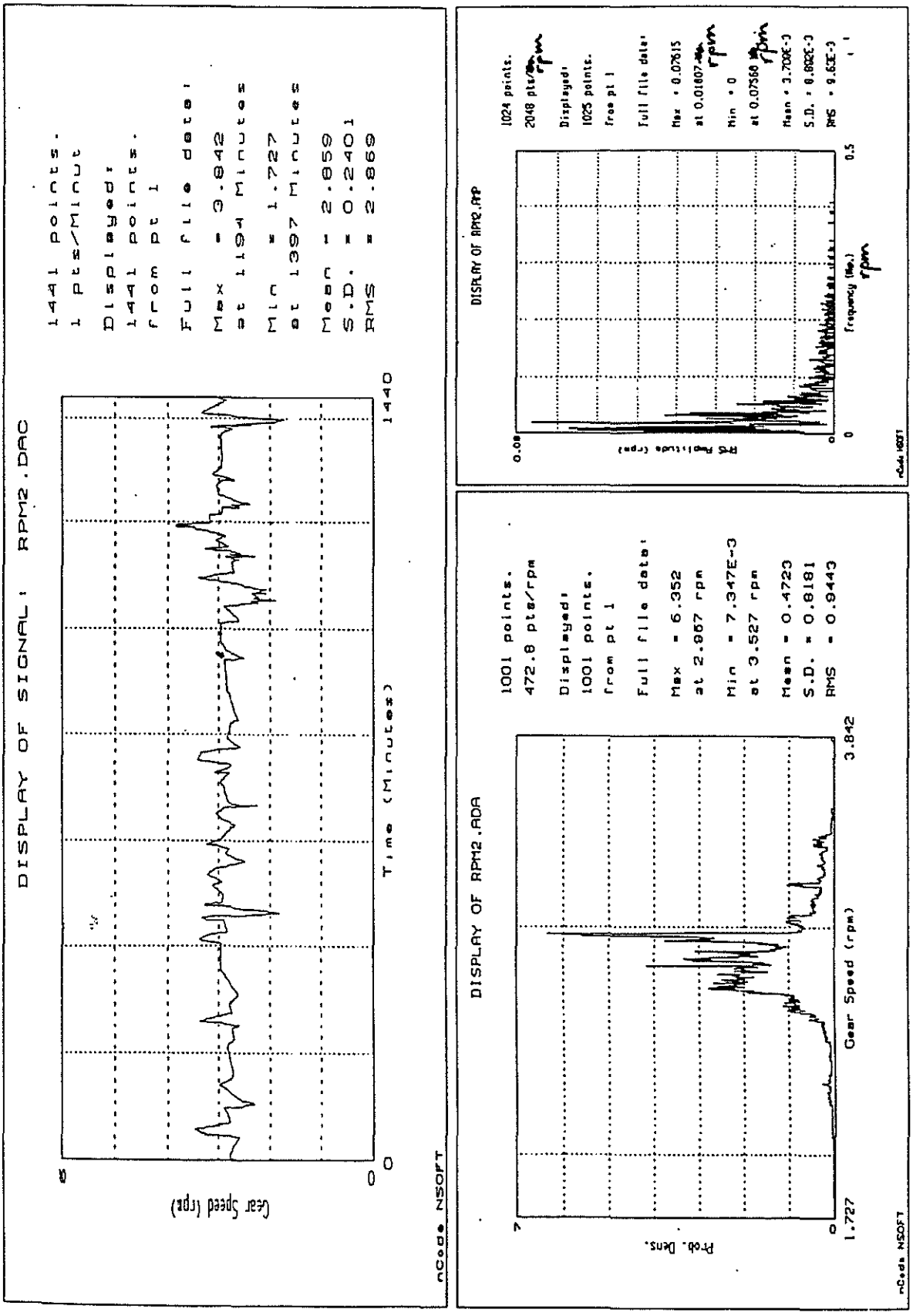

Figure 4.6 History, probability density and frequency spectrum plots for RPM2.

5.0 Initial 2D Finite Element Modelling of Spur and Pinion Gear Interaction

5.1 Geometry modelling

To assess the stress created by the transmission of torque between interacting gears, an accurate geometric model of the gear teeth must first be created. The tooth profiles for both the candidate pinion and wheel were produced using PATRAN from the specified dimensions. The final dimensions used in the geometry construction are as follows :

Overall	Pressure Angle	= 20 degrees
	Circular Pitch	= 5.0476 "
	Face Width	= 21 "
Spur	Number of Teeth	= 106
	Pitch Circle Diameter	= 170.310 "
	Addendum Circle Diameter	= 172.482 "
	Dedendum Circle Diameter	= 165.350 "
	Tooth Thickness	= 2.108 "
	Root Region Radius	≈ 15 mm (approximated from drawings)
Pinion	Number of Teeth	= 20
	Pitch Circle Diameter	= 32.134 "
	Addendum Circle Diameter	= 36.391 "
	Dedendum Circle Diameter	= 29.281 "
	Tooth Thickness	≈ 72.60 mm (approximated from drawings)
	Root Region Radius	= 0.688 "

On completion of the general teeth profiles, the geometry was divided into suitable patches in preparation for finite element meshing of the gear teeth. In addition, both the pinion and spur teeth were positioned so that they were contacting at their respective pitch circles. This allowed combined rotation of the teeth to view the contacting characteristics and to aid in the understanding of the meshing pattern. The line of contact, angle of recess and approach, the number of contacting teeth pairs at given positions were investigated. This knowledge proved important during the analysis of three pair of meshing teeth (Section 5.3). Figure 5.1 shows the basic geometry of one pair of mating teeth subdivided into patches. Note additional patches were attached to the spur tooth for analysis reasons only.

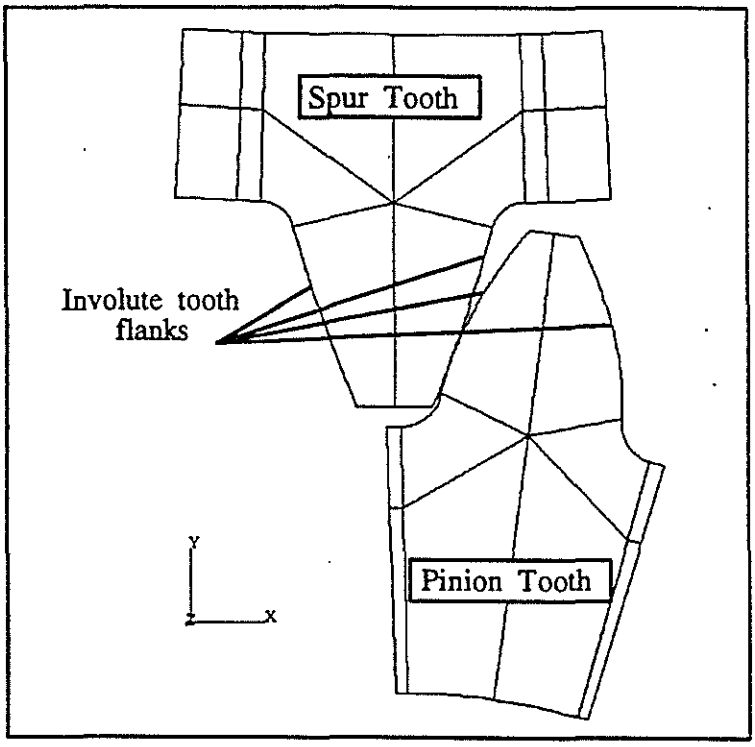

Figure 5.1 Basic geometry of one pair of mating gear teeth.

5.2 Analysis of single pair of meshing teeth

To make confident predictions regarding the effect and growth rate of a crack in the root region of a gear tooth, the stress intensity values experienced by the crack tip must be calculated. In order to calculate this value using fracture mechanics theory (Section 2.4), the reference stress or stress at the crack initiation point in the tooth for a particular load must be known. Of interest to this project are the cracks which have initiated from the root region of the spur teeth contacting flanks. As 'ABAQUS Standard' was the analysis code used for this project, only two dimensional contact problems were modelled. Hence only plane strain models were considered.

To understand and refine the modelling process for two contacting deformable bodies undergoing large displacements, a single pair of contacting teeth was initially analysed. Figure 5.2 shows the general element mesh arrangement used and highlights the regions of importance. This model consisted of 504 CPE8 (eight node biquadratic two dimensional plane strain) elements, 30 ISL21 (two node first order planar interface) contacting elements, 30 temporary beam elements (to aid in the contacting region slide line definition) and 2 MPCs (multi-point constraints) used in defining the boundary conditions. Figure 5.3 shows a close up of the mating teeth highlighting the location of the contact elements and the corresponding slide line.

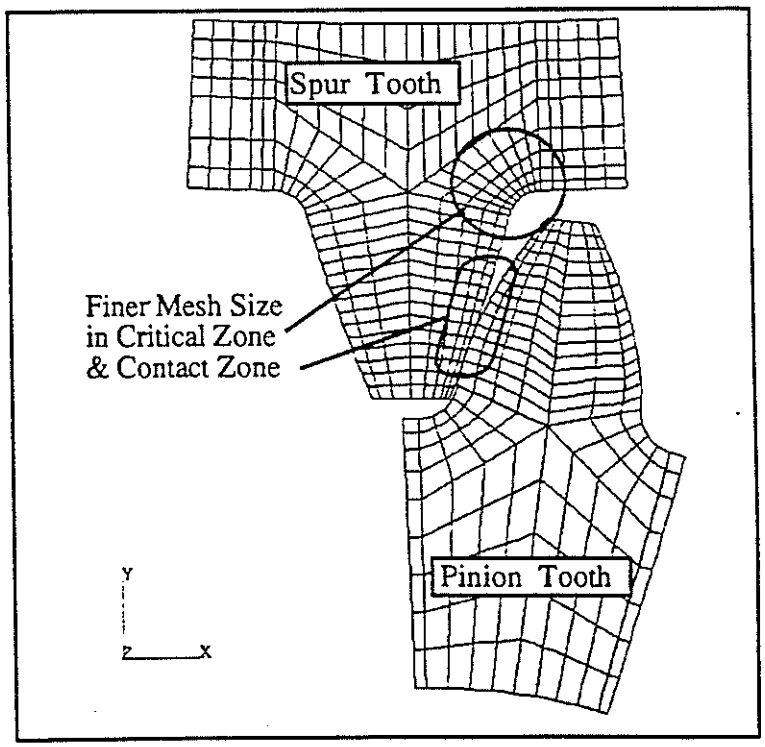

Figure 5.2 General mesh arrangement for single contacting pair model.

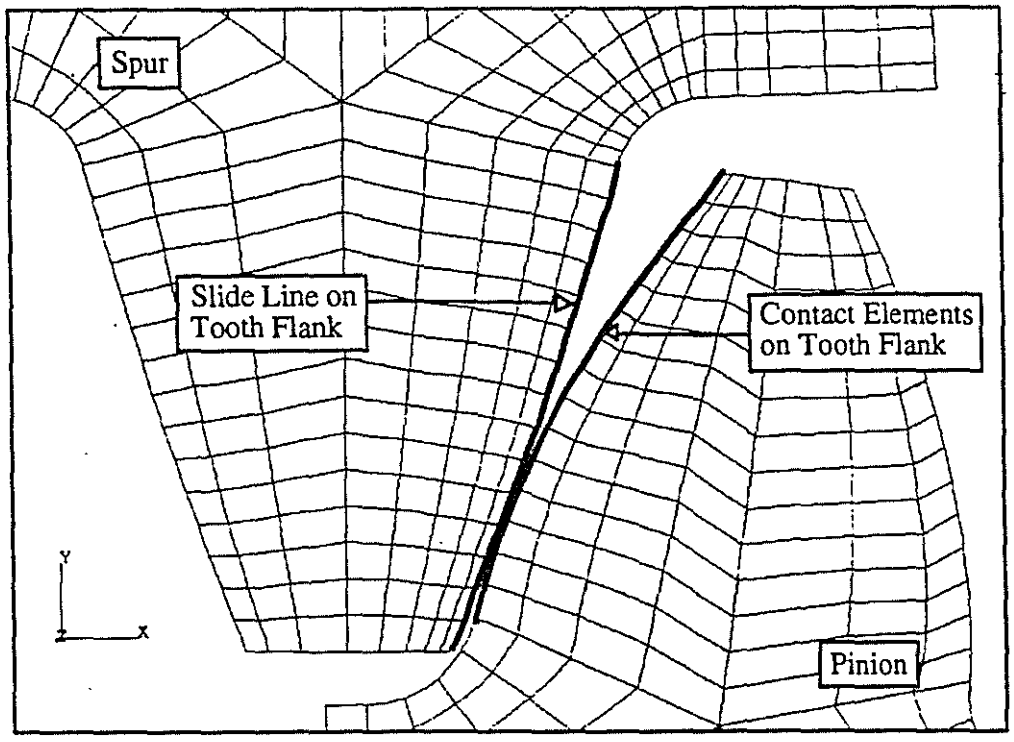

Figure 5.3 Position of contacting elements and slide line for single pair model.

Defining possible contact locations in a model requires the inclusion of an interface pair (contacting elements and a slide line) into the model definition. The slide line is basically a sequential list of nodes defining the surface of one deformable body (spur tooth). Contact elements are attached to the surface of the other deformable body (pinion tooth). During analysis, ABAQUS checks to see if the contacting elements pass through the slide line. If the contacting elements do penetrate the slide line, there is contact (load transferral) between the bodies and ABAQUS then iterates until an equilibrium is found where the contacting elements just touch the slide line. This procedure is continued as the gear teeth rotate and new contacting positions are encountered.

Before an analysis deck (model definition with restraint and load conditions) could be produced by PATRAN and solved by ABAQUS, the order in which torque loads and angular rotation were to be applied to the teeth was considered. After experimentation, a modelling procedure was agreed upon as shown diagrammatically in Figures 5.4 through 5.6.

The analysis involved two steps. Step 1 involved ramping the torque loading of the spur tooth up to a level (1 MNm) against the pinion tooth which was held stationary. This was found to be necessary to overcome contact problems due to dynamics. Step 2 involved the forced angular rotation (0.2 radians) of the pinion tooth against the spur tooth which was now loaded with a constant torque level (1 MNm) to simulate typical loading and speeds encountered by the candidate gear.

Figure 5.4 helps demonstrate the modelling procedure for the single pair of contacting teeth. Note the multi-point constraints (MPCs) which simply provide a means for rigidly connecting the pinion and spur teeth to the gear centres (nodes 1 and 2 respectively).

Figure 5.5 shows the application history of the torque loading to the spur tooth and the rotation of the pinion tooth.

The torque value of 1 MNm was chosen for this analysis as this was a typical value experienced by the candidate gear box (Section 4.3). The rotational speed of the pinion gear for this analysis was calculated to correspond to a rotational speed of 6 rpm for the spur gear. This value was used as it was the quoted maximum speed for the candidate spur gear. The coefficient of friction for the contacting surfaces was set at 0.1 as this is a typical value for lubricated steel on steel contact.

Figure 5.6 shows the initial and final position of teeth modelled.

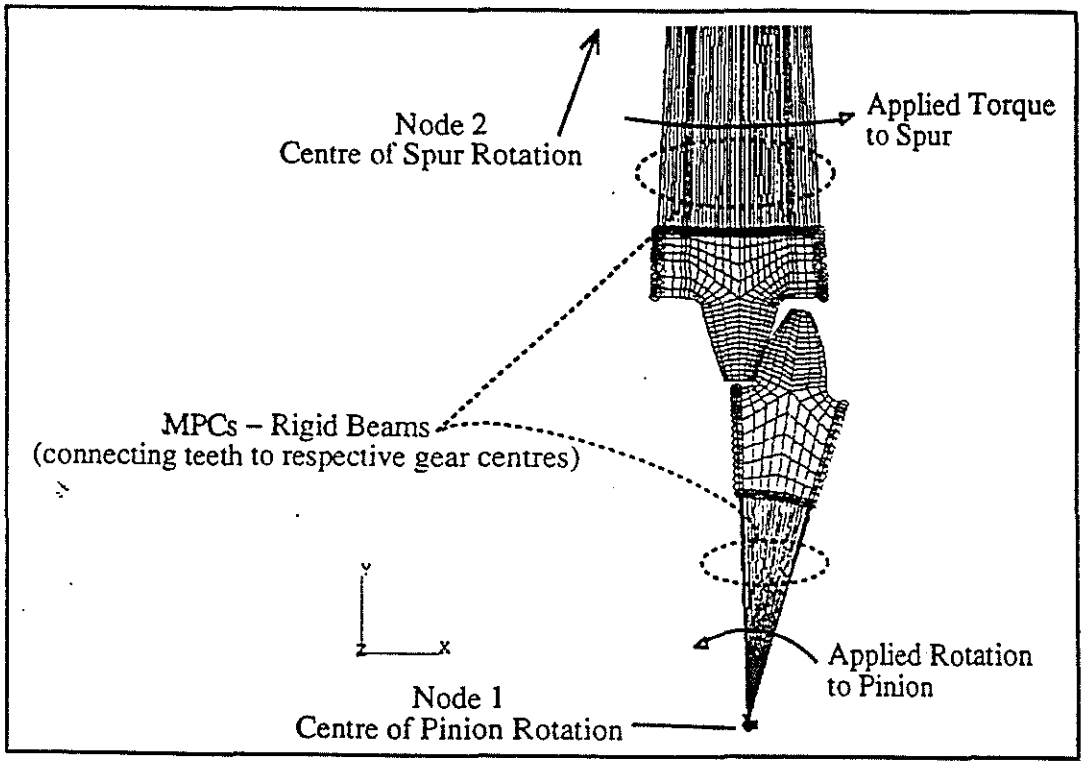

Figure 5.4 Single contacting tooth model showing general boundary conditions.

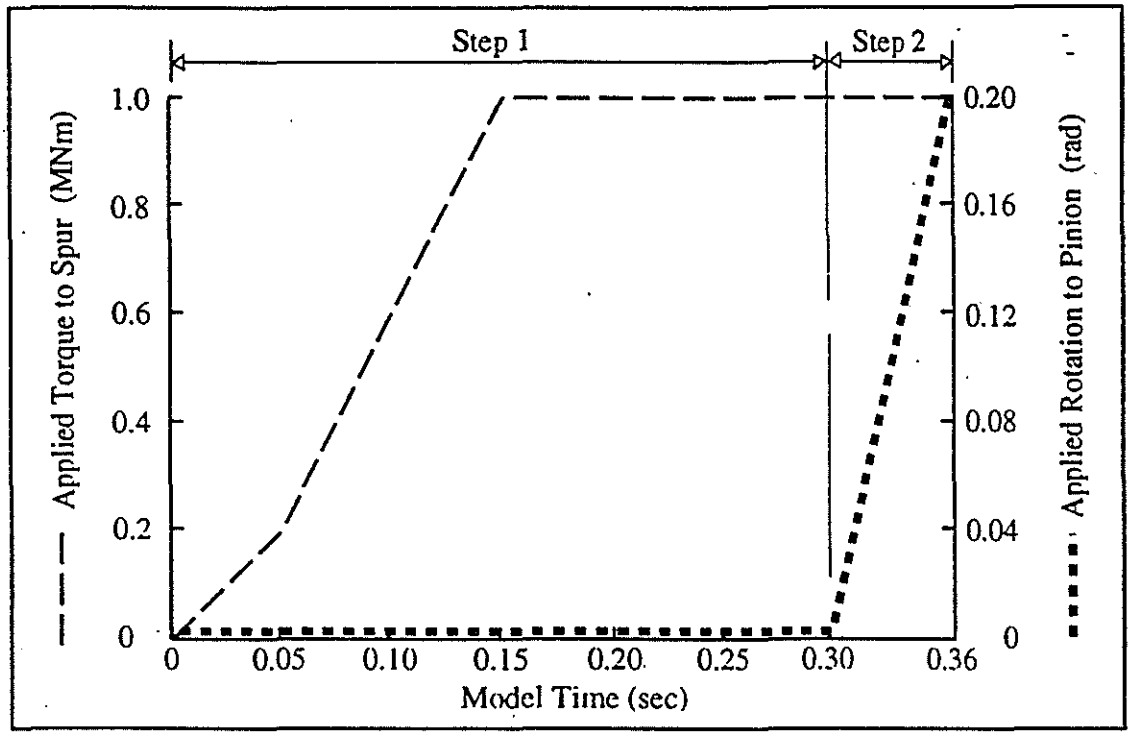

Figure 5.5 Diagram of spur torque loading and pinion rotation.

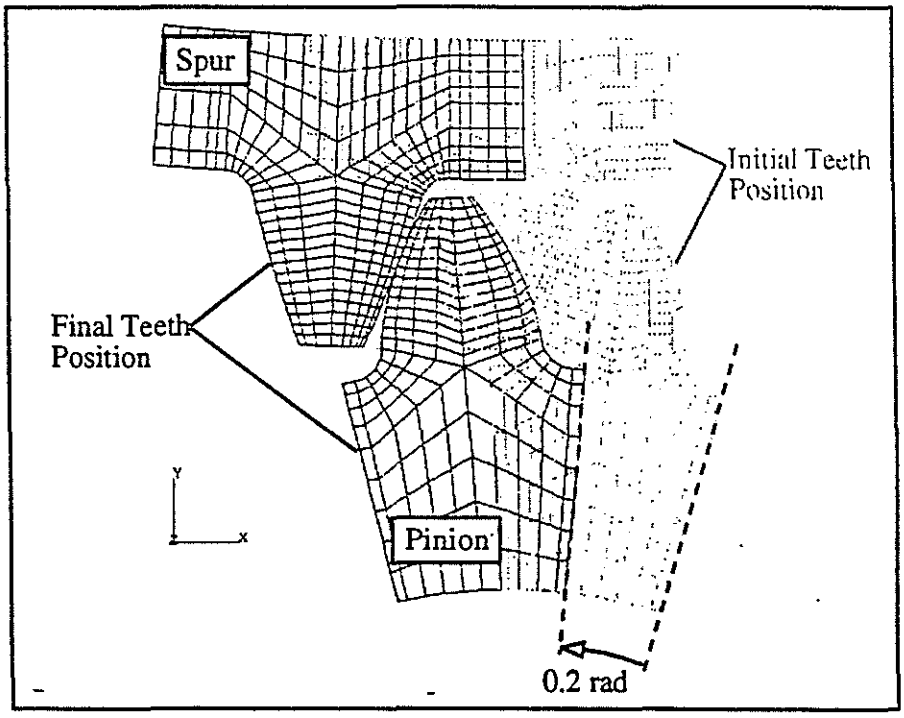

Figure 5.6 The position of teeth at the start and end of analysis.

ABAQUS Post allows the user to graph the history of a specified variable (eg. stress, strain) for any number of elements / nodes in a model. As this project is focused on the root region of the spur gear, several elements in this area were targeted for inspection. Figure 5.7 shows a close-up of the arrangement of elements in the root region. Highlighted are three elements from the root region whose average elemental maximum principal stress were plotted against the time duration of the analysis (Figure 5.8). As the maximum principal stress in the root region (Figure 5.9) drops sharply over the elemental area, the average stresses plotted in Figure 5.8 have lower values than the maximum principal stresses experienced by the root region's surface.

Figure 5.9 shows the stress state of the first increment of Step 2 which corresponds to the two mating gears contacting at their respective pitch circles under full torque load. The maximum principal stress experienced by the spur gear during the analysis was 64 MPa which occurred in the root region. However this value should be treated with reserve as the values were continuously fluctuating during the analysis.

This analysis is not representative of one complete tooth loading as the teeth began load transferral at their pitch circles. The modelling of multi-toothed sections of both the spur and pinion gear (Section 5.3) was required to calculate the stresses experienced by a spur tooth prior to, during and after contact under full torque load.

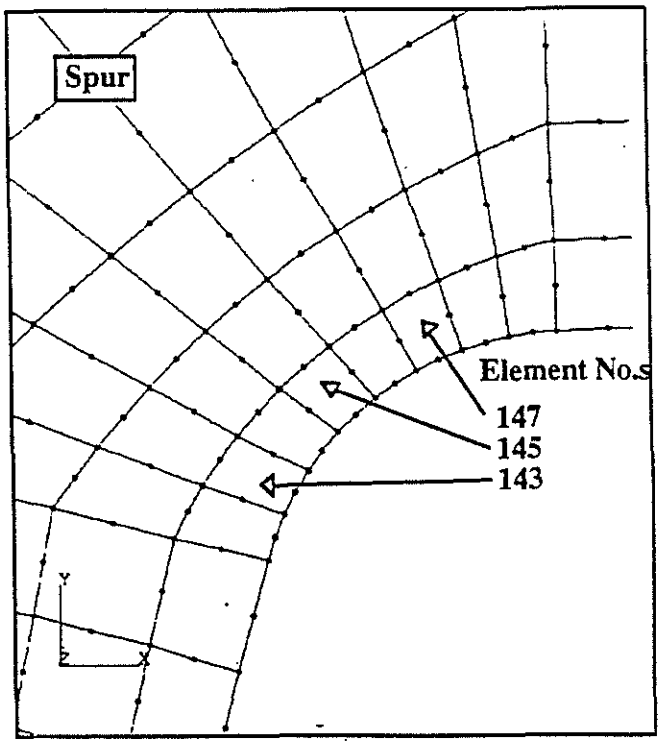

Figure 5.7 Close-up of root region elements under inspection.

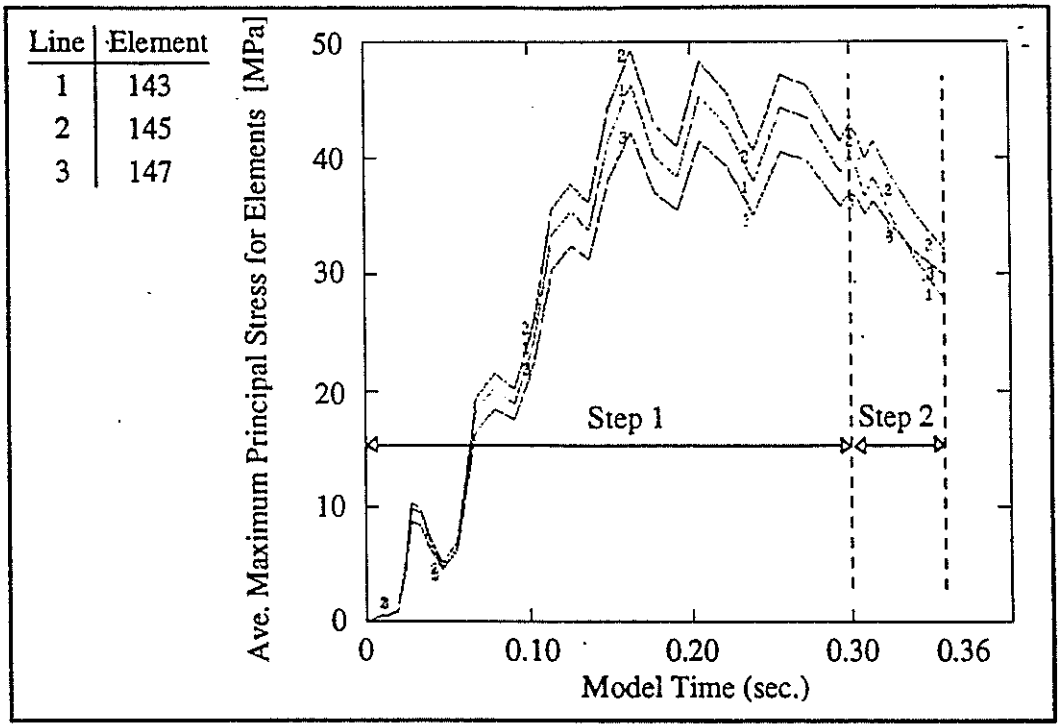

Figure 5.8 Ave. max. principal stress versus time for single contacting tooth analysis.

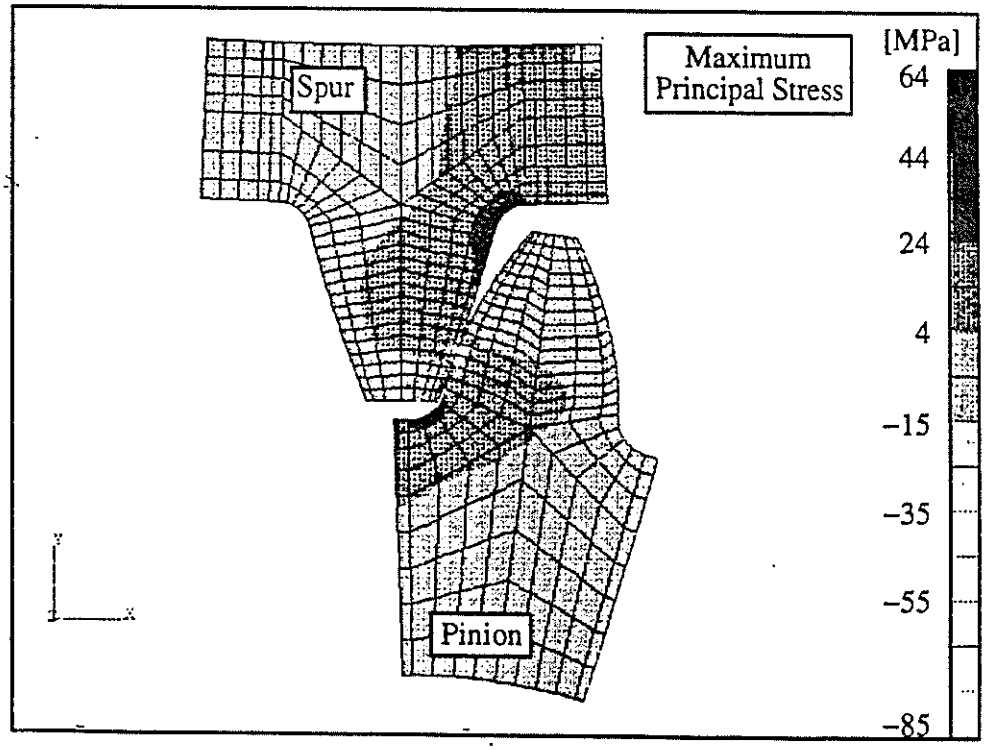

Figure 5.9 Max. principal stress plot for single contacting tooth analysis (time=0.305s).

5.3 Analysis of multiple meshing teeth

The analysis described in Section 5.2 aided with the understanding of the modelling process required for contacting gears. However, the analysis was far from comprehensive as the effect of varying the element mesh size and friction coefficient was not investigated for a complete tooth loading cycle. Hence, two multi-toothed models were analysed, initially to select a suitable mesh size for the final analysis and then to quantify the effect of the friction coefficient (lubrication characteristic).

The modelling procedure for the two, triple contacting pair models of differing element size was similar to that described in Section 5.2. Figure 5.10 shows the basic geometry used for the two triple teeth models with initial contact of the 1st pair of mating teeth contacting at their respective pitch circles. Figure 5.11 demonstrates the general model layout with MPCs, gear centre nodes and applied loading and rotation diagrams. Note the gear sections are not shown with mesh included as the mesh varies with the two models (shown later). Figure 5.12 shows the application history of the torque loading to the spur teeth and the rotation of the pinion teeth. This is notably similar to Figure 5.13 (single pair model) except that the rotation of the pinion is extended so that now three pair of teeth experience contact during rotation. Figure 5.13 shows the initial and final position of the teeth modelled. Appendix A3 contains a summarised input deck and status file for the finer mesh model's analysis.

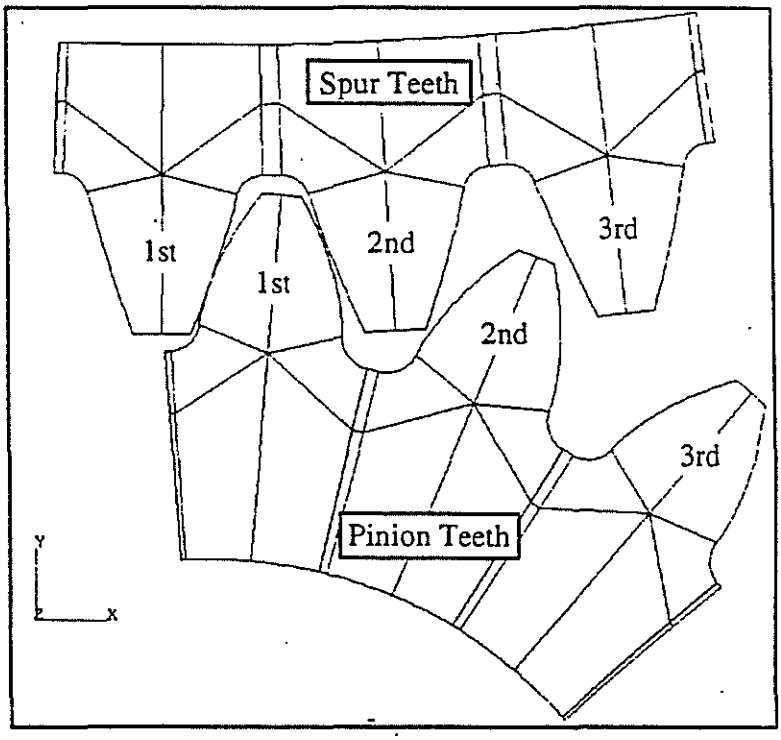

Figure 5.10 Basic geometry of three pair of mating gear teeth.

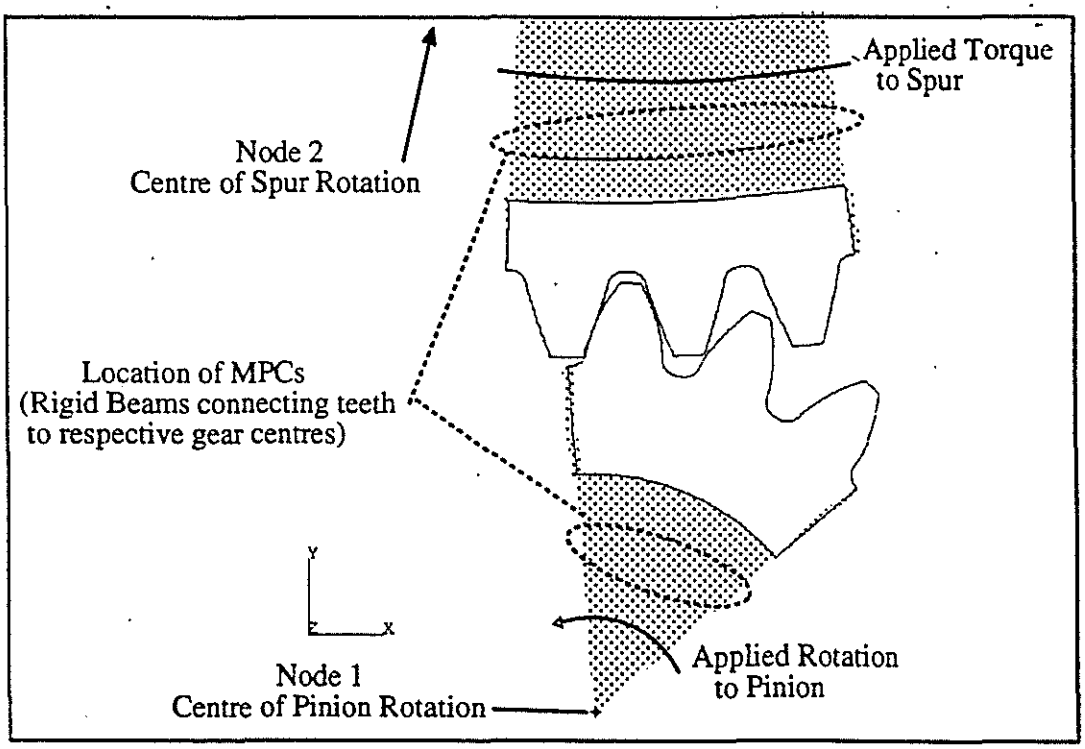

Figure 5.11 Triple contacting teeth model showing general boundary conditions.

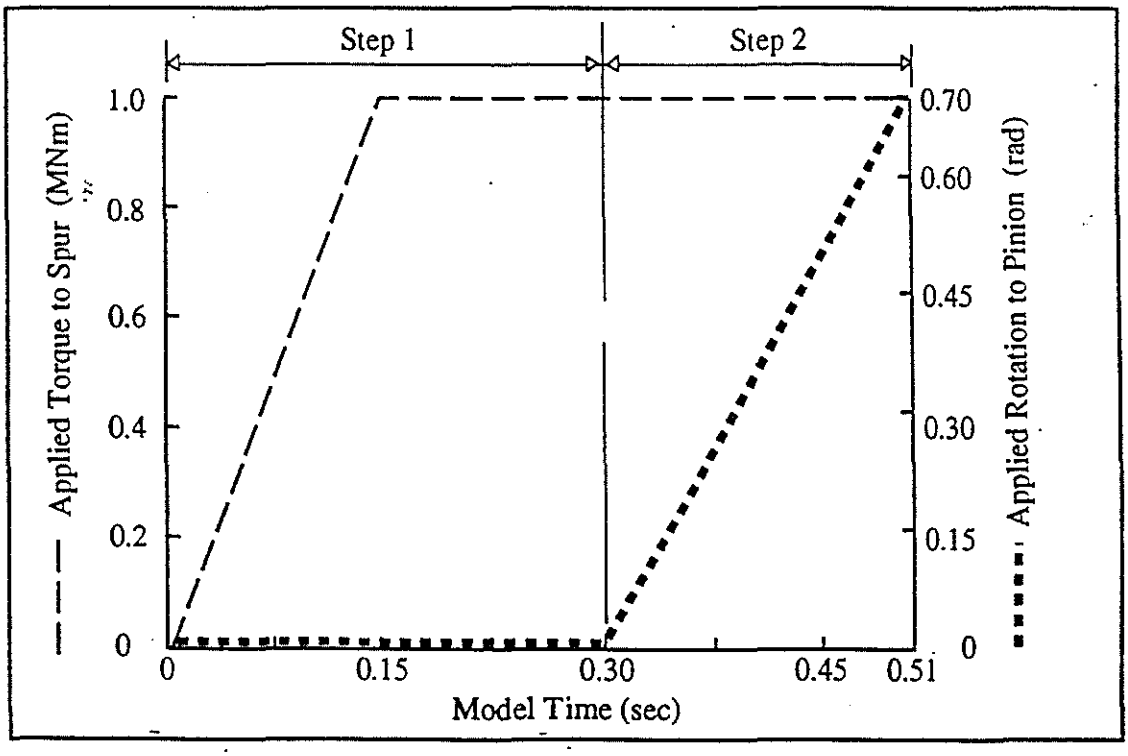

Figure 5.12 Diagram of spur torque loading and pinion rotation.

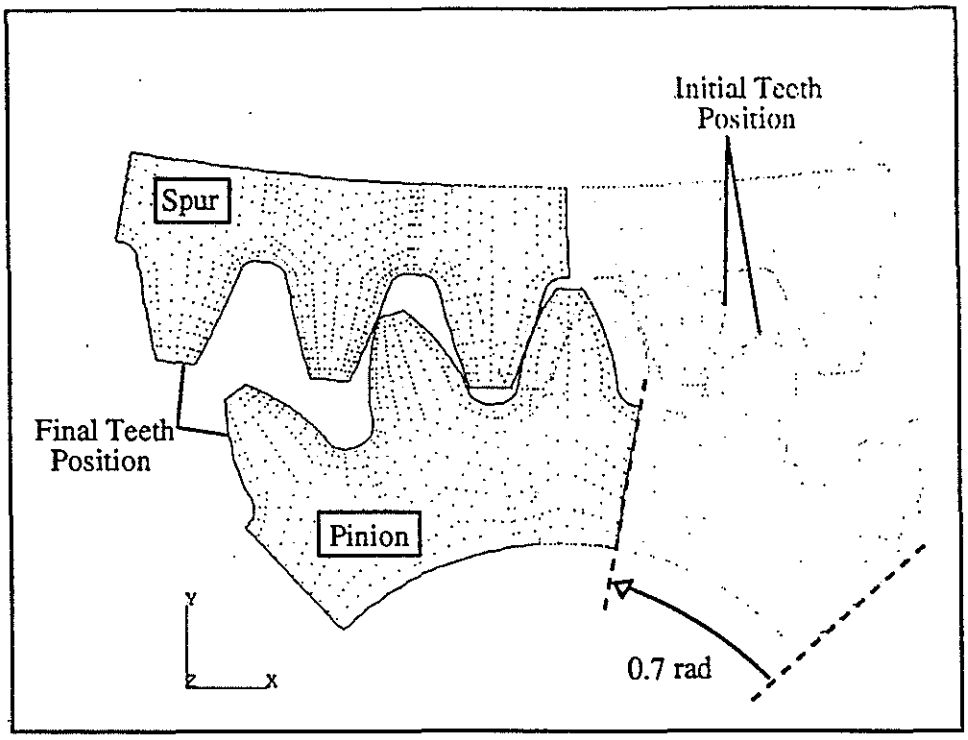

Figure 5.13 The position of teeth at the start and end of analysis.

5.3.1 Effect of mesh refinement on tooth stresses

Two models, each containing three pair of contacting teeth were analysed to quantify the effect of varying element size on tooth stress. The result of this investigation was to finalise an element size which gave reliable stress results without being over meshed. The first model analysed (coarse mesh model) was meshed using relatively large element sizes in the critical regions (root region and contact flanks) compared to the second model analysed (fine mesh model). The coefficient of friction was set at 0.1 (typical for lubricated steel on steel) for the following analyses.

The coarse mesh model (Figure 5.14) consisted of 536 CPE8 elements, 41 ISL21 contacting elements, 30 temporary beam elements for the slide lines and 2 MPCs used in defining the boundary conditions. The fine mesh model (Figure 5.15) consisted of 1112 CPE8 elements, 120 ISL21 contacting elements, 90 temporary beam elements for the slide lines and 2 MPCs used in defining the boundary conditions. Apart from different element sizes, the two models had slightly different contacting element and slide line positioning (Figures 5.16 through 5.17). The fine mesh model included modified contact definitions to account for tip relief which was not modelled in the coarse-mesh model. As the results show later, this tip relief modification removed the unexpected stress fluctuations experienced during tooth loadings with the coarse mesh model solution.

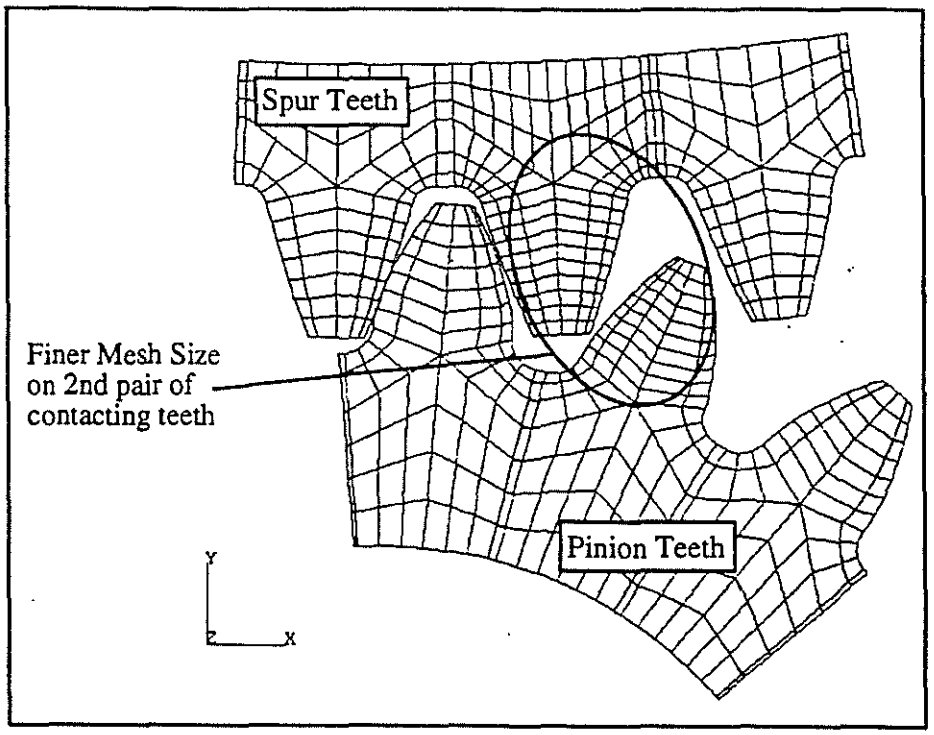

Figure 5.14 General mesh arrangement for triple teeth coarse mesh model.

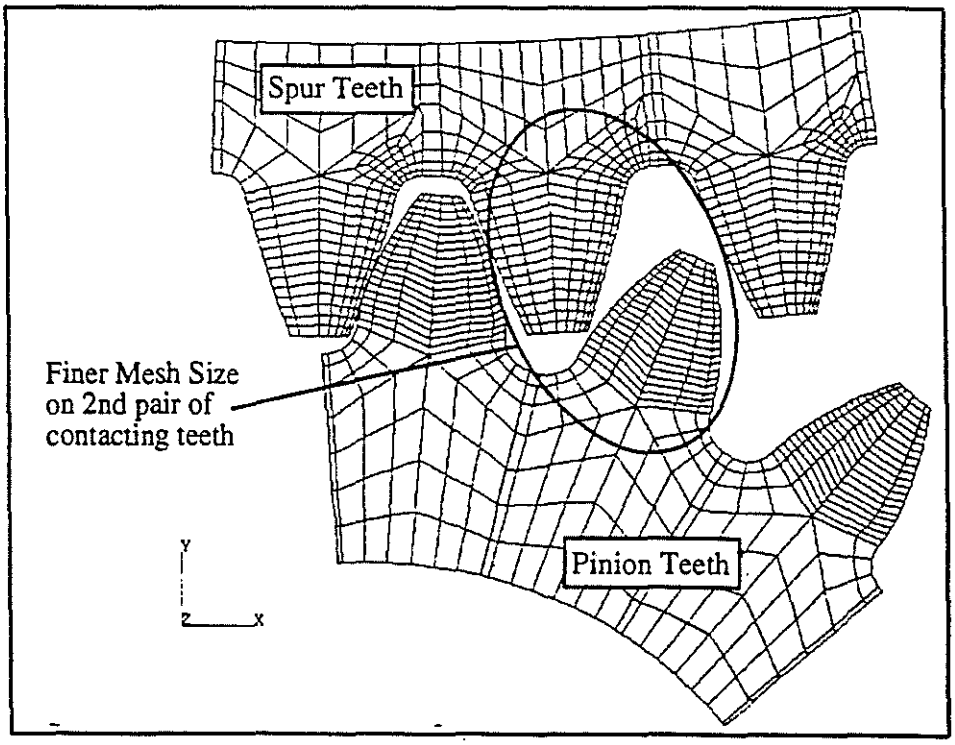

Figure 5.15 General mesh arrangement for triple teeth fine mesh model.

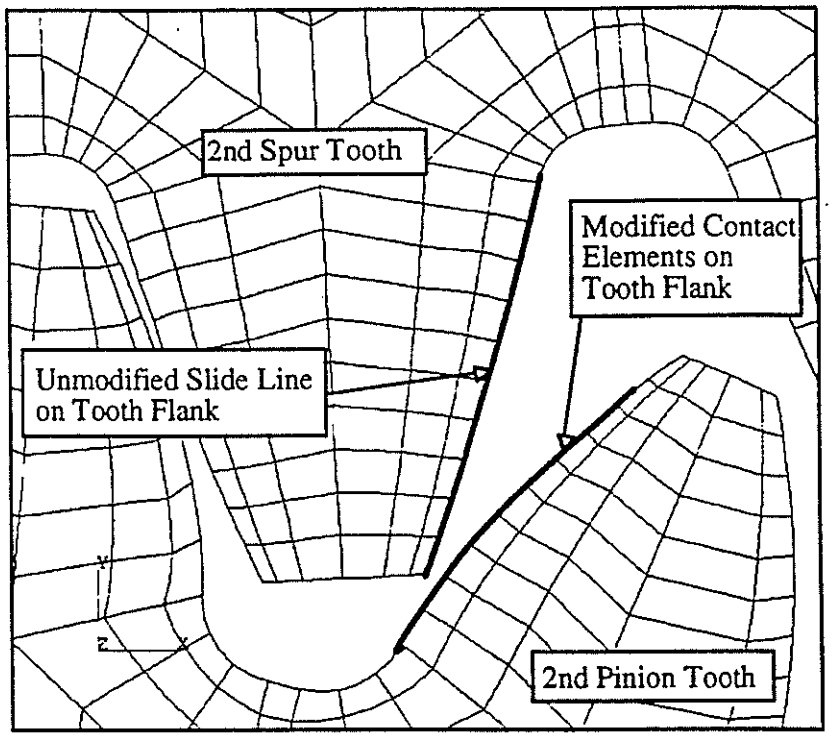

Figure 5.16 Position of contacting elements and slide lines for coarse mesh model.

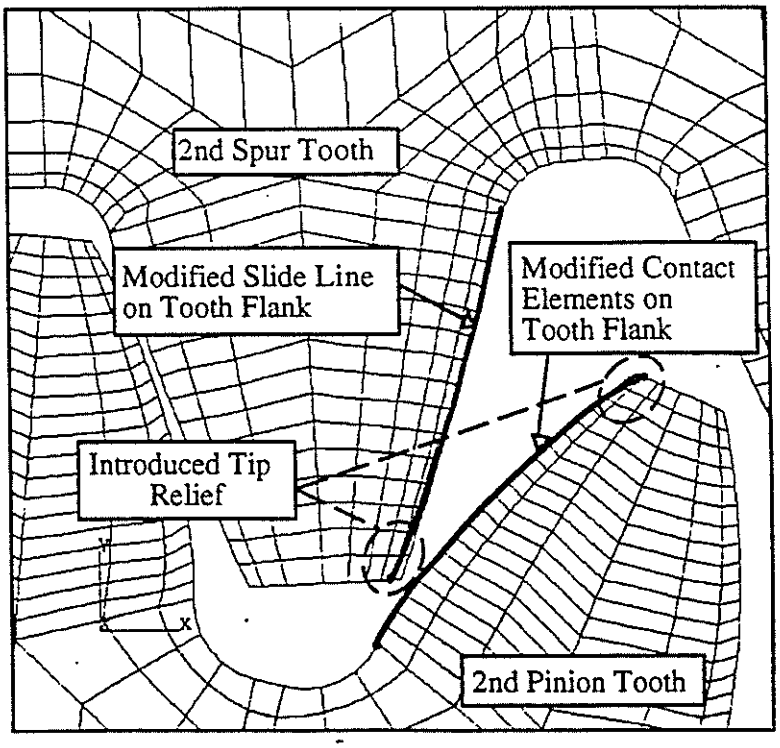

Figure 5.17 Position of contacting elements and slide lines for fine mesh model.

The analyses provided a general insight into the operation of the gears and the effect of mesh sizes on element stress. Throughout the post-processing, the root region of the second spur tooth was focused on as the stresses in this region are the least effected by boundary conditions and end effects. Figure 5.18 shows the stress state for the coarse mesh model when both the first and second pair of mating teeth are contacting simultaneously. Figure 5.19 shows the stress state for the coarse mesh model when the maximum principal stress is at its largest (65 MPa). In comparison, Figure 5.20 shows the stress state for the fine mesh model when the maximum principal stress is at its largest (62 MPa).

As in Section 5.2, certain elements in the root regions of the coarse and fine mesh models were targeted for inspection. Figure 5.21 highlights the six elements, spanning all three of the spur teeth root regions (coarse mesh model), whose average elemental stresses were plotted against the time duration of the analysis for Step 2 (full torque loading undergoing gear rotation / Figure 5.22). Similarly, Figure 5.23 highlights the six elements, spanning all three of the spur teeth root regions (fine mesh model), whose average elemental stresses were plotted against the time duration of the analysis for Step 2 (full torque loading undergoing gear rotation / Figure 5.24).

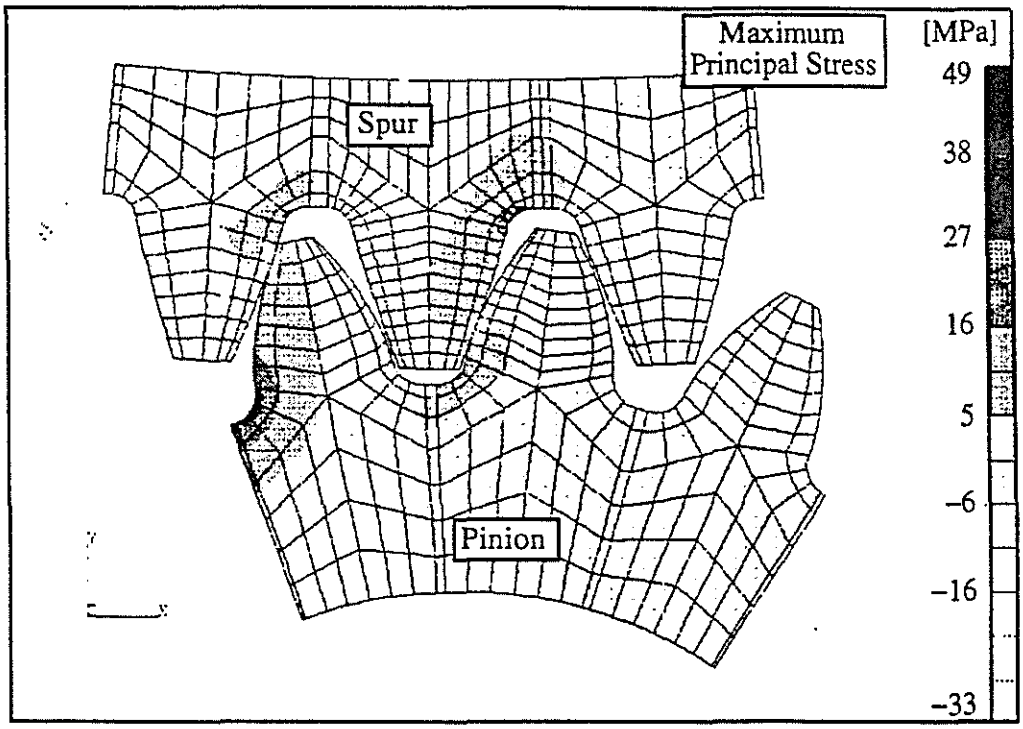

Figure 5.18 Max. principal stress plot for coarse mesh model showing shared contact between first and second pair of mating teeth (time=0.385s).

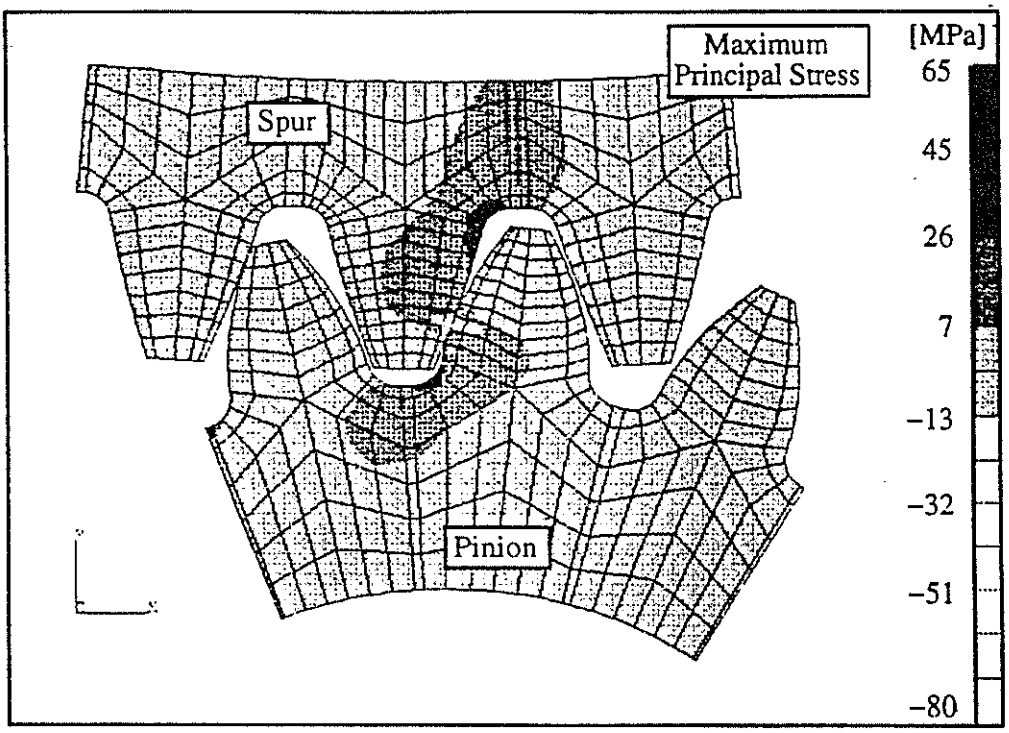

Figure 5.19 Max. principal stress plot for coarse mesh model (time=0.391s).

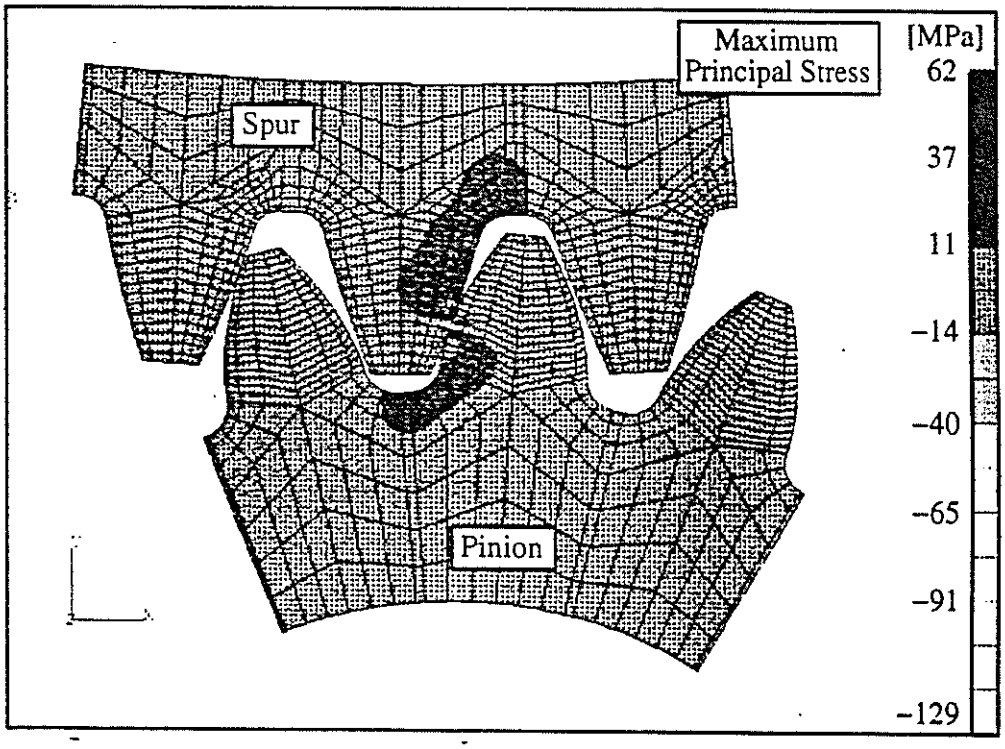

Figure 5.20 Max. principal stress plot for fine mesh model (time=0.395s).

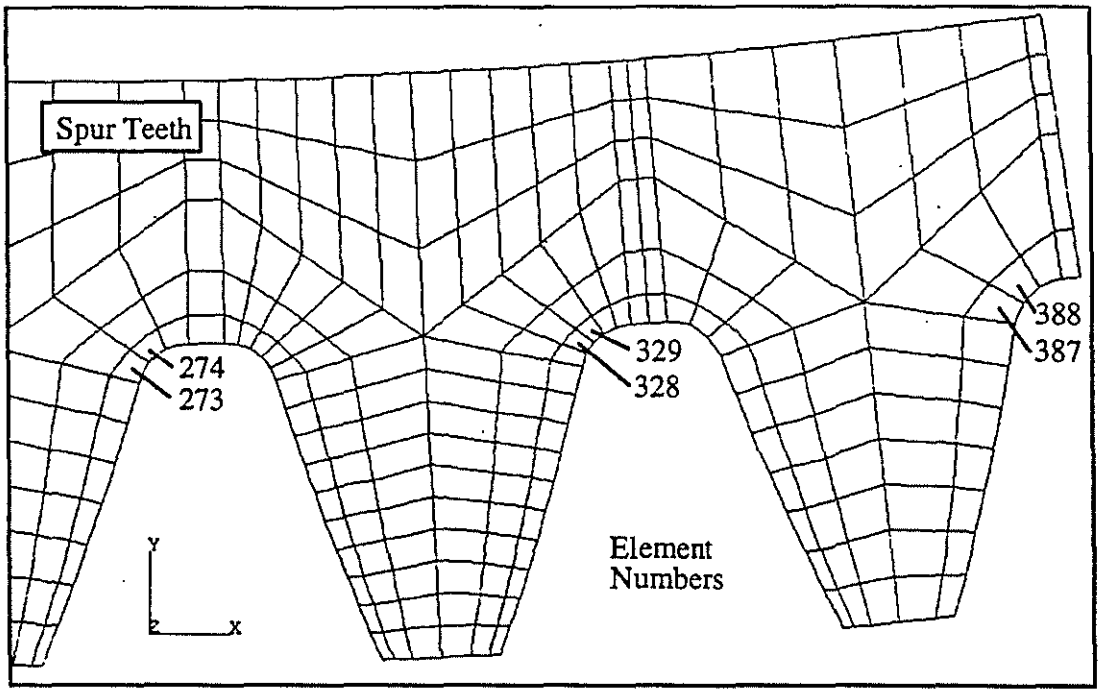

Figure 5.21 Close-up of root region elements under inspection (coarse mesh).

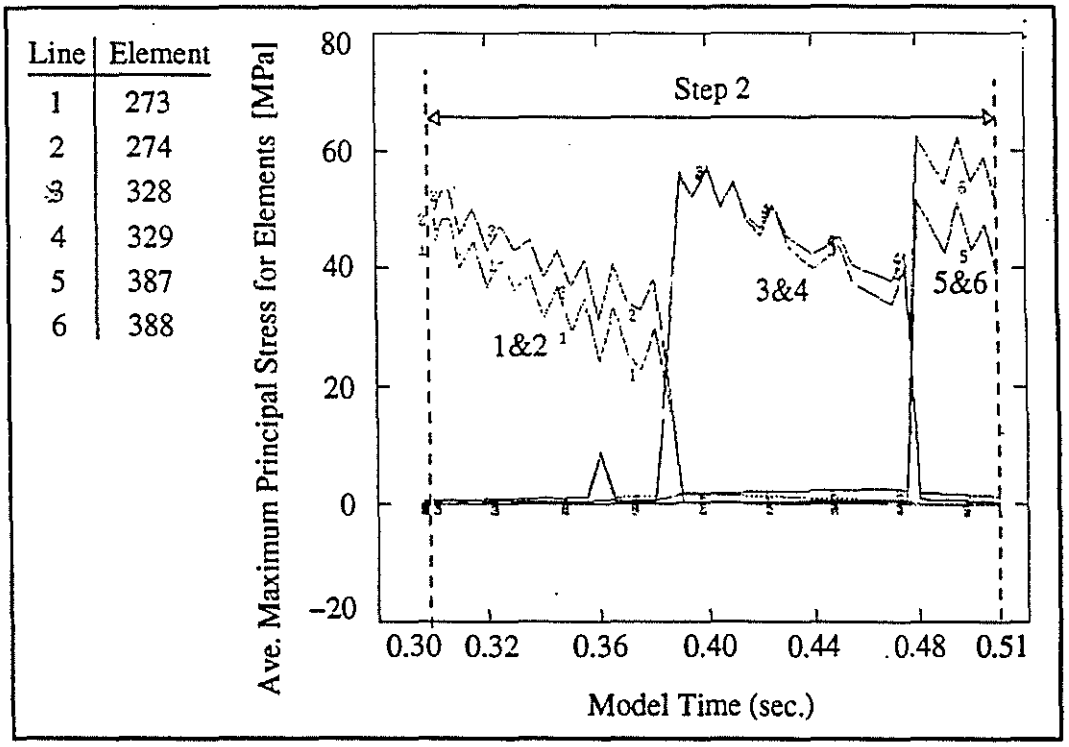

Figure 5.22 Ave. max. principal stress versus time for triple teeth model (coarse mesh).

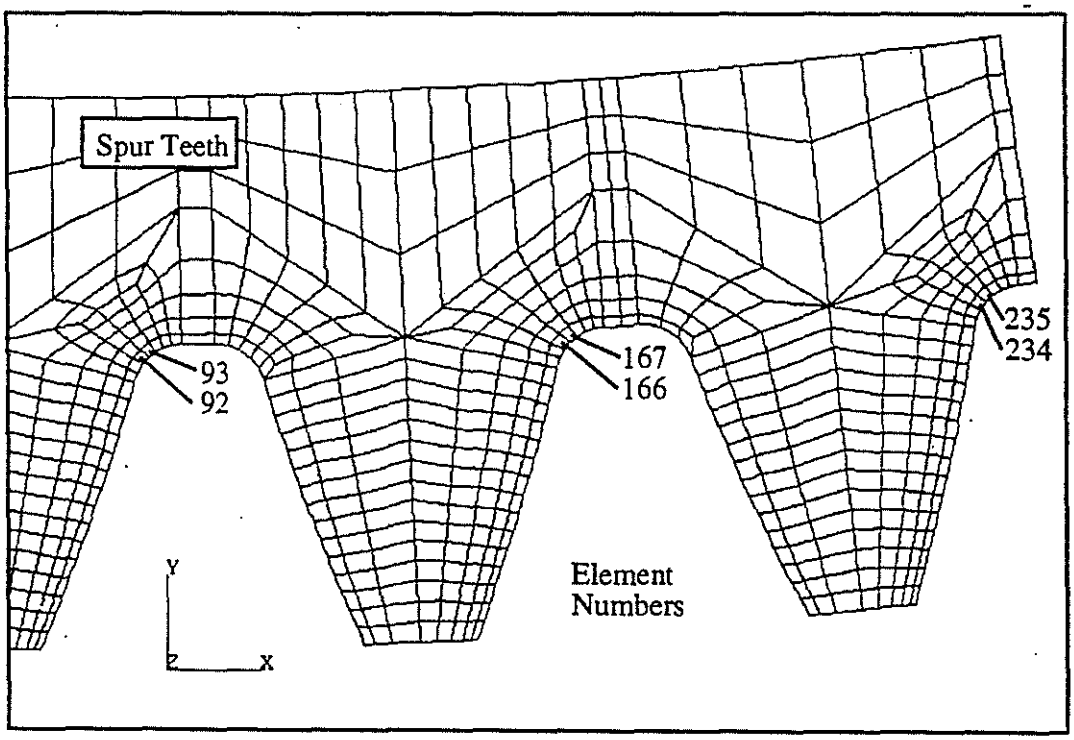

Figure 5.23 Close-up of root region elements under inspection (fine mesh).

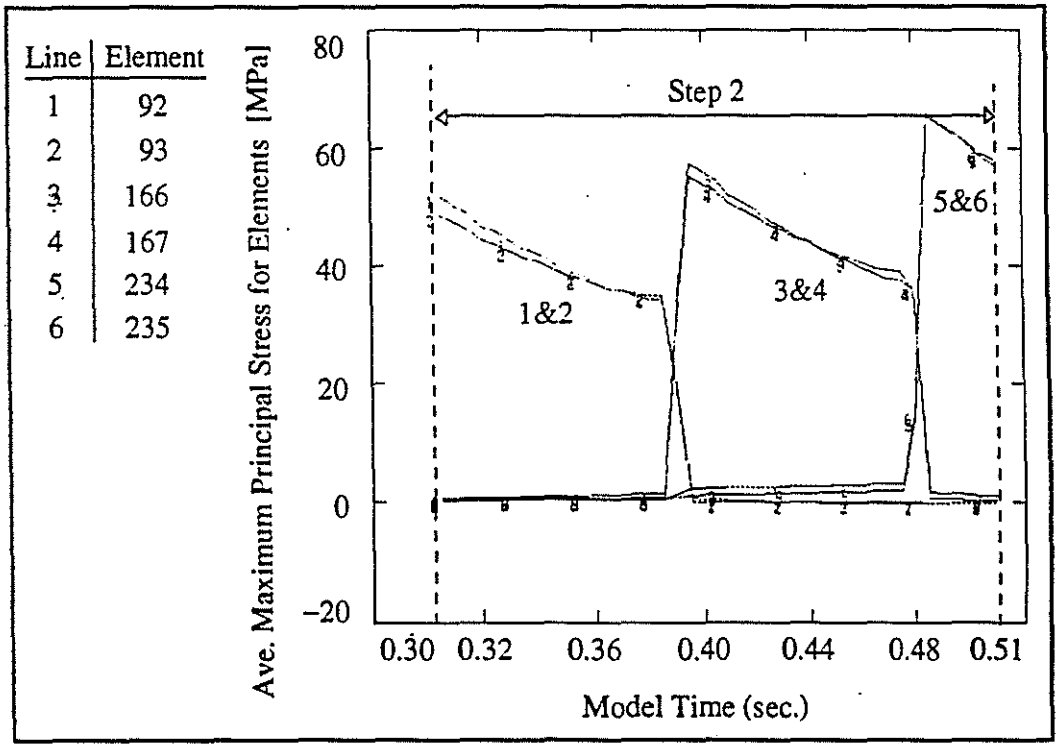

Figure 5.24 Ave. max. principal stress versus time for triple teeth model (fine mesh).

Direct comparison between the stress histories for the root region elements for the coarse and fine models (Figures 5.22 and 5.24 respectively) would not accurately quantify the effect of mesh size on stresses. This is because the history plots are of the average elemental stresses for different mesh sizes and not the maximum stresses. However, on comparing the maximum stresses for the coarse and fine meshes (65 MPa and 62.5 MPa respectively) it could be agreed that further mesh refinement would be unnecessary. In addition, the 65 MPa value for the coarse mesh, may have been recorded from the top of a stress fluctuation as seen in Figure 5.22. These fluctuations in stress readings are mainly due to the faceted effect of the contact elements on the pinion gear teeth. The effect of faceted contact characteristics is minimised by reducing the element size, thus smoothing the contact faces which results in smoother and more realistic stress histories. This can be seen when comparing stress history plots for the coarse and fine mesh models (Figures 5.22 and 5.24). Unrealistic boundary effects are evident in Figures 5.22 and 5.24 as the stresses in the root regions of the final pair of mating teeth are marginally higher ($\approx$ 8 MPa) than for the middle pair of mating teeth.

In conclusion, the stresses in the root region of a spur tooth induced via transferring torque of 1 MNm would oscillate from 0 to 62.5 to 0 MPa each spur gear revolution. This knowledge is used extensively throughout Chapters 6 and 7 regarding stress intensity calculations and crack growth rate predictions.

5.3.2 Effect of friction coefficient on tooth stresses

As the lubrication effects are not known with any confidence, the coefficient of friction was altered in the fine mesh solution from 0.1 to 0.4 to quantify the effect. The results of the analysis are shown in Figure 5.25 where the average maximum principal stresses were plotted for the elements shown in Figure 5.23. When comparing the results from the analyses of varying friction coefficients (0.1 and 0.4), it can be seen that there is minimal difference between the two results (Figures 5.24 and 5.25). This was expected as the contacting mechanism for mating teeth on the candidate gears consists mainly of a rolling action with only limited sliding between the teeth during load transferral. In addition, the sliding motion of the mating teeth occurs away from position of contact where the largest stresses are induced in the root region.

Modelling the effects of mesh refinement and friction coefficients proved beneficial as confidence in the accuracy of the stress results for the contacting teeth models was accomplished.

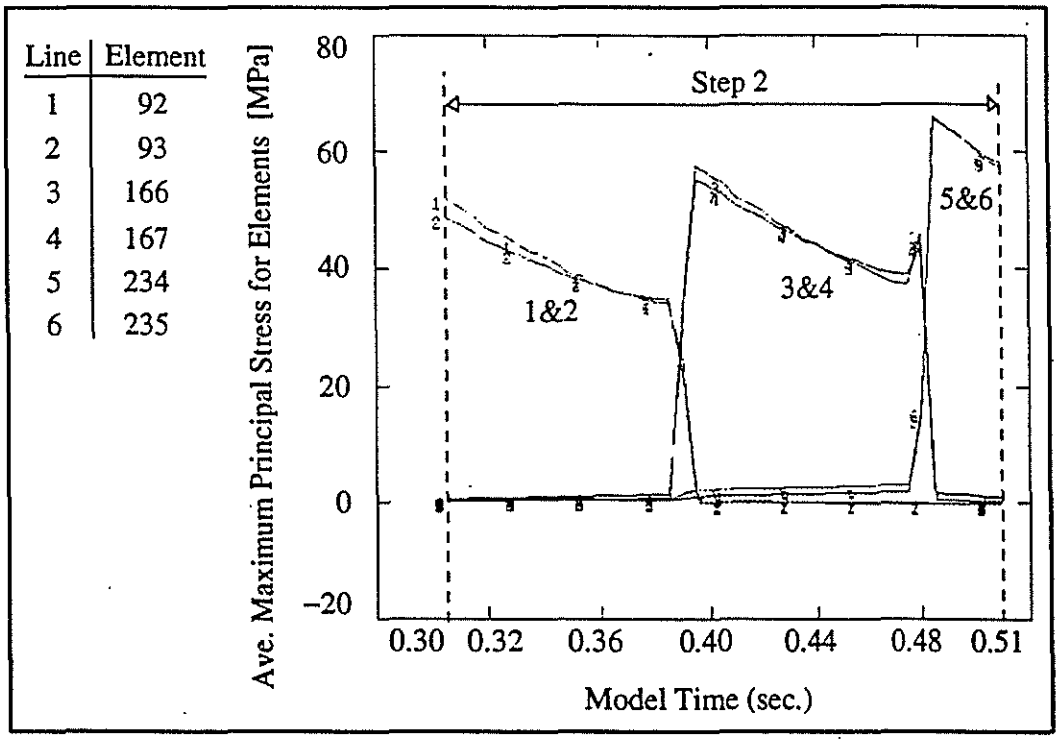

Figure 5.25 Ave. max. principal stress versus time for triple teeth model (fine mesh) (Friction coefficient was 0.4 for the contact definitions).

6.0 Stress Intensity Analysis (Plane Strain Approach)

6.1 Procedure for producing a geometry function

A necessary requirement for determining the growth rate of cracks in gears is finding a functional relationship between the stress intensity factor and the crack depth (equation 2.3), otherwise known as the geometry function as discussed in Section 2.4. This chapter is dedicated to obtaining a suitable geometry function for a propagating crack in the root region of the candidate spur gear. The geometry function required for input into the crack propagation prediction code, PFATIGUE, has to have a particular form (equation 2.4). L, in the equations below, is a generalised size parameter which will be discussed later.

$$K_I = \beta\left\{a/L\right\}\sigma\sqrt{\pi a} \qquad (2.3)$$

$$\beta\left\{a/L\right\} = C_1 + C_2\left(a/L\right) + C_3\left(a/L\right)^2 + C_4\left(a/L\right)^3 + C_5\left(a/L\right)^4 \qquad (2.4)$$

The procedure used to obtain the geometry function for the candidate spur tooth is known as the 'Virtual Crack Extension Method (VCEM)' [17,18]. This commonly used procedure utilises a combination of J-Integral estimations from finite element models with basic fracture mechanics theory. The following work assumes plane strain conditions for all the crack tips as only two dimensional contacting models were able to be solved in Chapter 5.

The VCEM commences with an uncracked spur tooth model loaded at a known torque loading (1 MNm) at the position which induces the largest maximum principal stress in the root region. In the case of the candidate spur gear, the highest stress level occurs when the gear is contacted at its pitch circle (Chapter 5). This analysis provides the reference stress in equation 2.3 at a known load. The next stage in the process is to introduce a crack into the root region of the spur tooth model at the location of highest surface stress in a direction normal to the maximum principal stress. The crack tip is surrounded with appropriate elements [19] and the model is loaded in exactly the same way as the uncracked model and analysed. From the solution, a J-Integral value is obtained for the crack tip. This J-Integral value can be transformed into a stress intensity value for that particular crack size using equation 2.7. Substituting the stress intensity value into equation 2.3 will result in a geometry function value for a particular crack length.

$$J = G_I = \frac{K_I^2\left(1-\nu^2\right)}{E} \qquad \text{(plane strain)} \qquad (2.7)$$

The direction in which a crack will proceed is usually in the direction of the maximum strain energy release rate, G_I, which is equal to the J-Integral (J) for elastic materials such as the candidate gear. Several analyses for each crack model are solved to find which direction, results in the largest J-Integral value and hence the direction for the crack to propagate. Another crack model can then be produced by extending the crack from the first model a short distance in the direction of greatest strain energy release. The second model can be solved to find another stress intensity value (hence geometry function value for a known crack size) and crack direction. This process is continued until the crack reaches a length where the stress intensity value reaches the fracture toughness for the material at expected loads or when the remaining section becomes too small and elastic theory is no longer relevant, resulting in computational errors.

Section 6.3 covers the stress analysis of the uncracked spur tooth model and Section 6.4 covers the stress analysis of the spur tooth with varying length cracks in the root region. In Section 6.5 a fourth degree polynomial is specified to enable prediction of the geometry function values for particular crack sizes.

6.2 Validation for using plane strain theory and the J-Integral solutions

This section deals with the simple but necessary calculations to see what assumptions result form using the plane strain theory and the tests performed to ascertain the accuracy of the J-Integral values obtained from the ABAQUS solutions.

As mentioned in Section 2.4, for a crack tip to have plane strain characteristics, the crack itself must be of a certain length for a particular depth or alternatively the component with a through crack must be of a certain width. Equation 2.5 describes the minimum crack length or component size required to ensure plane strain conditions at the crack tip.

$$Bs \geq 2.5\left(K_I/\sigma_{ys}\right)^2 \qquad (2.5)$$

Unfortunately, only limited material properties are known for the spur gear and so only an estimated crack size can be calculated. In addition, the expected stress intensities were yet to be calculated, so an approximate fracture toughness for the material was used to find a conservative crack size requirement. Hence, for a stress intensity of 60 MPa$\sqrt{m}$ and a yield stress value of 300 MPa, the resulting minimum crack size required for plane strain crack tip conditions would be 100 mm (remembering the spur teeth have a face width of 535 mm).

Two crack models of varying geometries were solved using ABAQUS to ensure the methods used to calculate J-Integral values were satisfactory.

The first model solved was a thick rectangular plate, containing an edge crack, that was loaded in tension as shown in Figure 6.1. This model contained 288 CPE8 (plane strain) elements. The elements surrounding the crack tip were suitably refined [19]. The purpose of this analysis was to understand the modelling process for J-Integral evaluations by comparing the solution value with the theoretical text value for a basic geometry.

Using the geometry function, quoted in Section 2.4 for such a geometry where the reference stress value is 100 MPa, the crack depth - width ration (a/W) is 0.25, the crack length is 25 mm, the material's elastic modulus is 207 GPa and Poisson ratio is 0.3, the theoretical value for the J-Integral would be 7.808 N/mm. The value obtained by solving the model was 7.785 N/mm which was a maximum for the crack to continue growing in the current direction (as expected). As the theoretical and model solution values compare well, confidence in the method and ABAQUS solution was achieved. Figure 6.2 shows the stress state for the cracked component.

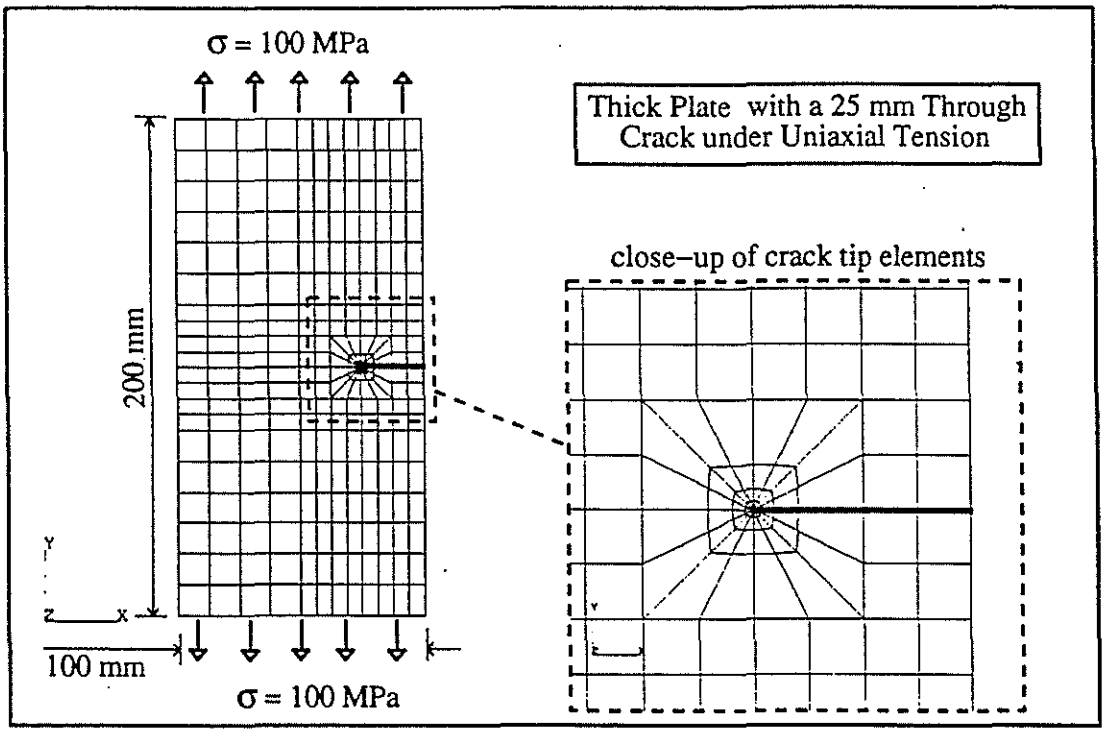

Figure 6.1 Diagram depicting first crack model solved showing boundary conditions.

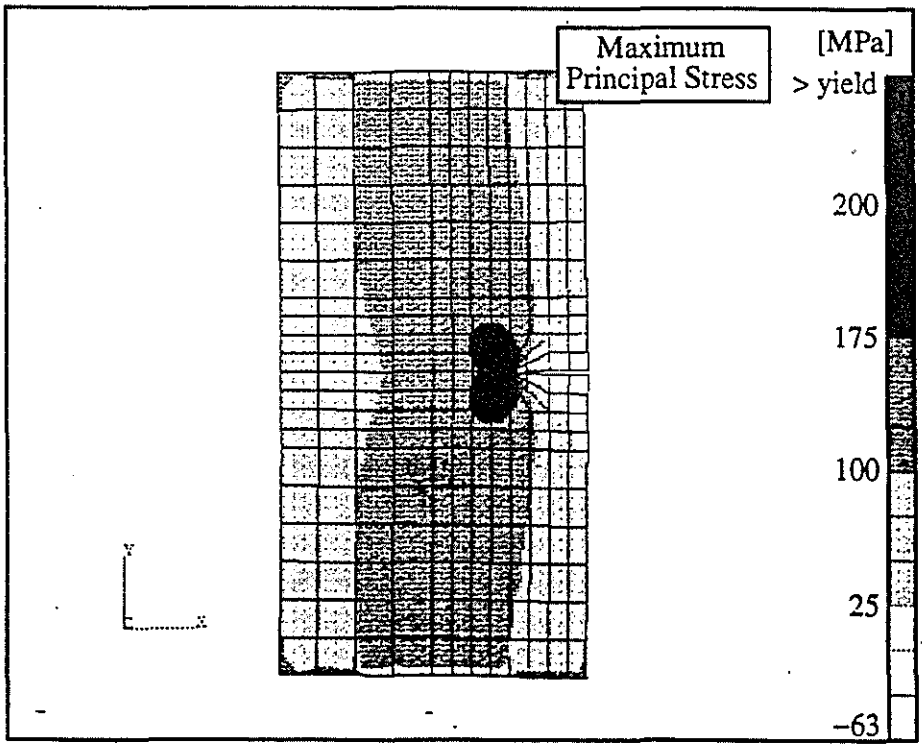

Figure 6.2 Max. principal stress plot for first crack model solved.

Generally, cracks propagate under a combination of modes, not solely by mode I crack opening. Although mode I is usually the major driving force behind propagating cracks, contributions from mode II (sliding mode) especially, have an impact on the overall effective stress intensity for a crack tip. Mixed mode crack propagation occurs when the component's geometry or the loading system is complex. As the loading system and geometry of a spur tooth can be considered complex resulting in mixed mode crack propagation, an investigation was undertaken to hopefully quantify the effective stress intensities relating from modelling of the cracked spur tooth models.

Theoretically [20], the J-Integral is related to the stress intensity factor and under mixed mode plane strain conditions has the form in equation 6.1.

$$J = \frac{\left(K_I^2 + K_{II}^2\right)\left(1 - \nu^2\right)}{E} \qquad (6.1)$$

In addition, the effective stress intensity ΔK_e (driving force for crack propagation) for correct use with the Paris Law in crack propagation predictions has the from in equation 6.2 [21].

$$\Delta K_e = \left(K_I^4 + 8K_{II}^4\right)^{1/4} \qquad (6.2)$$

From viewing equations 6.1 and 6.2, it would appear necessary to separate K_I and K_{II} to ensure feasible results for later use in the crack propagation analysis. However, separating K_I and K_{II} contributions, although possible, would not justify the time required to accomplish the task for every cracked gear model solved. For this reason, the J-Integral value was converted to a single K value for each model. This method introduced an error (intuitively small) into the stress intensity calculations but also reduced the analysis time several fold.

A second crack model (1272 CPE8 elements) was constructed and solved to confirm the relationship of J-Integral value with the mixed mode stress intensity contributions as in equation 6.1. A large thick plate (adequate size to reduce geometry function to 1) was modelled with a 20 mm 45^0 angled internal through crack and loaded as shown in Figure 6.3. Theoretically K_I and K_{II} have solutions as in equations 6.3 and 6.4 where α is the angle the crack makes with the direction of applied stress (100 MPa) and a is the half crack length (10 mm).

$$K_I = \sigma\sqrt{\pi a}\sin^2\alpha \qquad (6.3) \qquad K_{II} = \sigma\sqrt{\pi a}\sin\alpha\cos\alpha \qquad (6.4)$$

The theoretical value for J from combining equations 6.1, 6.3 and 6.4 was 0.691 N/mm, compared to a value of 0.693 N/mm output from ABAQUS. Of interest, the largest J value was obtained for a crack extending perpendicular to applied stress direction (as expected). Figure 6.4 shows the stress state for the second crack model (20 mm, 45^0).

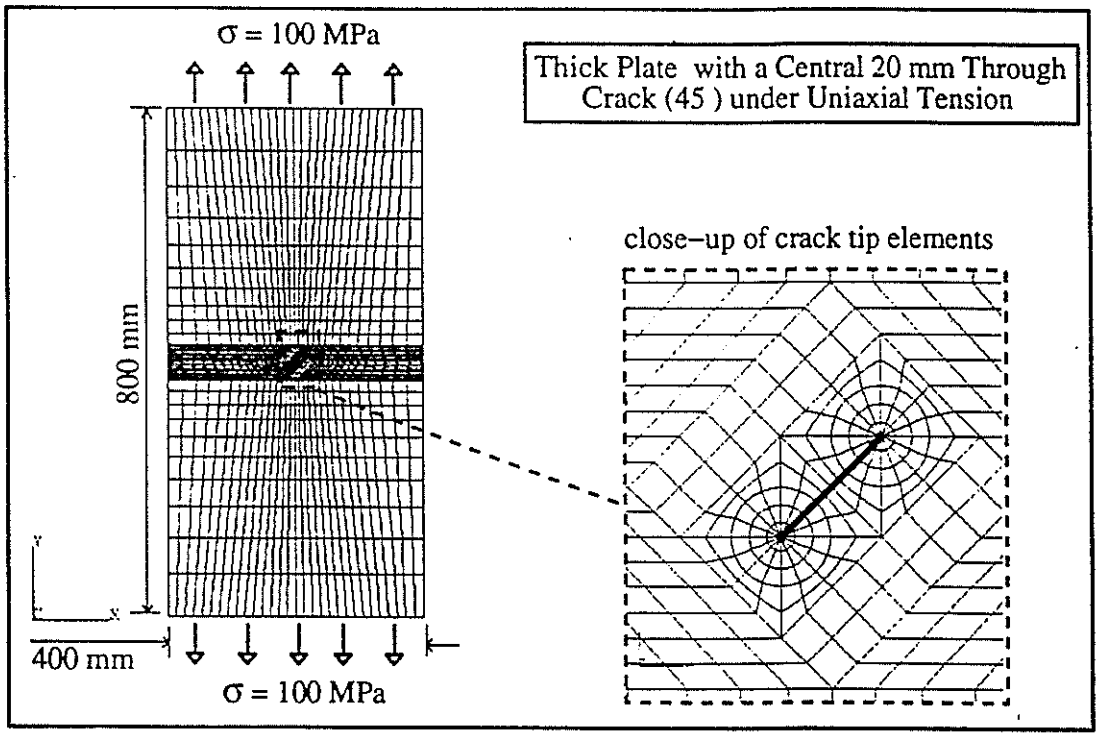

Figure 6.3 Diagram depicting second crack model solved showing boundary conditions.

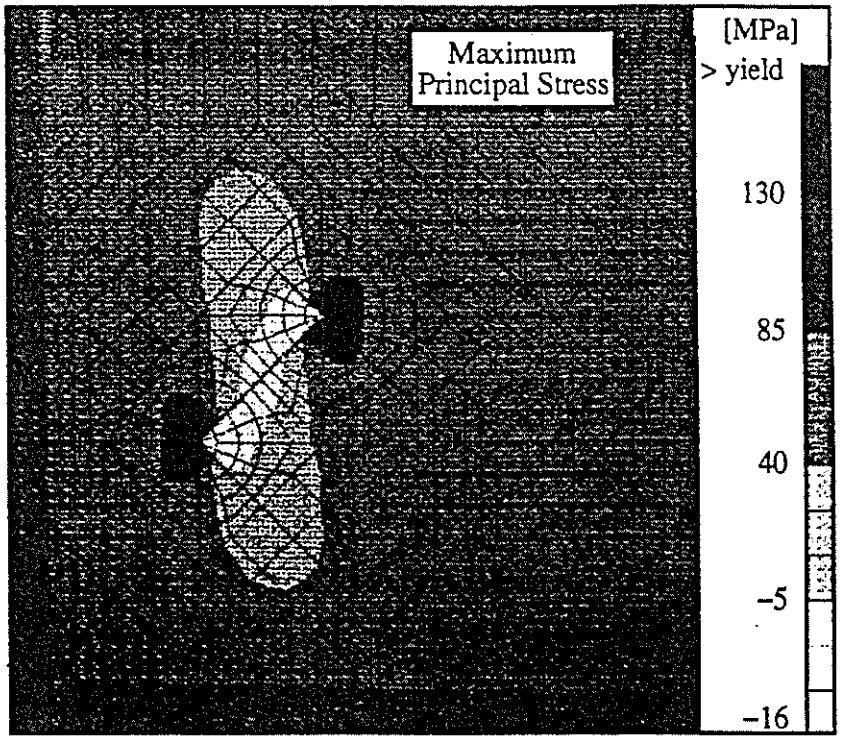

Figure 6.4 Max. principal stress plot for second crack model solved.

6.3 Reference stress for uncracked tooth

This section is dedicated to the analysis of an uncracked spur tooth to finalise a value for the reference stress to be used in the determination of a geometry function as previewed in Section 6.1. The objective of this modelling was to find the position and value for the maximum principal stress induced in the root region by a known torque loading (1 MNm) and the position (pitch circle) which causes the highest root region stress per gear revolution. From this information, the most likely location for a crack to initiate and its direction can be estimated and used in the creation of the cracked spur tooth modelling (Section 6.4).

The spur tooth model analysed consisted of 1613 CPE8 elements. The mesh size chosen was similar to that used in the triple teeth modelling (Section 5.3). Figure 6.5 shows the mesh arrangement and boundary conditions used. Figure 6.6 highlights the location of the maximum principal stress resulting from the static analysis. The maximum value to be used in future work is 62 MPa. This value was anticipated from completing the earlier analyses of the contacting teeth models experiencing the same loading. Figure 6.7 shows a close-up of the root region of the spur tooth and emphasises the magnitude and direction of the element principal stress. The location and direction of a root region crack used in the crack modelling is also indicated. Note that the direction of crack propagation is perpendicular to the maximum principal stress vector for the element closest to the crack initiation position.

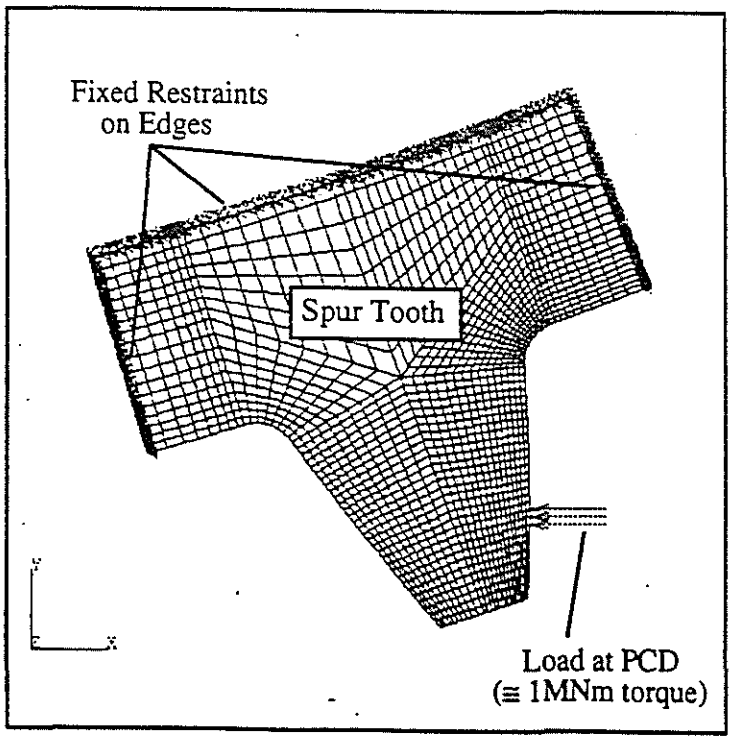

Figure 6.5 Spur tooth model showing mesh arrangement and boundary conditions used.

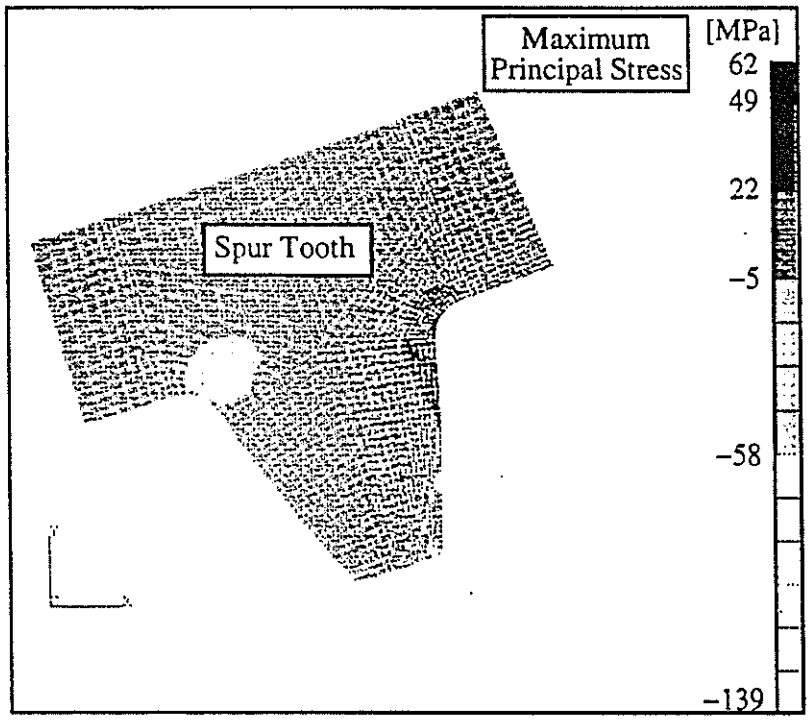

Figure 6.6 Max. principal stress plot for spur tooth model.

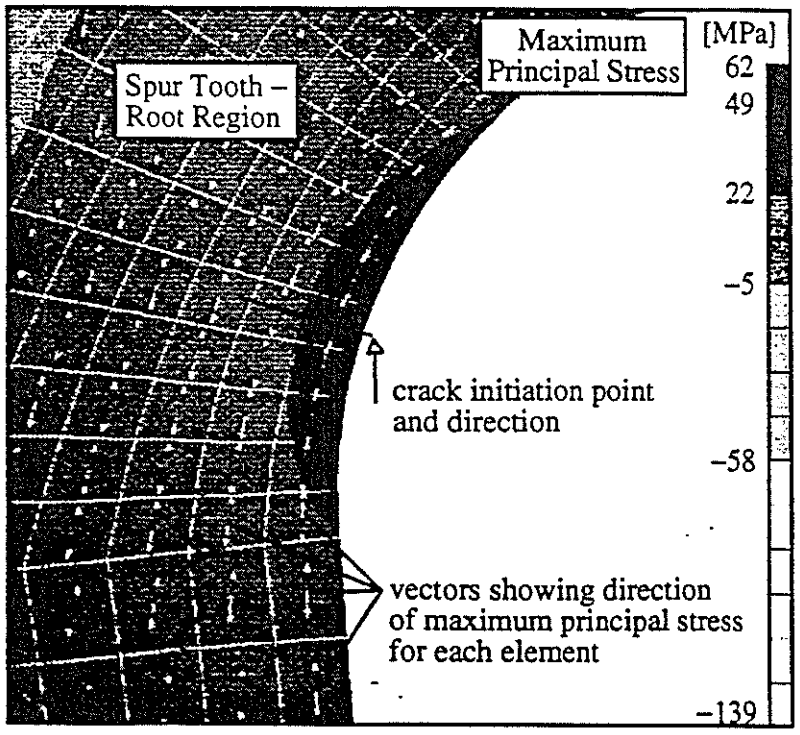

Figure 6.7 Spur tooth root region highlighting the max. principal stress vectors.

6.4 Stress analysis with varying length cracks in root region

This section is dedicated to the analysis of several cracked spur teeth models to finalise values for the stress intensity for varying length root region cracks. The objective of this modelling was to find the most likely propagation path for a crack that initiated in the root region. The torque loading (1 MNm) and boundary conditions used in the uncracked tooth modelling (Section 6.3) were again utilised for all crack models to minimise errors when comparing results.

Before commencing the first crack model, the minimum crack size for fracture mechanics to be considered valid, required estimation. The minimum crack size (or short crack parameter), l_o, is estimated using equation 6.5. This equation is a result of work done by Kitagawa [15] and is described graphically in Figure 6.8.

$$l_o = \frac{1}{\pi}\left(\Delta K_{th} / \Delta\sigma_o\right)^2 \qquad (6.5)$$

Approximate values for the threshold stress intensity (8 MPa $\sqrt{m}$, typical value obtained from PFATIGUE database) and the cyclic stress range (62 MPa) were used in equation 6.5. The gives an approximate initial crack size of 5 mm for commencement of crack tooth modelling.

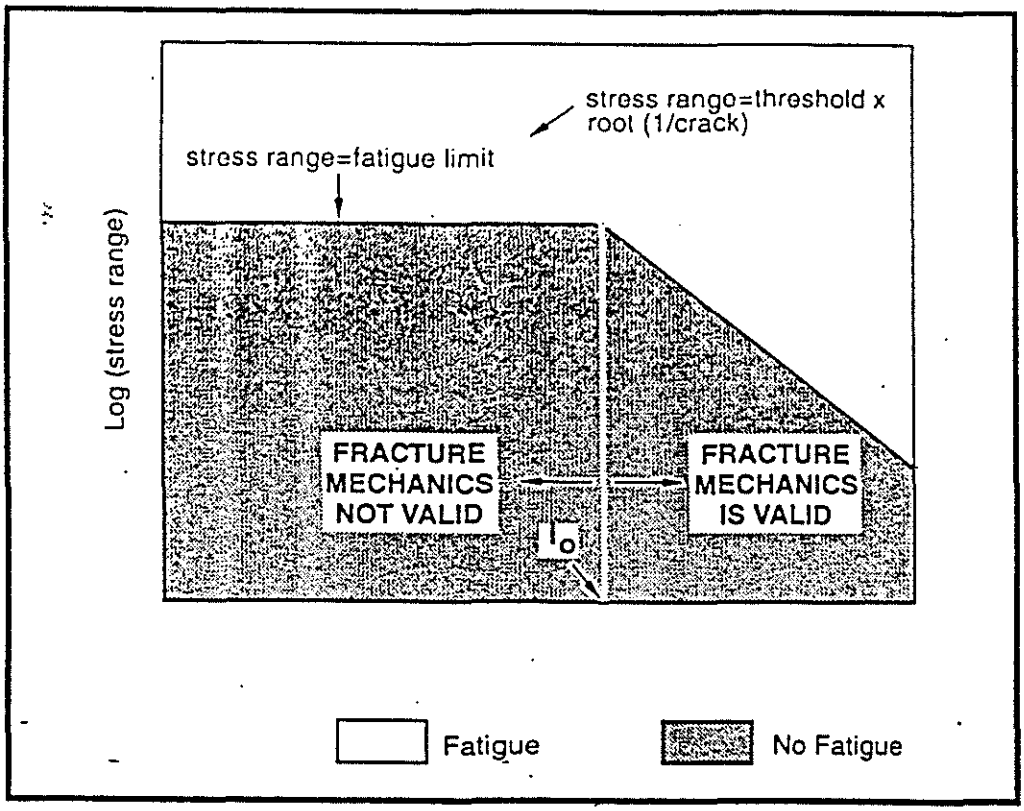

Figure 6.8 The 'Kitagawa Diagram' used to explain short crack parameter theory. [15]

Using the procedure for VCEM (Virtual Crack Extension Method) as explained in Section 6.1, a total of 18 consecutive crack models with varying root region cracks ranging from 5 mm up to 90 mm were analysed. The first crack model (5 mm crack) was analysed and the direction in which the crack would propagate was estimated by locating the direction which resulted in the highest J-Integral value. Through this J-Integral, the stress intensity for the particular crack size was calculated. In addition, the direction in which to extend the crack for the next model (10 mm) was also known. (Steps of 5 mm were chosen as a compromise between model numbers required and accuracy of crack path for certain sized crack extensions.) This process was continued until the crack reached 90 mm. At this stage the remaining tooth section was approximately 10 mm and the stress values across this region were reaching yield. Further crack growth would result in error since the analyses assumed linear elastic material behaviour.

Figures 6.9 through 6.11 show the spur tooth models containing root region cracks of lengths 10 mm, 90 mm and 50 mm respectively. These figures highlight the typical mesh arrangements and boundary conditions used for all the crack models along with surface plots showing the crack positions. A summarised input deck and results file for the 50 mm crack model (932 CPE8 elements) can be found in Appendix A4. Figure 6.12 shows the stress state for the 50 mm crack model with exaggerated deformation to help visualise the crack opening.

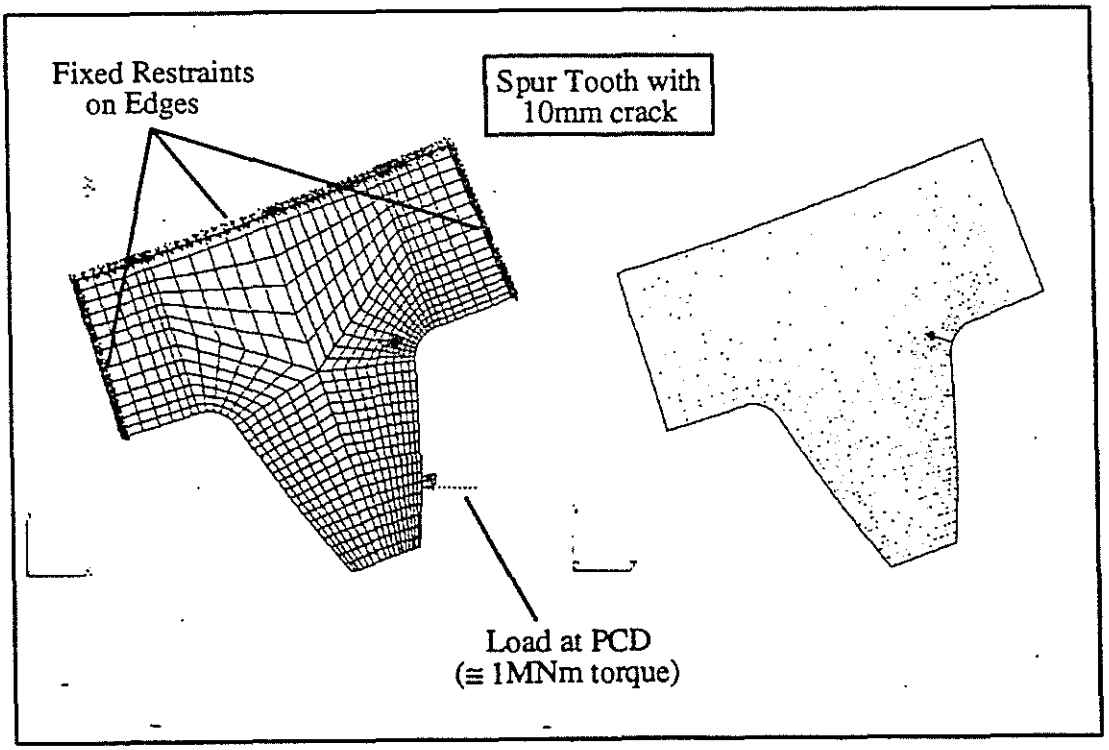

Figure 6.9 10 mm crack model showing mesh arrangement and boundary conditions.

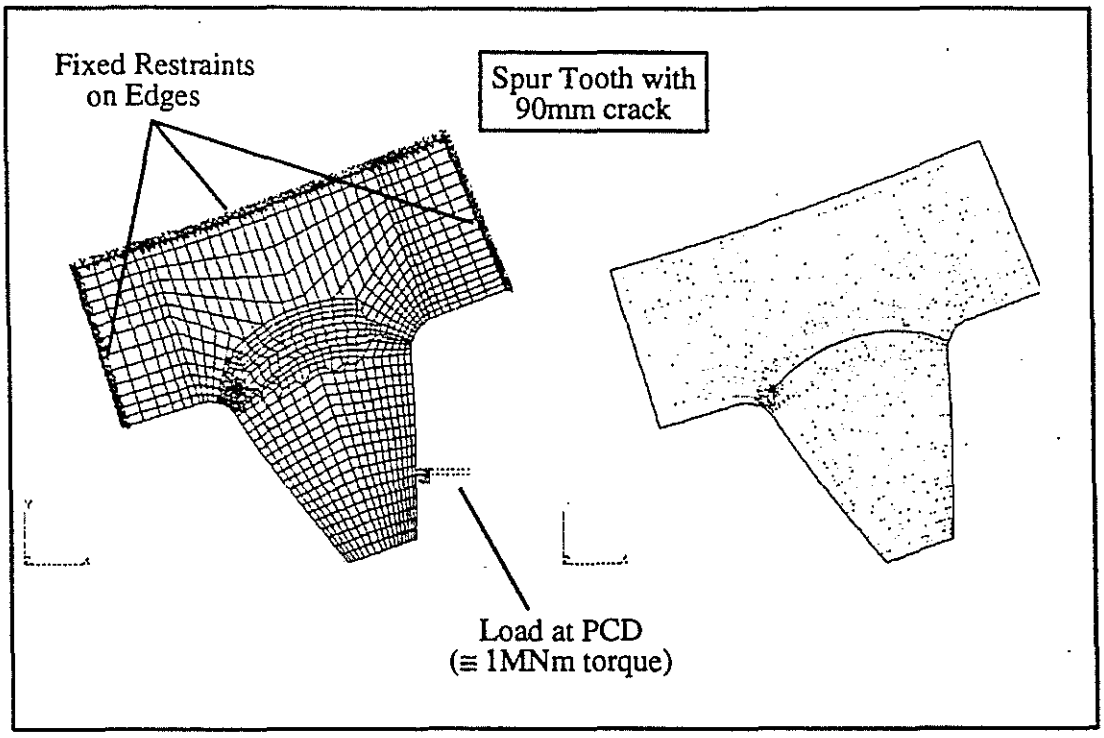

Figure 6.10 90 mm crack model showing mesh arrangement and boundary conditions.

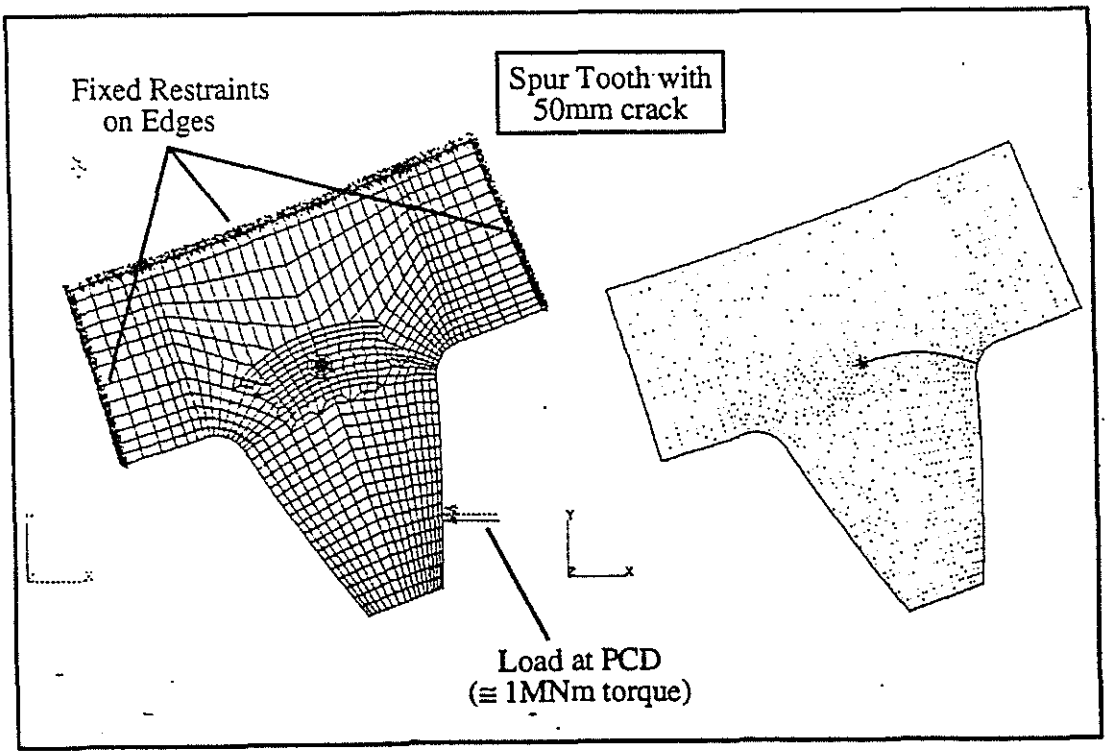

Figure 6.11 50 mm crack model showing mesh arrangement and boundary conditions.

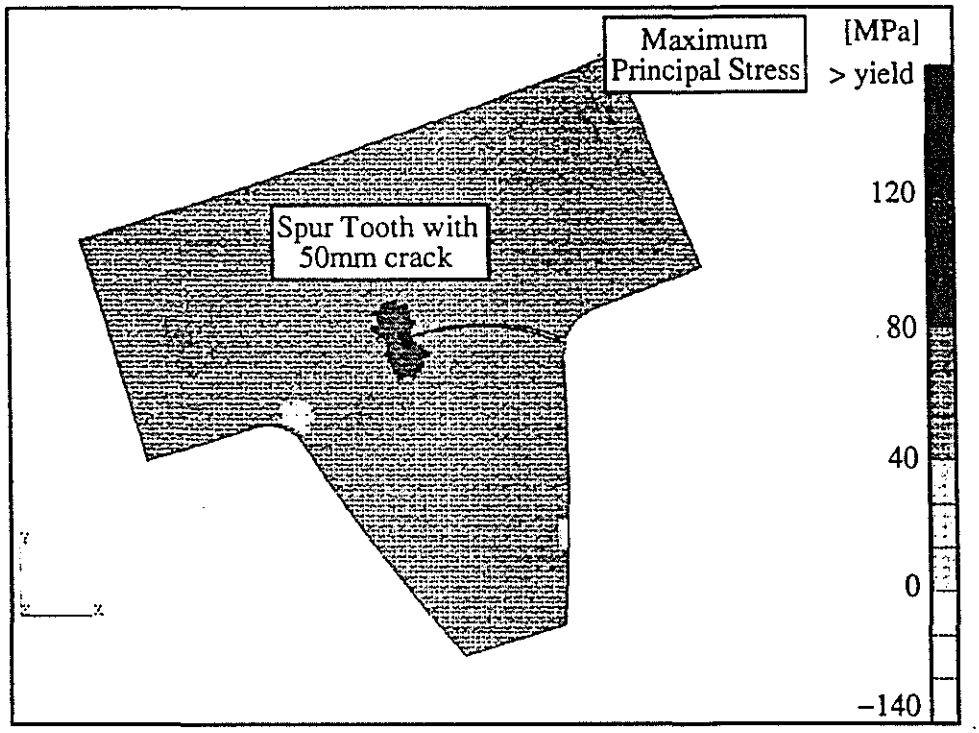

Figure 6.12 Max. principal stress plot for the 50 mm crack model.

Following the analysis of the sequential crack models, some additional analyses were undertaken to gauge the effects of load variations on crack direction and J-Integral values. Several randomly chosen crack models were analysed using torque loads of 0.8 MNm and 1.2 MNm. Results from the 1 MNm loaded crack models are tabulated in Table 6.1. From these analyses it was concluded that load variations did not effect the direction of crack propagation and the J-Integral results were as expected using equations 2.3 and 2.7. Further analysis of the data can be found in Section 6.5.

A model was also constructed with a straight crack beginning at the crack initiation point and ending at the position where the 50 mm crack from an earlier model was found to end (Figure 6.13). The direction for crack extension for the straight 50 mm crack model and original 50 mm crack model were in close agreement with similar J-Integral results (Table 6.1). It can be concluded from this analysis that preliminary modelling of a known crack size can be completed using a straight line approximation for the crack path (instead of numerous intermittent crack models to find the crack path), resulting in feasible stress intensity values. This concept would prove beneficial to future analyses regarding cracked gearing in the Sugar Industry.

Table 6.1 Summary of J-Integral values for Crack Models. (Torque = 1 MNm)

Model Description - Crack Size [mm]	Crack Direction Angle above -X axis	Max. J-Integral [N/mm]
5	17.2	0.1326
10	12.0	0.1705
15	7.0	0.1997
20	2.0	0.2322
25	-2.0	0.2699
30	-6.25	0.3194
35	-9.75	0.3824
40	-13.75	0.4650
45	-17.25	0.5775
50	-20.75	0.7349
50 straight	-20.75	0.7333
55	-24.25	0.9638
60	-28.0	1.311
65	-31.75	1.874
70	-35.5	2.850
75	-39.75	4.740
80	-43.5	8.954
85	-47.75	20.81
90	-52.0	70.58

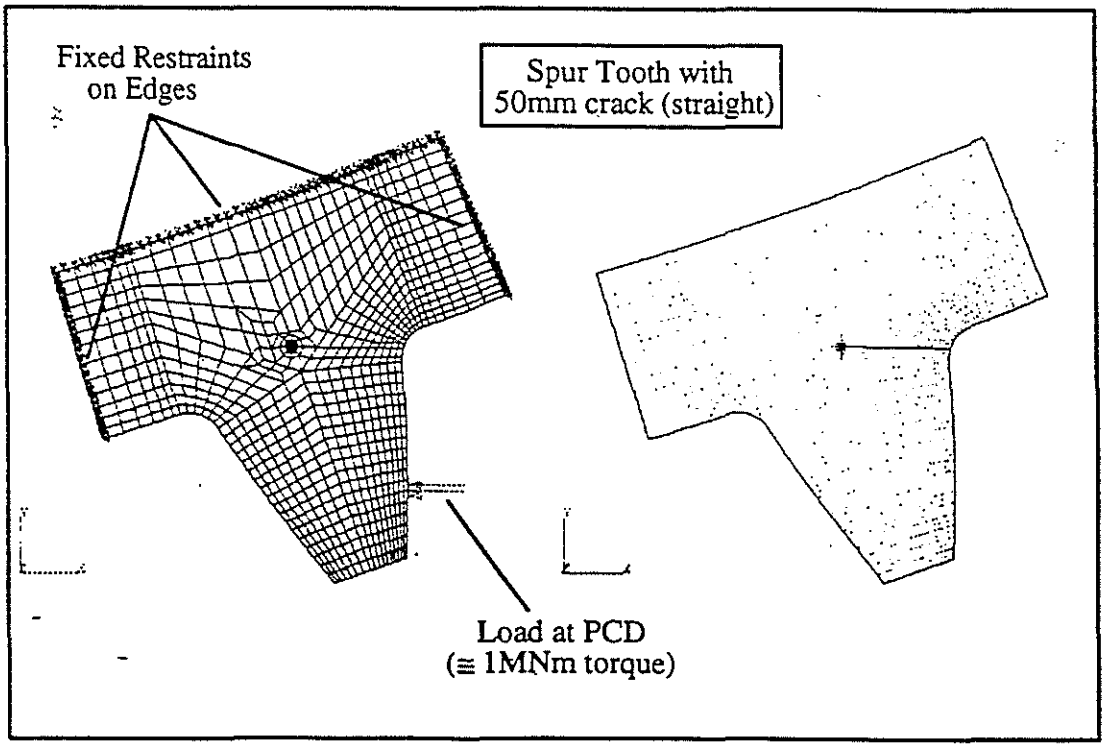

Figure 6.13 Straight 50 mm crack model analysed.

6.5 Calculation of geometry function and feasibility

This section deals with the final manipulation of J-Integral results (Section 6.4) into a geometry function in preparation for cracked gearing life predictions. Using equations 2.3 and 2.7, the J-Integral values and their respective crack lengths can be transformed into stress intensities (assuming plane strain conditions) and non-dimensional values from which a geometry function can be fitted. Plotting the geometry function values against the normalised crack lengths (a/L), a line of best fit can be found (fourth degree polynomial (equation. 2.4)). L, the generalised size parameter was set at 100 mm (final fracture crack length for the spur tooth) for the geometry function calculations. Table 6.2 lists the results used to find the geometry function for a crack in the root region of the candidate spur tooth.

$$J = \frac{K_I^2}{E(1-\nu^2)} \qquad (2.7) \qquad\qquad K_I = \beta\left\{a/L\right\}\sigma\sqrt{\pi a} \qquad (2.3)$$

$$\beta\left\{a/L\right\} = C_1 + C_2(a/L) + C_3(a/L)^2 + C_4(a/L)^3 + C_5(a/L)^4. \qquad (2.4)$$

Table 6.2 Data used to find the line of best fit for geometry function.

(Torque = 1 MNm, E = 207 GPa, ν = 0.3, σ = 62 MPa)

Crack Length a [mm]	J-Integral Value J [N/mm]	Stress Intensity K [MPa $m^{0.5}$]	Geometry Value $\beta(a/L)$	Normalised Crack Length (a/L)
5	0.1326	5.49	0.706	0.05
10	0.1705	6.23	0.562	0.10
15	0.1997	6.74	0.497	0.15
20	0.2322	7.26	0.464	0.20
25	0.2699	7.84	0.447	0.25
30	0.3194	8.52	0.444	0.30
35	0.3824	9.33	0.450	0.35
40	0.4650	10.28	0.464	0.40
45	0.5775	11.46	0.488	0.45
50	0.7349	12.93	0.522	0.50
55	0.9638	14.81	0.570	0.55
60	1.311	17.27	0.636	0.60
65	1.874	20.65	0.731	0.65
70	2.850	25.46	0.869	0.70
75	4.740	32.84	1.082	0.75
80	8.954	45.13	1.440	0.80
85	20.81	68.80	2.130	0.85
90	70.58	126.71	3.813	0.90

Figure 6.14 shows the geometry function values plotted against the normalised crack lengths. A fourth degree polynomial (equation 6.6 / shown in Figure 6.14) was fitted to the data points with a correlation coefficient of 0.98. This equation will be used for the crack propagation predictions (Chapter 7) using the PFATIGUE code. As can be seen, the fitted curve deviates above the data points for the higher values of normalised crack lengths (a/L). This will cause overestimation of the stress intensities and hence the crack propagation rates for larger crack sizes (> 70 mm) in the fatigue modelling analyses. However, depending on the loading conditions of the tooth and the material's fracture properties, real life cracks may become unstable and cause failure before they reach such lengths. Therefore, the final curve fitted to the data was considered satisfactory for use in crack propagation modelling as the curve accurately described the data for smaller sized crack geometry values.

$$\beta\left\{a/L\right\} = 1.027 - 7.814\left(a/L\right) + 36.516\left(a/L\right)^2 - 69.544\left(a/L\right)^3 + 47.147\left(a/L\right)^4 \qquad (6.6)$$

For future use with crack modelling codes or software which can use more complex equations for defining geometry functions, a ninth degree polynomial (equation 6.7) was fitted to the data shown in Figure 6.14. This curve accurately matches the data points.

$$\beta\left\{a/L\right\} = 0.869 - 2.106\left(a/L\right) - 49.590\left(a/L\right)^2 + 702.666\left(a/L\right)^3 - 4123.822\left(a/L\right)^4 + 13490.247\left(a/L\right)^5$$
$$-26260.250\left(a/L\right)^6 + 30228.782\left(a/L\right)^7 - 19005.661\left(a/L\right)^8 + 5036.652\left(a/L\right)^9 \qquad (6.7)$$

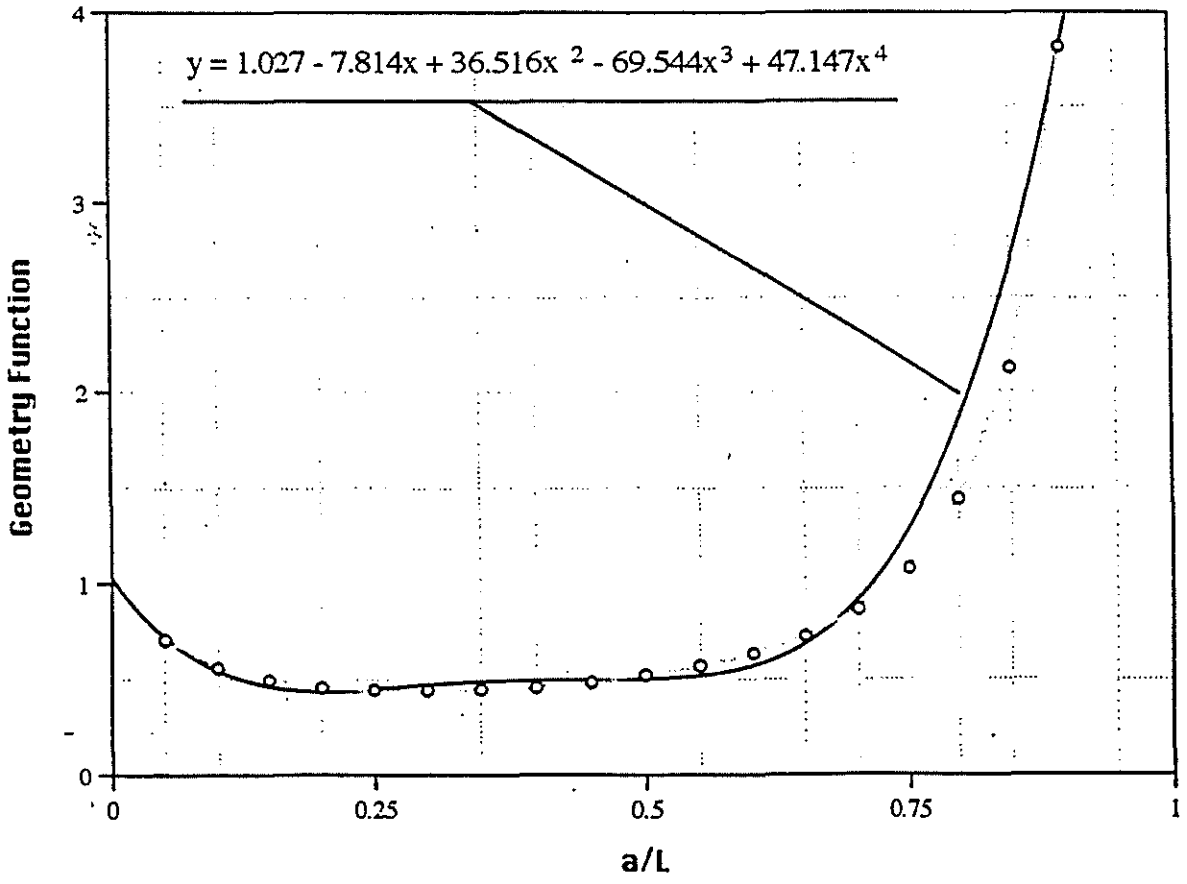

Figure 6.14 Geometry function values versus normalised crack lengths.

7.0 Prediction of Crack Propagation Rates

This chapter describes the approach taken to analyse the growth characteristics of root region cracks. Crack propagation results and a sensitivity analysis follow.

The general procedure for calculating crack growth in a component made of a certain material under nominated load conditions is outlined in Figure 7.1. As shown, the three inputs, component geometry, material properties and loading history must be specified before any successful crack propagation calculations can be completed. The PFATIGUE code used in this section combines the three inputs with the Paris Law theory and outputs such information as time to crack fracture, the length of the crack at fracture and monitors the growth of the crack throughout its life.

Fracture related properties for the candidate gear were not available for this project. Consequently precise crack propagation predictions for this gear were not possible. However, the remaining inputs, geometry and loading history were known with some confidence and therefore analyses of the root region cracks could be completed using a 'best estimate' of the properties obtained from PFATIGUE database. Section 7.1 involves crack propagation results for a gear under nominal loading conditions and Section 7.2 reports on several sensitivity analyses undertaken to explore the effect of varying material properties and loading characteristics on crack propagation rates.

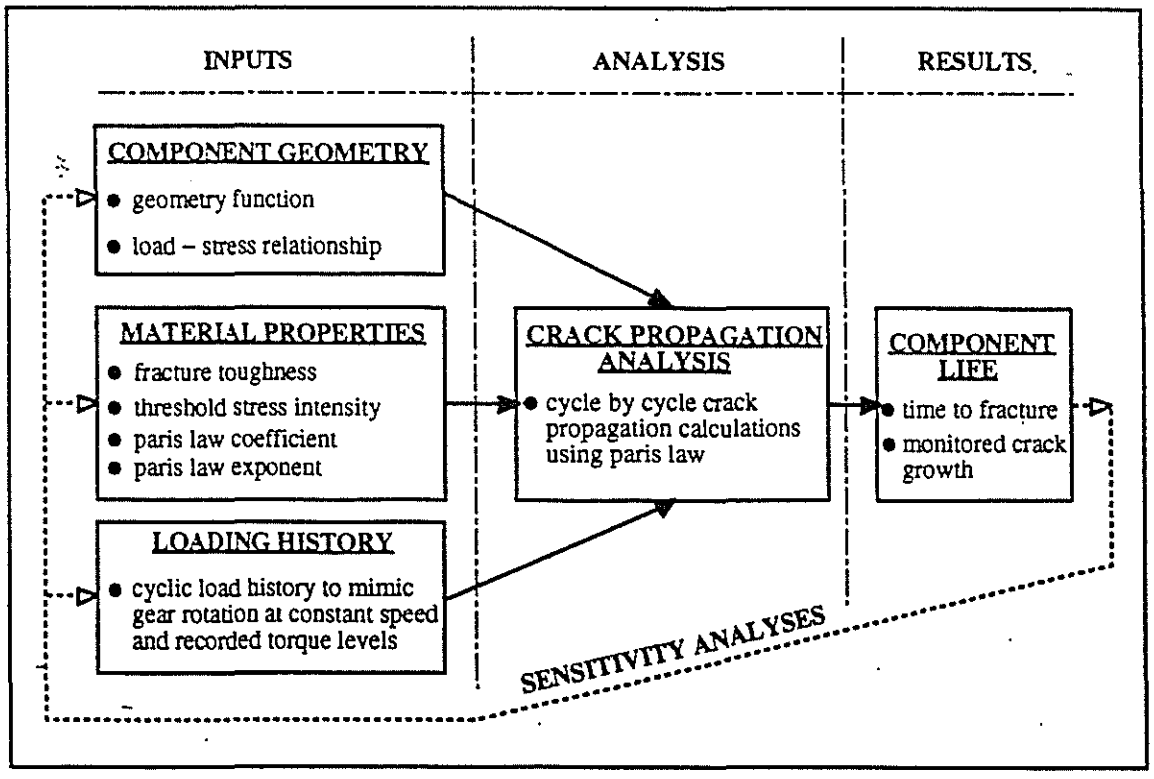

Figure 7.1 General analysis procedure involved with crack propagation predictions.

7.1 Crack propagation analysis and results under nominal loading conditions

The following analysis of a cracked spur tooth assumes that the gear is experiencing nominal loading conditions (torque and speed histories analysed in Section 4.3) with no misalignment between the mating gears. Non-uniform tooth loading and other load severities are covered in Section 7.2. For all analyses, the geometry function used was that obtained in Chapter 6 (equation. 6.6).

$$\beta\left\{{}^{a}/_{L}\right\} = 1.027 - 7.814\left({}^{a}/_{L}\right) + 36.516\left({}^{a}/_{L}\right)^{2} - 69.544\left({}^{a}/_{L}\right)^{3} + 47.147\left({}^{a}/_{L}\right)^{4} \qquad (6.6)$$

As the fracture properties were not known for the candidate gear, PFATIGUE's materials database was searched in an attempt to find a substitute material with similar properties such as Young's modulus and the ultimate tensile strength to that of the gear. In total there were 22 materials with fracture material properties supplied. This selection was reduced by filtering out the materials with dissimilar properties to the gear (Grade C, BS592-1967). The remaining materials and their general properties are listed in table 7.1 for comparison. Note the ultimate tensile strength (UTS) for the candidate gear was quoted at a minimum of 532 MPa. C and m in Table 7.1 are the Paris Law coefficient and exponent respectively (equation 2.8). The threshold stress intensity and fracture toughness are also tabulated.

$$da/dN = C(\Delta K)^{m} \qquad (2.8)$$

Table 7.1 Most suitable replacement materials and their properties.
(UTS for gear is 532 MPa, E used in modelling was 207 GPa)

Material	A533B	MANTEN
UTS [MPa]	552	552
Y [MPa]	345	324
E [GPa]	200	203
C	4.77 E-13	3.00 E-12
m [m/cycle]	3.73	3.43
K_{1c} [MPa.m$^{0.5}$]	100	121
ΔK_{th} [MPa.m$^{0.5}$]	4.65	8.00

It was decided that A533B would be used as the substitute material for the candidate gear as it had the lower threshold stress intensity and fracture toughness of the two possible materials (Table 7.1). Although A533B is not the exact gear material, it properties would result in more conservative life predictions than MANTEN.

The finite element model used for the crack propagation analyses was the refined mesh spur tooth model analysed in Section 6.3. The initial static load solution for this model when coupled with the geometry function complete the requirements for the geometry inputs needed for a crack propagation model. The maximum principal stress state for the tooth under a known torque load of 1 MNm and the predicted propagation path for a root region crack are shown in Figure 7.2 to aid in the understanding of the following analyses.

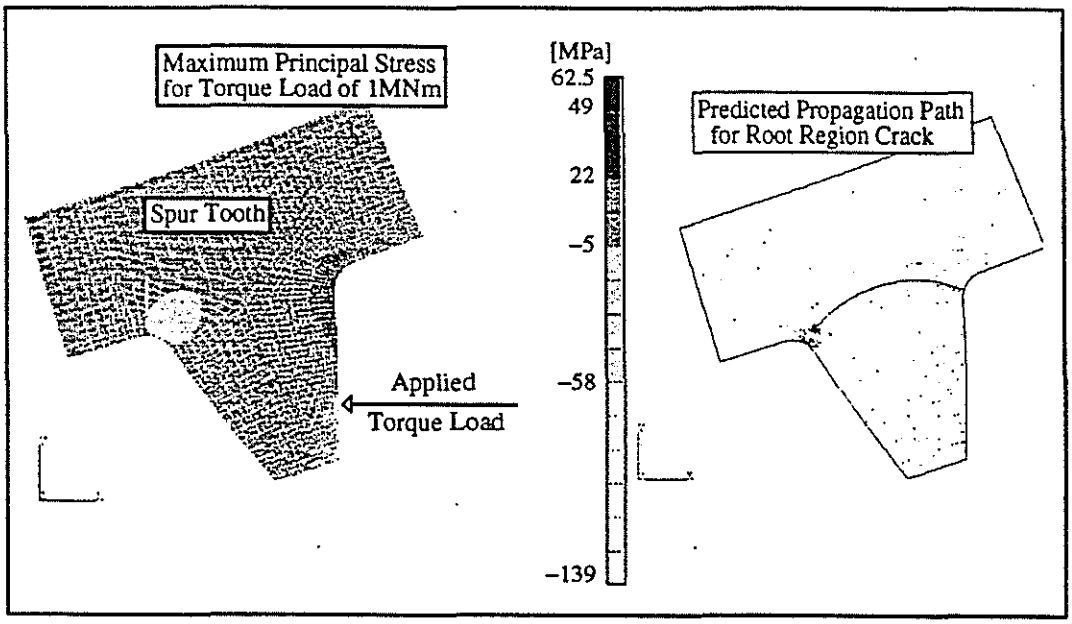

Figure 7.2 Spur tooth model used for the crack propagation analyses.

Now that the geometry and material inputs are specified, only the loading history needs refinement before propagation solutions can commence. Of the two torque histories investigated in Section 4.3, the first torque history (TOR1) was chosen to be adapted for application as it had the highest mean value (0.957 MNm compared to 0.944 MNm) and highest corresponding gear rotational speed (3.69 rpm compared to 2.859 rpm).

The torque history, TOR1, was sampled at 1 reading / minute and a loading history for the model required load oscillations at the gear rotational speed and measured torque values to simulate gear rotation at nominal torque transmission loads. To simplify the creation of a suitable load history file, the method displayed in Figure 7.3 was utilised. The original torque history (TOR1) was multiplied by a calibrating trace consisting of a triangular wave oscillating at 4 rpm with a magnitude between 0 and 1. The result was a torque history adapted from actual measured data with an oscillation speed at 4 rpm. This history when used in the crack propagation models would simulate cyclic spur tooth loading at measured torque levels and at a rotational speed of 4 rpm. Simple calculations from the predicted crack life times could account for changes in rotational speeds.

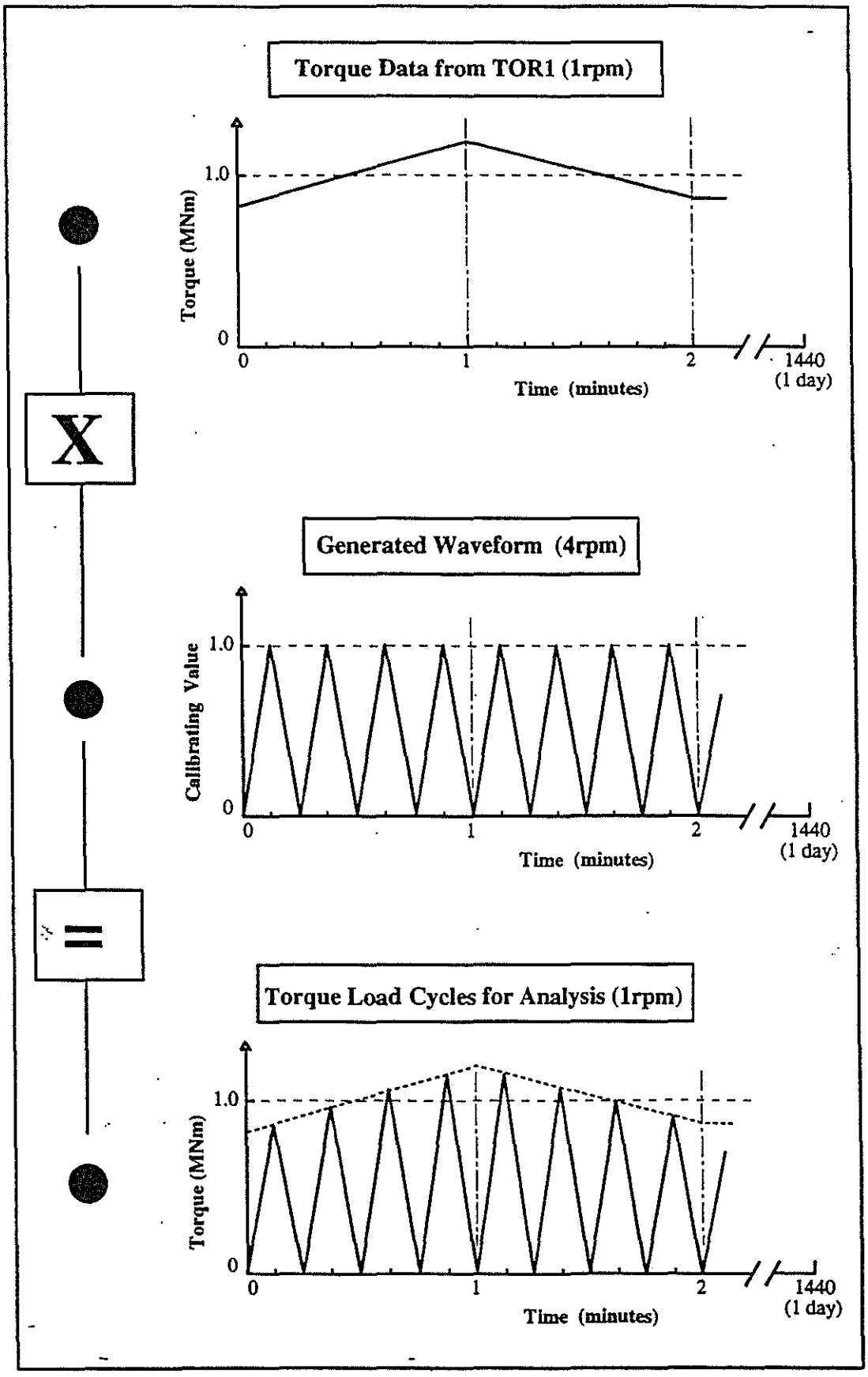

Figure 7.3 Method used to produce suitable load trace for crack propagation analyses.

In total, four crack propagation analyses were undertaken for the cracked spur gear tooth made of A533B. Each of the models differed by the initial crack size used (10 mm, 20 mm, 40 mm, 50 mm). The crack length for each model was recorded after the analyses had reached 500 crushing days (Table 7.2.). Note, the analyses assumed full teeth contact (no misalignment) in an 'AIR' environment.

Table 7.2 Crack propagation results under nominal loading conditions.
(Material used was A533B, load history was TOR1 at 4 rpm)

Initial crack length [mm]	Crack length at 500 crushing days [mm]	Change in crack length after 500 crushing days [mm]
10.0	10.00	0.00
20.0	20.02	0.02
40.0	41.57	1.57
50.0	53.66	3.66

To view the crack propagation with time, the model with an initial crack size of 50 mm was monitored until tooth fracture occurred. Figure 7.4 shows the crack length versus time as expressed in crushing days. The crack length at fracture was 77.4 mm under nominal load conditions (no misalignment) . The solution suggested that it would take 1115 crushing days under such loading conditions to reach the critical length.

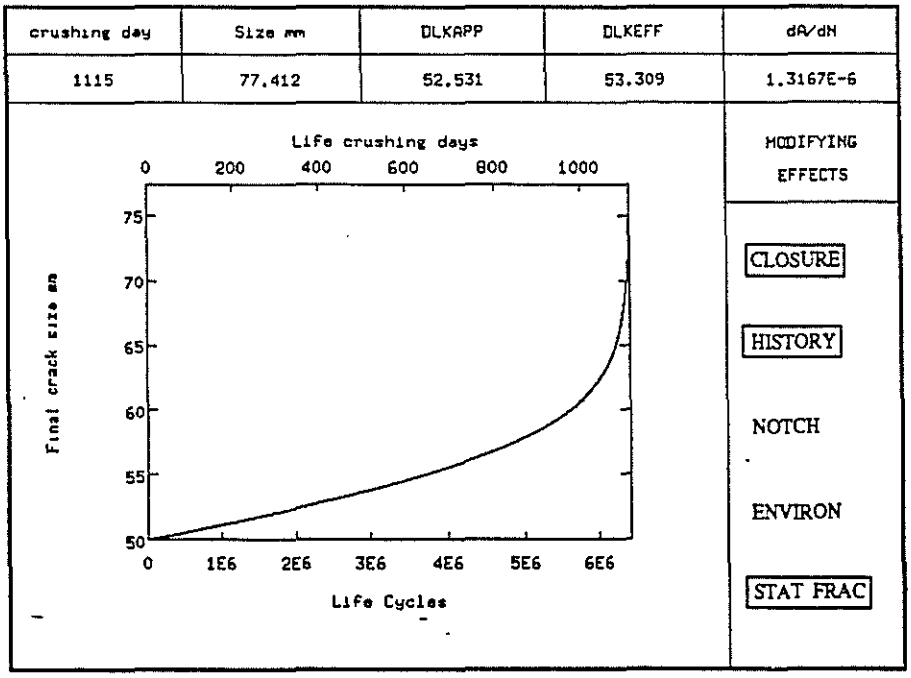

Figure 7.4 Crack length versus time under nominal load conditions for a A533B gear tooth.

7.2 Sensitivity analysis

It was decided that sensitivity analyses were necessary for this project to account for the shortfalls in information necessary for accurate modelling of the cracked candidate gear. As the material properties, misalignment between the pinion and spur gear and possible future loading conditions were not known with any certainty, modelling was carried out to explore the effects of varying these parameters. Section 7.2.1 describes the effects of varying the material behaviour and properties on the crack growth characteristics. Section 7.2.2 describes the effect of varying the torque transmission loads on the crack gearing and finally Section 7.2.3 describes the effect of non-uniform loading (eg. misalignment) across the face of the spur tooth face.

7.2.1 Effect of varying material properties and behaviour

Varying the fracture material properties would intuitively effect the remaining life predictions for a cracked gear tooth under known loading conditions. Quantifying the effect of varying material properties is relevant for this project as the exact material properties for the candidate gear are unknown. However, as there are numerous fracture properties that determine how cracks in certain material behave, it would require many solutions to cover all possible combinations of fracture properties. This process would result in many useful parametric charts from which a combination of fracture properties and possible loading conditions could be combined for a particular crack size to give a single value for the remaining life of a gear tooth. Unfortunately, this process would in itself be very time consuming. To gain some appreciation of the effect of varying material properties, four crack propagation analyses were undertaken for the cracked spur gear tooth, this time made of MANTEN (Table 7.1), using the same method as described in Section 7.1 for a tooth made of A533B. The results of the analyses are listed in Table 7.3.

Table 7.3 Crack propagation results under nominal loading conditions.
(Material used was MANTEN, load history was TOR1 at 4 rpm)

Initial crack length [mm]	Crack length at 500 crushing days [mm]	Change in crack length after 500 crushing days [mm]
10.0	10.00	0.00
20.0	20.00	0.00
40.0	40.46	0.46
50.0	51.76	1.76

Comparing the results for the gear tooth made of A533B and MANTEN (Tables 7.2 and 7.3 respectively) under nominal loading conditions, it can be seen that the change in material properties resulted in differing crack propagation characteristics. As an example, a crack of 20 mm depth in a MANTEN tooth resulted in no crack propagation whereas for a similar sized crack in a A533B tooth there was some crack extension for nominal loading conditions. This can be explained by comparing the threshold stress intensity values for the two materials. The induced crack tip stress intensity for the tooth was just sufficient to produce crack propagation in A533B ($\Delta K_{eff} > 4.65$ MPa.m$^{0.5}$ = K_{th}) but not high enough to produce crack propagation in MANTEN ($\Delta K_{eff} < 8.00$ MPa.m$^{0.5}$ = K_{th}). The difference in Paris Law coefficients and exponents for the two materials also effected the rate at which the cracks grew under similar loading conditions.

The MANTEN model with an initial crack size of 50 mm was monitored until tooth fracture occurred. Figure 7.5 shows the crack length versus time as expressed in crushing days. The crack length at fracture was 81.176 mm under nominal load conditions (no misalignment) . The solution suggested that it would take 1709 crushing days under such loading conditions to reach the critical length.

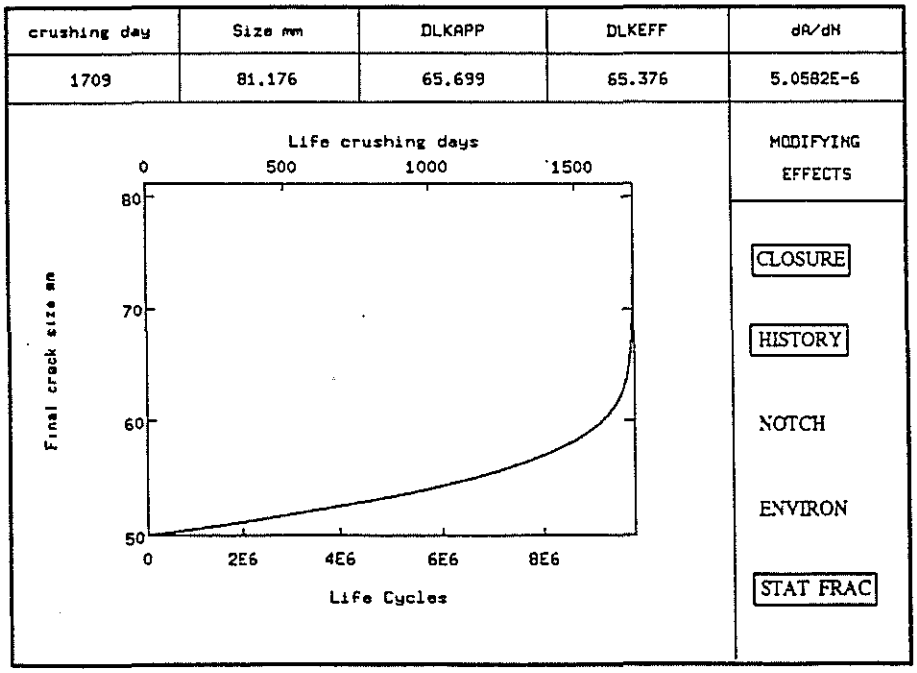

Figure 7.5 Crack length versus time under nominal operating for a MANTEN gear tooth.

7.2.2 Effect of varying torque transmission loads

Increasing the torque loads transmitted between the mating spur and pinion teeth results in increased root region stresses and hence increased crack propagation rates and reduced fracture crack lengths. As the analysis is based on linear elastic fracture mechanics, an increase in torque load induces a proportional rise in the stress. Therefore doubling the torque load would double the stress in the root region and hence an increase in stress intensity and propagation rate for a particular crack length according to the Paris Law theory (equation 2.8) and the general fracture mechanic's equation (equation 2.3).

$$da/dN = C(\Delta K)^m \qquad (2.8)$$

$$K_I = \beta\{a/L\}\sigma\sqrt{\pi a} \qquad (2.3)$$

Several numerical analyses were undertaken to obtain an understanding of the effect increasing the torque transmission load (increased root region stresses) on the life of cracked gearing. Two of these analyses are presented below. The first analysis considered a tooth made of A553B with an initial root region crack of 10 mm length that was loaded with double the nominal torque loading until fracture occurred. The second analysis was identical except the material was changed to MANTEN. Table 7.4 lists the results.

Table 7.4 Crack propagation results for varying torque transmission loads.
(. crack length = 10 mm, spur gear speed set at 4 rpm.)

Tooth material.	Torque transmission loads. [% of nominal torque loading]	Critical crack length. [mm]	Time to fracture. [crushing days]
A533B	100	no growth	∞
A533B	200	67.47	1930
MANTEN	100	no growth	∞
MANTEN	200	71.58	2956

Figures 7.6 and 7.7 show the crack growth characteristics for the analyses involving double the torque loading on the A533B and MANTEN gear teeth respectively. In conclusion, it appears as though propagation of the existing cracks in the candidate gear would only occur if there was increased root region stresses induced via increased torque transmission loads or by misalignment which results in non-uniform loading across the spur teeth (Section 7.2.3). However, it must be noted that the materials used to form this conclusion were not that of the actual gear material.

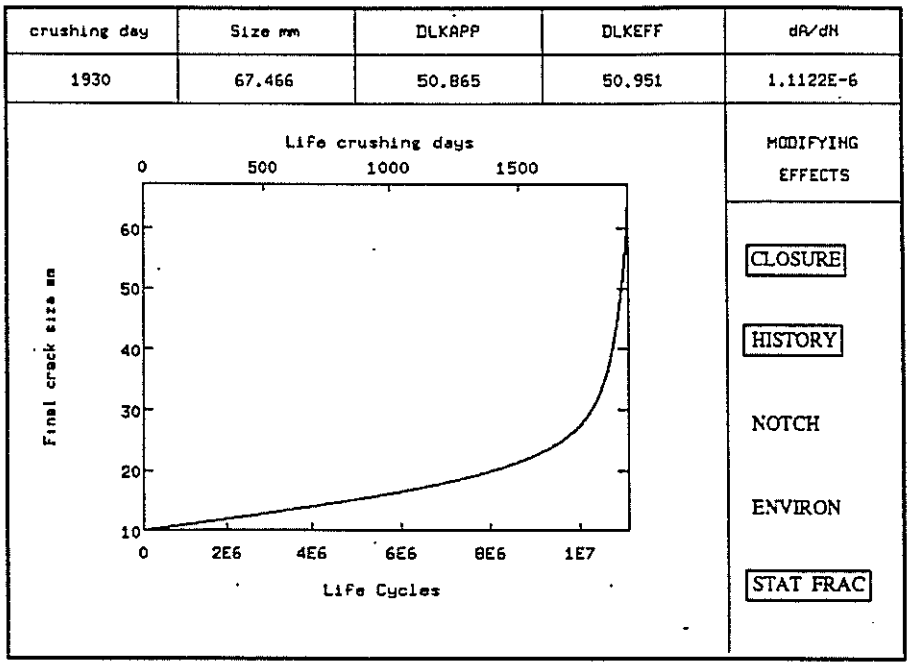

Figure 7.6 Crack length versus time for a A533B gear tooth under 200% loading.

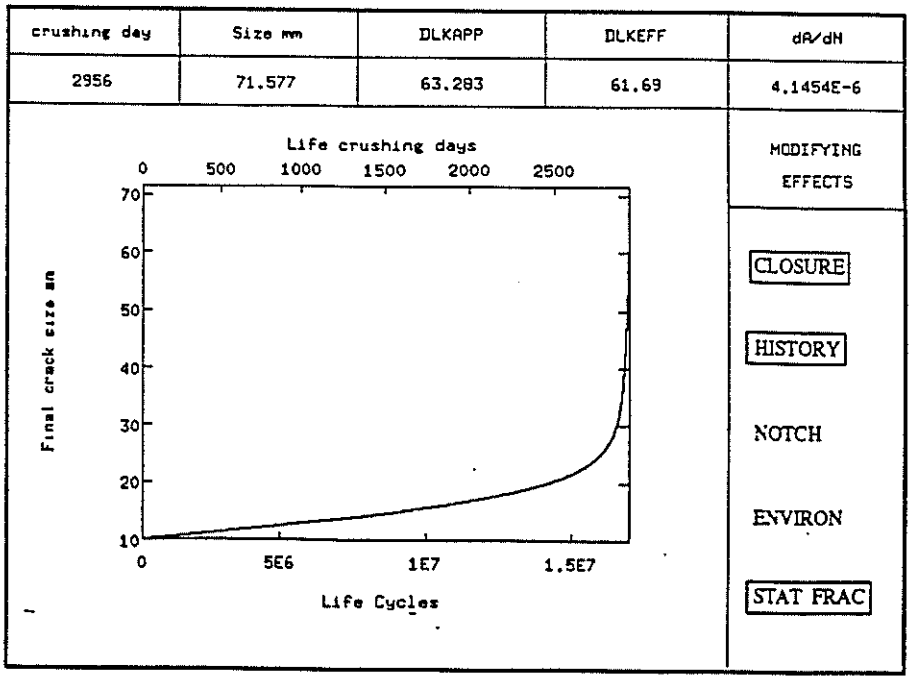

Figure 7.7 Crack length versus time for a MANTEN gear tooth under 200% loading.

7.2.3 Effect of non-uniform loading across the spur tooth face

Non-uniform loading across the spur tooth face can result from either misalignment between the mating gears resulting from assembly errors, deflection of the gear shafts causing misalignment or by tooth profiles which only allow contact over a certain percentage of the tooth width. The effect of non-uniform loading is very similar to increasing torque transmission loads as both induce higher root region stresses. Note that the previous stress calculations for the two dimensional (2D) spur tooth models assumed uniform contact across the full width of the tooth face.

To quantify the effect of non-uniform tooth loading, several three dimensional (3D) finite element models were solved using different pressure loading distributions (≈ 1 MNm torque) at the pitch circle. Each 3D model incorporated (3168 3D solid elements). These were calibrated against the results of a 2D model (198 plane strain elements) which assumed uniform tooth loading. Figure 7.8 shows the stress state and model definition for the calibrating 2D model. As expected, a torque loading of 1 MNm resulted in a maximum root region stress of 63 MPa. Figures 7.9 and 7.10 show the first 3D model with uniform loading (≈ 1 MNm torque) applied and the resulting stresses (65 MPa maximum) respectively. The difference in stress levels for the 2D and 3D uniform loading cases is a result of the plain strain assumption for the 2D case. Figures 7.11 and 7.12 show the second 3D model with a tapered loading distribution across the tooth face (≈ 1 MNm torque) and the resulting stresses (110 MPa maximum) respectively. Figures 7.13 and 7.14 show the third and final 3D model with double the loading distributed across only one half of the tooth face (≈ 1 MNm torque) and the resulting stresses (130 MPa maximum) respectively.

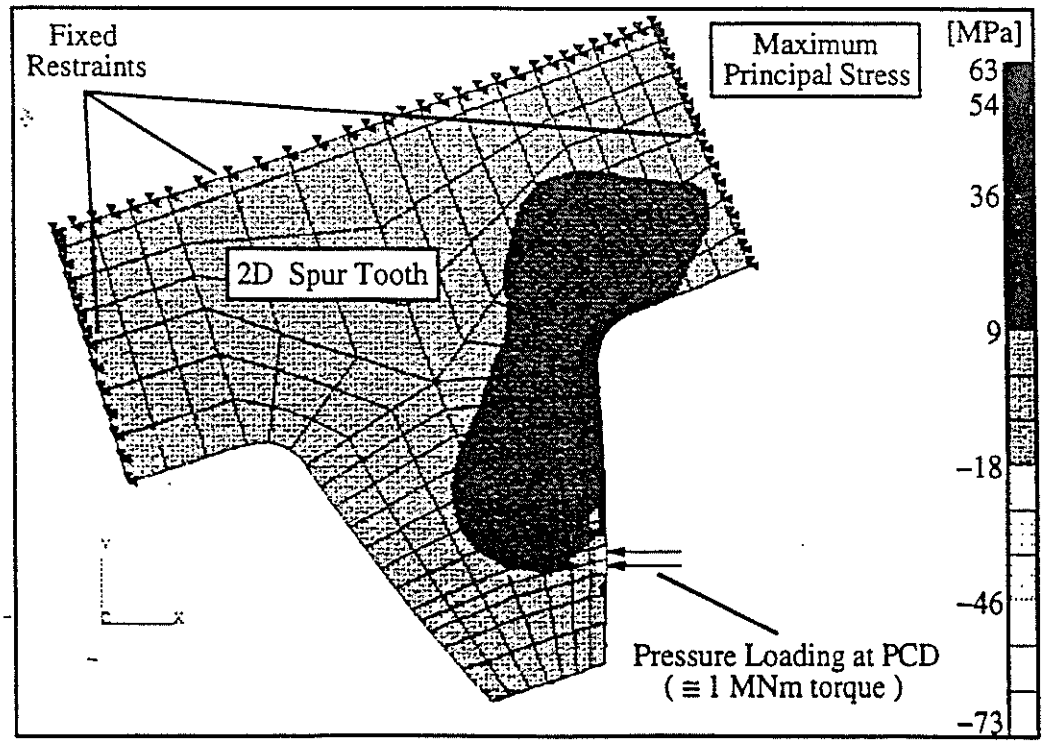

Figure 7.8 Stress state and boundary condition placement for 2D model.

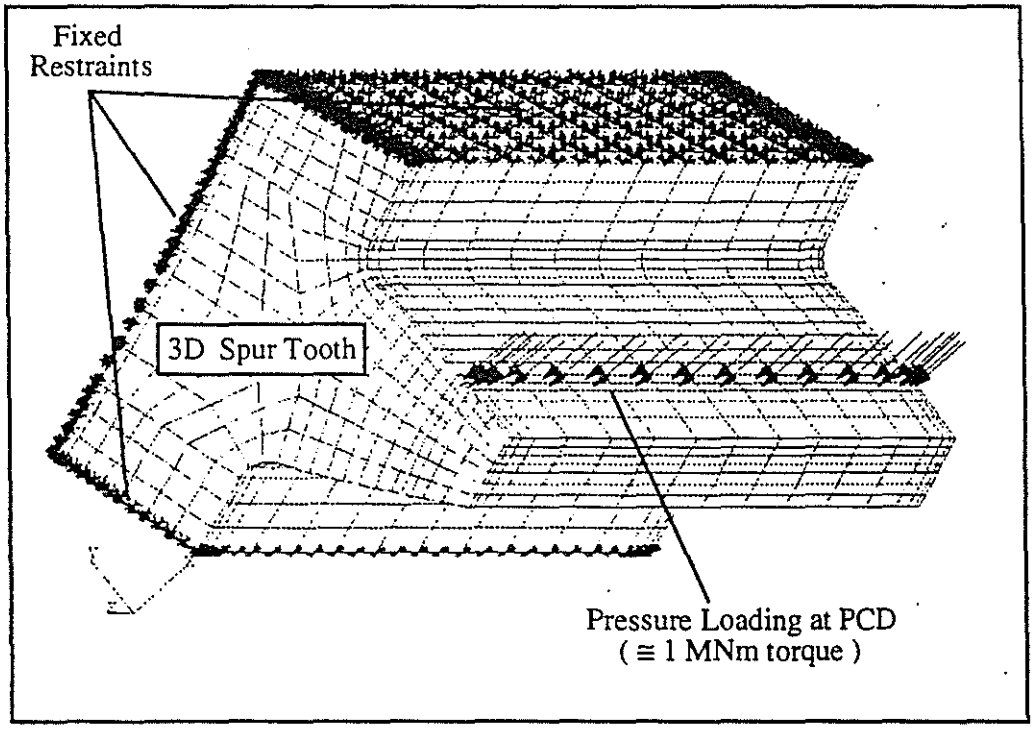

Figure 7.9 First 3D model showing uniform tooth loading and restraints.

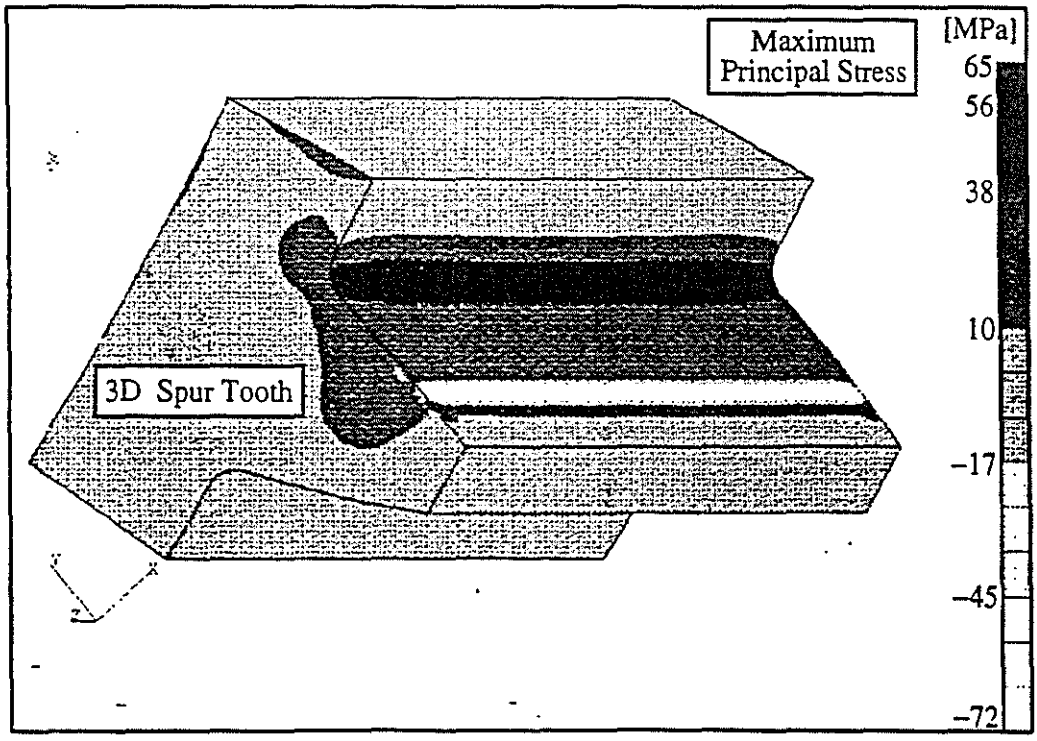

Figure 7.10 Maximum principal stress plot of the first 3D model with uniform tooth loading.

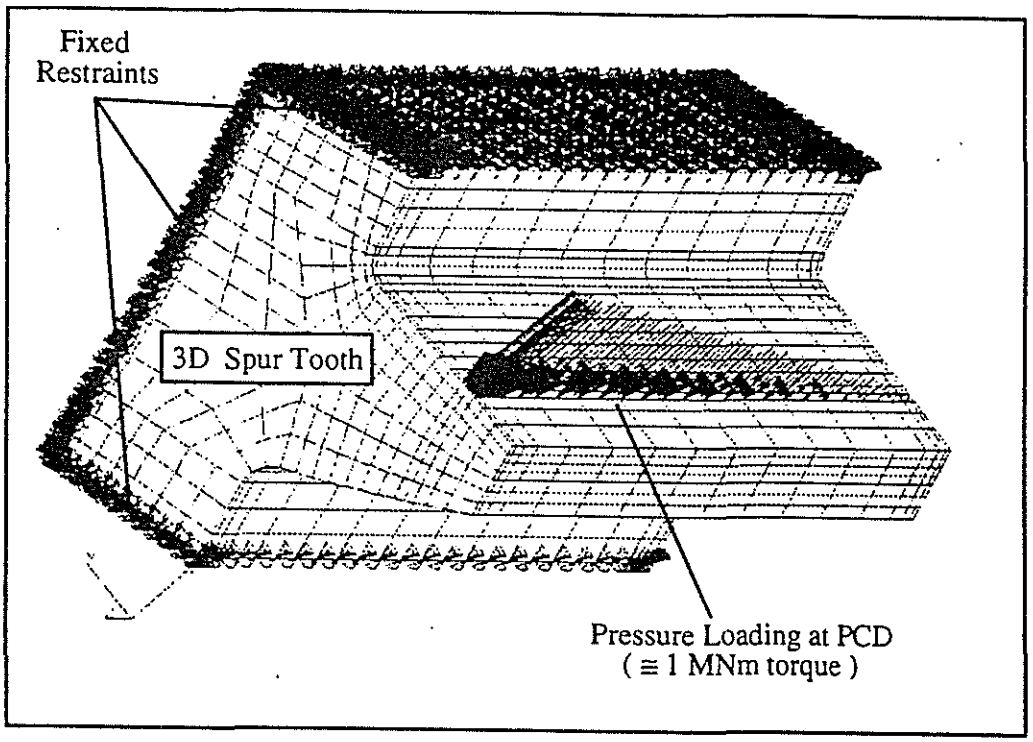

Figure 7.11 Second 3D model showing tapered tooth loading and restraints.

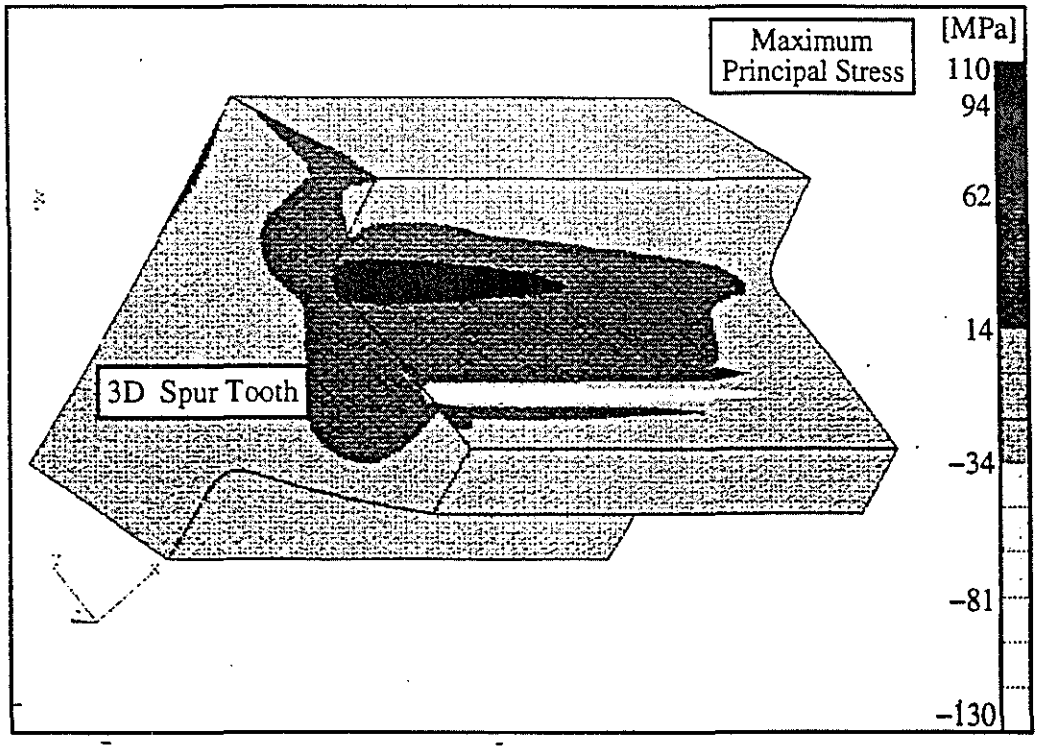

Figure 7.12 Maximum principal stress plot of the second 3D model with tapered tooth loading.

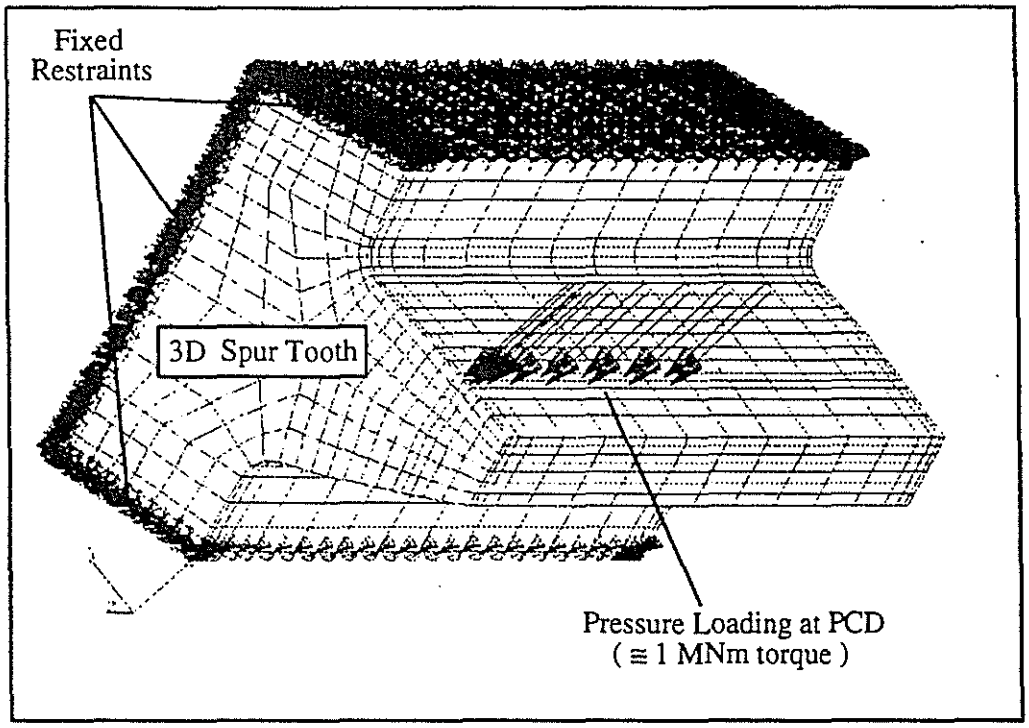

Figure 7.13 Third 3D model showing non-uniform tooth loading and restraints.

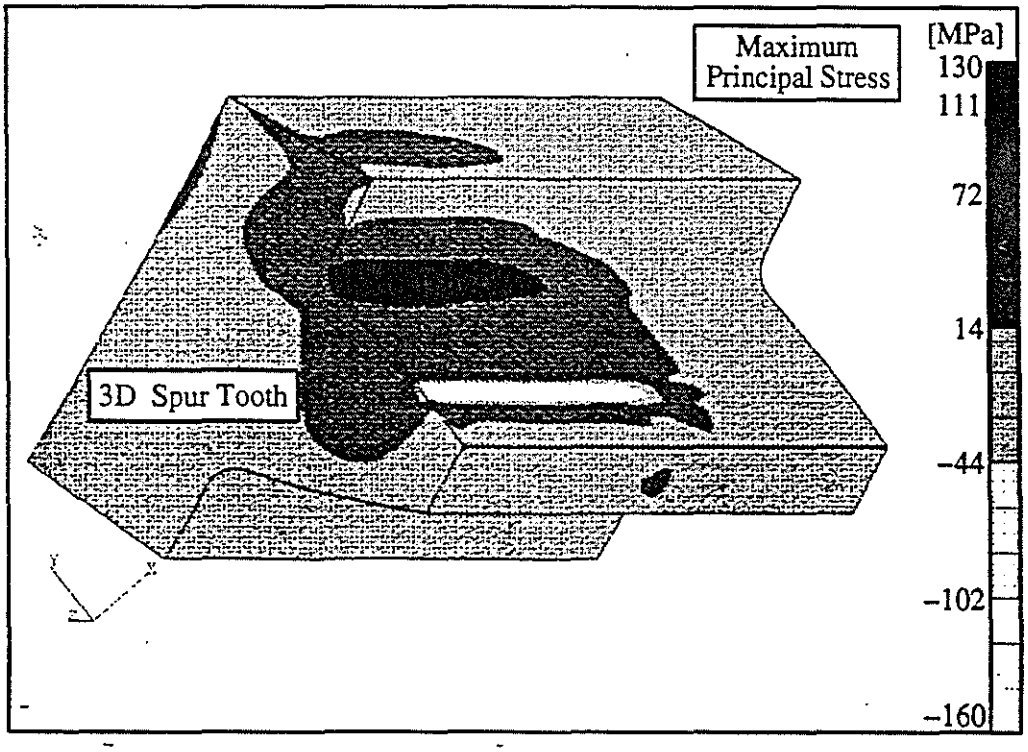

Figure 7.14 Maximum principal stress plot of the third 3D model with non-uniform tooth loading.

From summarising the results from the 3D models, a pattern between the root region stress levels for a torque loading of 1 MNm and the area of torque load application became evident. It can seen from the stress plots that the root region stresses are seemingly limited to root region directly under the contact region where the majority of the torque load was applied. On comparison of the first (uniform pressure loading across entire tooth face) and third (doubled pressure loading across one half of the tooth face) model, the stresses in the root region doubled when the loading was concentrated onto half the face width.

As previously mentioned, increasing torque transmission loads would have similar effects on a crack's characteristic as would decreasing the contact area on the tooth face for a nominal torque load transmission, as both involve an increase in the root region stress. Hence, for the purpose of a sensitivity analysis regarding non-uniform tooth loading, reference need only be made to the results from Section 7.2.2.

From the results of the 3D models, an approximate inverse relationship between the stresses induced in the root region and the percentage of the tooth face contacted during gear operation exists. For example, 50 per cent tooth face width contact under nominal torque would have a similar effect to doubling the torque with 100 per cent contact. This result pertains to the findings of gearing standards which conclude that non-uniform tooth loading, due to misalignment, acts like an additional stress concentration.

8.0 Project Limitations

8.1 Insufficient fracture properties and surface / heat treatment details for spur gear material

Throughout this report the shortfall in material properties available has been highlighted. Although a suitable method for predicting the behaviour of root region cracks in gear teeth has been established, this lack of fracture properties has rendered the final predictions of the remaining life in the cracked gearing hypothetical. The sensitivity of life predictions to changes in material properties was emphasised in Section 7.2.1.

Apart from the lack of fracture properties, the uncertainty of heat and surface treatment details also restricted the success of this project. Heat and surface treatment of gear teeth is a common practice by manufacturers to increase the hardness of gear teeth and to introduce residual compressive stresses in the surface of the teeth to increase the fatigue resistance of the gear. The induced residual stresses come in two distinct stages [18]. The outer surface of a treated tooth has residual compressive stresses, which would reduce crack propagation rates (as compared to case where compressive stresses were non-existent) in that region. The compressive stresses are replaced by tensile stresses at some distance in from the surface. In this region, these tensile stresses would increase crack propagation rates (as compared to case where tensile stresses were non-existent). A method to account for the inclusion of residual stresses [5] is well documented and could be utilised to improve the remaining life predictions for cracked gearing if such information was supplied by gear manufacturers.

Although this project was completed without the knowledge of the exact material properties or heat treatment details, a method for predicting the remaining life of cracked gearing when this information is provided has been established.

8.2 Accuracy of torque measurements, tooth profile and possible gear misalignment details

The torque measurements analysed in Section 4.3 were obtained from the 'Bailey' computer based supervisory control system. The recorded torque level, (one sample every minute) is calculated empirically from turbine chest pressure. Appendix A5 shows the typical graphs used to calculate torque loads as supplied by Victoria mill. The error in torque predictions could be as high as 20 per cent. Although the effect of varying the torque transmission loads on the growth characteristics of root region cracks was analysed in Section 7.2.2, more realistic predictions of crack behaviour may result if torque telemetry equipment was fitted.

As torque loads directly effect the level of root region stress and hence the propagation rates of cracks, so does the tooth profile. Gear tooth manufacturing techniques such as crowning and end relief [22] both reduce the contacting area on the tooth face during operation. As discovered in Section 7.2.3, the reduction in tooth face contact area results in an increase in the root region stress, hence increased crack propagation rates. Unfortunately, the exact tooth manufacturing details for the candidate gear were not available with the tooth profile drawings.

Gear misalignment occurs frequently in the assembly of gear trains. Thermal telemetry methods have been established to calculate the angular misalignment between mating gears by analysing the operational temperature differences across the face width of the gear teeth. The effect of misalignment on the root region stress and hence crack propagation rates was analysed in Section 7.2.3. Gear misalignment has similar effects on gear tooth stress as does crowning and end relief of tooth profiles as they both effectively reduce the contact area on the tooth face.

To reduce the error in cracked gearing life predictions, torque measurements, effective gear misalignment and tooth profile geometry should be known with some accuracy.

9.0 Project Outcomes and Recommendations

9.1 General results and conclusions

This project has focused on the application of finite element methods and durability analyses to predict the life of cracked gearing under routine operating conditions. This is the first application of finite element methods and durability analyses to the tooth region of large spur gears, typical of those operating in the Australian Raw Sugar Industry.

Replacement bull gears cost upwards of $200 thousand, depending on the size. These large gears operate under arduous conditions. The milling units they drive, are generally set according to the allowable torque that can be transmitted through the gearing. When cracks appear, the mill settings should be reviewed to enable the gear to survive until a replacement can be manufactured. From the time of order for a replacement gear to time it is constructed, transported and installed is typically 16 weeks. At the commencement of this project there was no rapid technique available to assess the onset of cracks in gear teeth, although sugar factories often rely on annular condition monitoring techniques to keep a check on existing cracks and their growth behaviour. The aim of this project was to use finite element methods in combination with fracture mechanic's theory to predict the characteristics of cracks under nominal operating conditions with the final result being an understanding of root region crack growth so that the remaining life of the cracked gearing, the critical crack lengths for varying operating conditions and optimal timing for non-destructive testing could be estimated.

Background information relating to the problem of cracked gearing was reviewed to commence this project. Information such as gear terminology and design, fracture mechanics and crack propagation theory, appropriate computer software codes and historical torque data, material properties and non-destructive testing records which would aid in the life predictions for cracked gearing were investigated. From this review, a suitable computational modelling procedure was developed.

Finite element models began with the geometric construction of the candidate spur and pinion gear teeth, followed by two dimensional analyses of a single pair of meshing teeth through to three pair of meshing teeth to estimate the stress levels experienced in the root region of the spur teeth under nominal loading. Further two dimensional models of a spur tooth were modelled to ascertain the effect of introduced cracks of increasing length in the root region of the spur tooth and to produce the most likely path for a root region crack to propagate. A geometry function resulted from the stress intensity modelling which was later used in the life predictions.

Several three dimensional models of the spur tooth were analysed with varying load distribution patterns on the tooth faces to investigate the effect of non-uniform tooth loading (gear misalignment or modified tooth profiles) on the root region stresses and hence the propagation rates for cracks in that region. The project was then completed with sensitivity analyses which involved remaining life predictions and critical crack lengths for cracked spur gear teeth under various operating conditions.

Although the majority of computational analyses were restricted to two dimensions and the material properties for the candidate gear were only 'best estimate', a suitable method was refined for predicting the growth characteristics for root region cracks in slow speed gearing. Given appropriate data (torque history, gear geometry, material properties etc.), a method now exists to produce estimations relating to the remaining life of a cracked gear tooth.

As a result of this investigation, a possible approach to assess cracked gearing is suggested:

1. Collection of relevant information regarding cracked gearing.
   - geometry of gear and teeth
   - any non-destructive records of gear
   - approximate shape and location of crack
   - adequate torque and speed data
   - basic material and fracture properties
   - heat and surface treatment

2. Assessment of cracked gearing.
   - If crack is in the root region then life predictions are possible. If not, the life predictions for the crack would be too difficult.
   - If the tooth geometry is similar to the candidate gear modelled in this report then the assessment may be as simple as a hand calculation. If not, then an additional model of the exact gear tooth would be required.
   - If the fracture properties for the gear are known then life predictions are possible. If not, then life predictions will be hypothetical with sensitivity modelling required.

Recommendations for future work as a result of completing this project are discussed in Section 9.2.

9.2 Future research possibilities

9.2.1 Obtaining accurate material and fracture properties from gear samples

The engineering properties for gear steels are known with reasonable accuracy. However, the need for accurate material and fracture properties is critical if feasible crack propagation predictions are to be calculated. To obtain these properties, samples of steel with the same composition and heat treatment as the material of the gear under review should be tested. Fracture properties such as the fracture toughness, threshold stress intensity, the Paris Law coefficient and exponent should be investigated. Additional tests to confirm the standard material properties such as elastic modulus, the ultimate tensile strength and yielding stress should also be undertaken.

9.2.2 Creating methods for back-calculating properties from crack histories

At the onset of this project it was evident that adequate fracture properties for the candidate gear would be unavailable. To counter this shortfall, it was considered that from non-destructive testing records, fracture properties could be back-calculated. However, crack history records only contain surface length dimensions and not depth which is required for analysis. In addition, back-calculating parameters using linear elastic fracture mechanics theory in combination with inadequate data such as misalignment and torque history details would result in errors.

This method of back-calculating fracture properties (still a possibility) should only be considered if other data such as crack propagation and torque loading histories, misalignment details and engineering properties are known with confidence. Also of concern is that crack geometry does not always suit plane strain analysis.

9.2.3 Producing a rapid method for analysing cracked gears of varying geometries

The production of a code which asks for certain information about a meshing gear pair (geometry, material properties, load history and crack geometry) from the user and outputs a geometry function for root region cracks and a selection of other relevant details, possibly torque loading levels which would ensure that a cracked gear would last its initial design life would be desirable. Such a code would be ideal to any industry which relies on continuous operation of large slow speed gearing. However, the time it would take to produce a code / program which produces and analyses all the models covered during this project in one operation would intuitively be great.

9.2.4 Modelling effects of misalignment and 3D crack shapes using ABAQUS (Explicit)

The analysis contained in this report was restricted to two dimensions (plane strain). This was a result of the modelling capabilities of the available software ABAQUS (Standard) for the duration of the project. Static three dimensional models were analysed in order to investigate non-uniform tooth loadings which would result from gear misalignment. Although interesting, these three dimensional models were considered a preliminary analysis for the modelling of misalignment effects. In addition, the cracks modelled throughout the project were assumed to be 'through' cracks or partial 'through' cracks of rectangular shape. Realistically, such root region cracks would generally have elliptical shapes. However, the implementation of modelling two dimensional cracks is considered feasible under certain operating conditions (plane strain cracks) and satisfactory for an investigation such as this.

In future, modelling of elliptical cracks and misalignment between gears could be modelled using ABAQUS (Explicit) which is capable of modelling three dimensional contact and crack geometries.

References

[1] Shigley J.E. (1986). *Mechanical Engineering Design. 1st Metric Edition.* McGraw-Hill.

[2] Townsend D.P. (1991). *Dudley's Gear Handbook. 2nd Edition.* McGraw-Hill.

[3] AGMA (1976). *ANSI B6.14-1976. American National Standard. Gear Nomenclature (Geometry). Terms, Definitions, Symbols, and Abbreviations.'*

[4] AGMA (1980). *ANSI / AGMA 110.04. AGMA Standard. Nomenclature of Gear Tooth Failure Modes.*

[5] Beale R.F. and Dan P.A. (1979). *The Specification and Evaluation of Heavy Gearing - The Mining Industry's Viewpoint.* Paper from International Conference on Mining and Machinery, Brisbane, 1979.

[6] AGMA (1988). *ANSI / AGMA 2001-B88. American National Standard. Fundamental rating Factors and Calculation Methods for Involute Spur and Helical Gear Teeth.*

[7] SAA (1987). *AS 2938-1987. Gears - Spur and Helical - Guide to Specification and Rating.*

[8] SAA (1990). *ISO/DIS 6336-3 - Calculation of the Load Capacity for Spur and Helical Gears - Part 3: Calculation of Tooth Strength.* Draft ISO International Standard.

[9] Broek, D. (1986). *Elementary Engineering Fracture Mechanics. 4th Edition.* Martinus Nijhoff Publishers.

[10] Ashby M.F. and Jones D.R.H. (1982). *Engineering Materials. An Introduction to their Properties and Applications.* Pergamon Press.

[11] Blackmore P. (1994). *Fatigue Theory and Applications.* Lecture Notes from Fatigue Workshop, Compumod, Sydney, 1994.

[12] Anon. (1993). *PATRAN 3 User's Manual.* PDA Engineering.

[13] Anon. (1993). *ABAQUS User's Manuals - V 5.3.* Hibbit, Karlsson and Sorensen, Inc.

[14] Anon. (1993). *NSOFT Products User's Manuals - V 4.10.* nCode International Ltd.

[15] Anon. (1993). *PATRAN 3 - P3 / Fatigue User's Manual.* PDA Engineering.

[16] Goel V.S. (1985). *Fatigue Life: Analysis and Prediction.* International Conference and Exposition on Fatigue, Corrosion Cracking, Fracture Mechanics and Failure Mechanics. American Society of Metals.

[17] Glodez S., Flasker J., Ren Z. and Pehan S. (1995). *Three- Dimensional Numerical Analysis of Crack Propagation in Gear Tooth Root.* Anon.

[18] Stanley P. (1977). *Fracture Mechanics in Engineering Practice.* 1976 Annual Conference of the Stress Analysis Group of the Institute of Physics, University of Sheffield, England. Applied Science Publishers Ltd.

[19] Goldthorpe M.R. (1992). *Finite Elements, Linear Elastic Fracture Mechanics and Structural Integrity.* Document from nCode International Ltd.

[20] Aliabadi M.H. and Rooke D.P. (1991). *Numerical fracture Mechanics.* Computational Mechanics Publications.

[21] Smith R.N.L. (1991). *Basic Fracture Mechanics.* Butterworth-Heinemann Ltd.

[22] SAA (1991). *AS 2075 - 1991. Glossary of Terms and Notations for Gears.*

Recommended Reading

ASM (1979). *Fatigue and Microstructure.*

ASTM (1976). *Cracks and fracture.* Proc. of the 9th National Symposium on Fracture Mechanics, University of Pittsburgh.

ASTM (1976). *Properties Related to Fracture Toughness.* 78th Annual Meeting.

AWRA (1980). *AWRA Technical Note 10. Fracture Mechanics.*

Beale R.F. and Moy B.W. (1982). *Rating of Heavy Gearing - Experiences with Alignment and Gear Accuracy.* Queensland Division Technical Papers.

Berry B.W. (1968). *Fracture toughness.* The Iron and steel Institute, London.

Buch A. (1988). *Fatigue Strength Calculation.* Trans. Tech. Publications.

Fagan M.J. (1992). *Finite Element Analysis. Theory and practice.* Longman Scientific and Technical.

Hall T.D. (1988). *Applying AS 2938 to Manufacturing.* Report from David Brown Gear Industries Limited.

Harris W.J. (1961). *Metallic fatigue.* Pergamon Press.

Jebe E.H. and Little R.E. (1975). *Statistical design of Fatigue Experiments.* Applied Science Publishers Ltd.

Larsson L.H. (1983). *Elastic - Plastic Fracture Mechanics.* Proc of the 4th Advanced Seminar on Fracture Mechanics, Joint Research Centre, Ispra, Italy. D. Reidel Publishing Company.

Michalec G.W. (1966). *Precision Gearing: Theory and Practice.* John Wily and Sons.

Neale M., Needham P. and Horrell R. (1991). *Couplings and Shafts.* Mechanical Engineering Publications Limited.

Owen D.R.J. and Fawkes A.J. (1983). *Engineering Fracture Mechanics: Numerical Methods and Applications.* Pineridge Press Ltd.

Rassweiler G.M. and Grube W.L. (1959). *Internal Stresses and Fatigue in Metals.* Proc. of the Internal Stresses and Fatigue in Metals, Detroit, 1958. Elsevier Publishing Company.

Rice R.C. (1988). *Fatigue Design Handbook.* Society of Automotive Engineers.

Steele J.M. (1989). *Applied Finite Element Modeling.* Marcel Dekker.

Stokes A. (1992). *Gear Handbook. Design and Calculations.* Butterworth-Heinemann Ltd.

Appendix A1

INTICO (QLD) PTY. LTD.
INDEPENDENT TESTING & INSPECTION COMPANY

Page 1/1

NONDESTRUCTIVE TEST REPORT

Client: C.S.R. Victoria Mill

Description of Job (incl. Method): E.M.D. testing of secondary gearing associated with milling Trains 4th

Client's Order No.: Date of Inspection: 6-2-1991

Job No.: Mill Gearing Report No.: 3005 ET 01

Item No.: N° 1 & 4 'B' Train Correlation No.: 3005.

Instrument: T T I EMD III Material: Cast Steel

Consumables: Probe Tips Construction Code: N/A

Test Specifications: Clients requirements

Test Requirements: To determine the presence of cracking associated with the root area of each tooth.

Testing Procedure: Each tooth root area was scanned down its entire length using a hand held probe The S.M.R Lubricating oil was only removed to confirm the presence of Crack like Indications.

Results: B. TRAIN Bull Gears only.

N° 1 mill Bull Gear :- No cracklike indications were detected.

N° 4 mill " " :- " " " " " however

10 off Known cracks were washed down and examined by M.P.I. to determine the amount of Crack propagation since last years servey.

Cont

Test Restrictions: The above gears were examined on the end faces only due to the molylube type lubricant

Pinions were not available for test due to the new guards.

Ref W/V 16861

Signed M Dodson

INTICO (QLD.) PTY. LTD.

N° 4 mill B Train Bull gear

M.P.I of Known Cracks.

Tooth N°	Crack length
9-10	335 - 530 mm
12-13	430 - 530 mm
14-15	490 - 515 mm
15-16	350 - 535 mm
16-17	310 - 535 mm
17-18	310 - 460 mm
18-19	295 - 490 mm *
19-20	380 - 420 mm
20-21	300 - 520 mm
31-32.	450 - 475 mm

No significant crack propagation other than on the tooth marked with the * was detected. Tooth 18-19 propagated by 20 mm in length, the same tooth also propagated by 25 mm in the previous Survey.

LINKWELL PTY. LTD.
A.C.N. 010 818 717
26 Leyland Street, Townsville. Qld. 4814
Postal Address : P.O. Box 40, Hermit Park. Qld. 4812
Telephone : (077) 79 0411 Fax : (077) 25 1180

cc Zmdi

FILE in CE office.

REPORT NO: VRA 91-12-12 - 1 DATE: 13TH DECEMBER 1991

CLIENT: CSR VICTORIA MILL
CONTACT: MR C. ARNOLD
PHONE: 764211
ORDER NO: HRO 6936
SUBJECT: MAGNETIC TESTING OF DRIVE GEARS
EXAMINER: RON QUIRK

EXAMINATION DATE: 12/12/91
LOCATION: VICTORIA MILL
TEST SPECIFICATIONS: AUSTRALIAN STANDARD 1171
EQUIPMENT: PORTABLE MAGNETIC TESTING EQUIPMENT

MATERIAL SPECIFICATION: AS SUPPLIED
SURFACE FINISH: MACHINED
FURTHER REQUIREMENTS: NIL

RESULTS: REFER ATTACHED

.....
RON QUIRK
LINKWELL PTY LTD

AA 91-12-12-1 13TH DECEMBER 1991

Magnetic Particle Inspection of Drive Gears A1, B1 and B4 was carried out at random locations and the known cracks located on Drive B4.

Drive Gear A1 - Eight random teeth were inspected. Nil crack indications evident.

Drive Gear B1 - Six random teeth were inspected. Tooth number 71-72 revealed a crack 7mm in length, located in a heavy area of spalling. Refer to diagram Number 1 for location.

Drive Gear B4 - Eight known cracks were inspected. Of these, eight cracks, three cracks have propagated since last inspection. Another six random teeth were inspected. Nil crack indications evident.

B4 Known Cracks:

Tooth		Crack Length	
9-10	155	335 - 530mm	
12-13	160	430 - 530mm	
14-15	25	490 - 515mm	
15-16	155	340 - 535mm	10mm Growth
17-18	180	310 - 490mm	30mm Growth
18-19	200	290 - 490mm	5mm Growth
20-21	220	300 - 520mm	
31-32	25	450 - 475mm	

Tooth 18-19 has reported growth on the last two inspections.

All crack indications on Drive Gear B4 were centre punched to give a more accurate indications of growth at the next inspection.

RA 91-12-12-1 13TH DECEMBER 1991

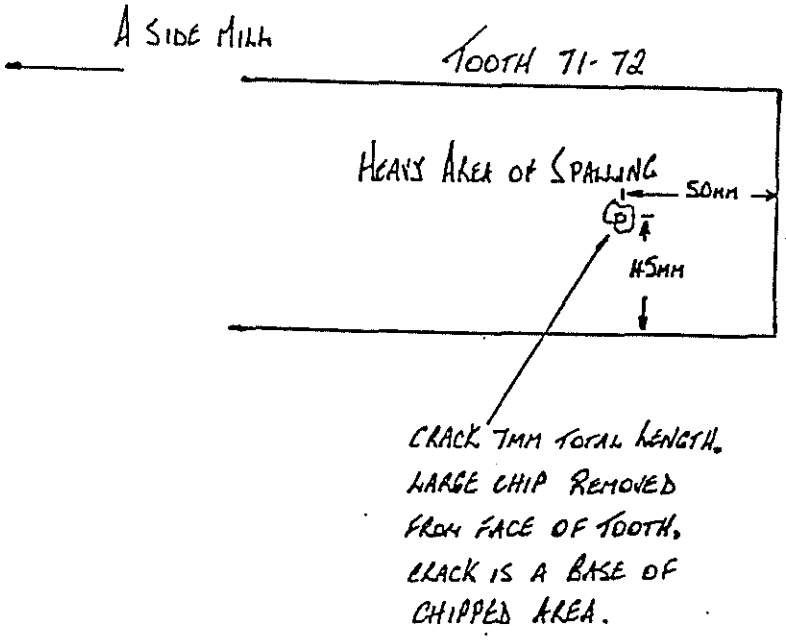

Diagram No 1

LINKWELL PTY. LTD.
A.C.N. 010 619 717
26 Leyland Street, Townsville. Qld. 4814
Postal Address : P.O. Box 40, Hermit Park. Qld. 4812
Telephone : (077) 79 0411 Fax : (077) 25 1180

Ref:f:\linkndt\report.16

REPORT NO: VRA 93-03-02 DATE: 5 MARCH 93

CLIENT:	CSR VICTORIA MILL	EXAMINATION DATE: 2-4 MARCH 93	
CONTACT:	MR C ARNOLD	LOCATION: VICTORIA MILL	
PHONE:	764 211	TEST SPECIFICATIONS: AS 1171	
ORDER NO:	TBA		
SUBJECT:	DRIVE GEARS B1,BA, A2 AND A4		
EXAMINER:	RON QUIRK	EQUIPMENT: ARDROX PORTABLE MAGNETIC TEST EQUIPMENT	

MATERIAL SPECIFICATION: AS SUPPLIED

SURFACE FINISH: -

FURTHER REQUIREMENTS: NIL

RESULTS:

1. Magnetic particle testing of Drive Gear B1 was carried out on four (4) random teeth. Nil cracks evident.

2. Tooth No.71 Drive Gear B1 has a crack 7mm in length, previously reported. Nil growth.

.....
RON QUIRK
LINKWELL PTY LTD

LINKWELL PTY. LTD.
A.C.N. 010 818 717
26 Leyland Street, Townsville. Qld. 4814
Postal Address : P.O. Box 40, Hermit Park. Qld. 4812
Telephone : (077) 79 0411 Fax : (077) 25 1180

REPORT NO: VRA 93-03-02 **DATE:** 5 MARCH 93

3. Magnetic particle testing of drive gear B4 was carried out on the eight (8) known crack locations. New crack indications were detected on four of the teeth tested. All new cracks detected were located on the edge of the tooth adjacent to the 'B' side mill, running down the face of the gear.

4. B4 Known Cracks

Tooth		Crack Length	
9-10	195	335-530mm	Nil Growth
12-13	190	430-530mm	New Crack 20mm
14-15	25	490-515mm	Nil Growth
15-16	195	340-535mm	New Crack 3mm
17-18	180	310-490mm	Nil Growth
18-19	200	290-490mm	Nil Growth
20-21	220	300-520mm	New Crack 25mm
31-32	25	450-475mm	New Crack 48mm

5. Magnetic particle testing was carried out on Drive Gear A2. The following teeth were tested. Nil crack indications evident.

Tooth 7-8, 21-22, 38-39, 58-59. 74-75 and 105-106.

6. Magnetic particle testing was carried out on Drive Gear A4. The following teeth were tested, 32-33, 43-44, 73-74, 85-86, 93-94, 102-103, 114-115. Nil crack indications evident. Tooth 58-59 exhibited a crack indication located 8mm from the base of the tooth length 6mm.

7. Refer attached diagrams for new crack locations and orientation.

LINKWELL PTY. LTD.
A.C.N. 010 819 717
26 Leyland Street, Townsville. Qld. 4814
Postal Address : P.O. Box 40, Hermit Park. Qld. 4812
Telephone : (077) 79 0411 Fax : (077) 25 1180

REPORT NO: VRA 93-03-02 **DATE:** 5 MARCH 93

DRIVE GEAR B4

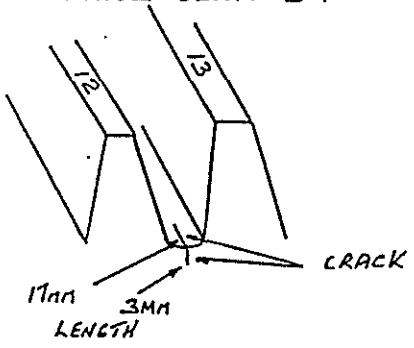

DRIVE GEAR B4

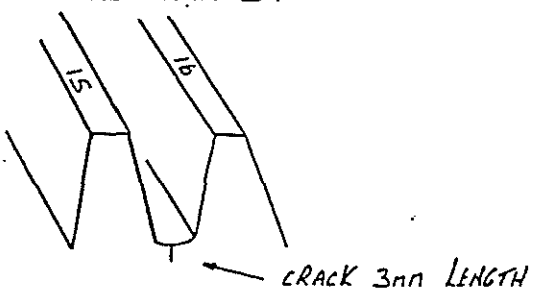

LINKWELL PTY. LTD.
A.C.N. 010 819 717
26 Leyland Street, Townsville. Qld. 4814
Postal Address : P.O. Box 40, Hermit Park. Qld. 4812
Telephone : (077) 79 0411 Fax : (077) 25 1180

REPORT NO: VRA 93-03-02 DATE: 5 MARCH 93

DRIVE GEAR B4

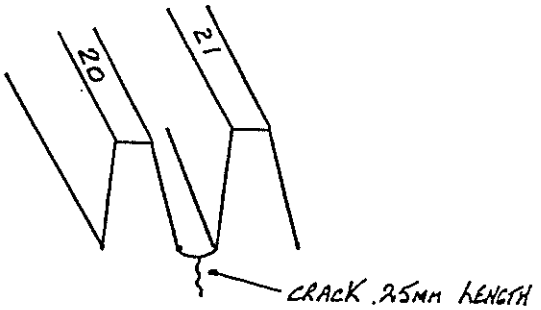

DRIVE GEAR B4

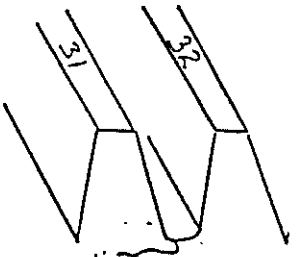

C/E
This one has been almost ground out - 5mm deep.

Area of grinding

Appendix A2

WALKERS LIMITED
ENGINEERS & FOUNDERS
A.C.N. 009 656 848

JN/MK

13th September, 1994

James Cook University of North Queensland,
JCU Sugar Advanced Technology Unit,
Department of Mechanical Engineering,
TOWNSVILLE QLD 4811.

Attention: Mr. Jeff Loughran

Dear Sir,

STUDY OF GEARWHEEL CRACKS

With reference to your request regarding details of the final motion gear and pinion for No. 4B Mill at Victoria Mill we enclose a copy of

Drawing	MG 4AX/A	-	Spurwheel
	MG 3AD	-	Pinion

I understand the wheel and pinion in question was made in 1975 to our Order No. 39-00-3901. This seemed to be confirmed by the Factory.

Unfortunately there are no metallurgical records dating back to that time and therefore we cannot offer you any chemical analysis or heat treatment data, etc.

The toot profile template of the wheel however was located in our tool room and I have enclosed a tracing of same.

From our conversation I understand this information is required to assist you in modelling crack propagation of existing cracks in this wheel which are an ongoing concern to the Factory. We would be interested to receive a copy of your analysis and conclusions in due course.

Best Regards

J. Nagel.

J NAGEL
DESIGN SUPERINTENDENT

P.O. BOX 211,
MARYBOROUGH QLD 4650 AUSTRALIA
23 Bowen Street, MARYBOROUGH QLD 4650
Telephone: (071) 21 8100 Fax (071) 22 4400
Telex: AA49718 ITOLZAK
A MEMBER OF THE EVANS DEAKIN INDUSTRIES GROUP

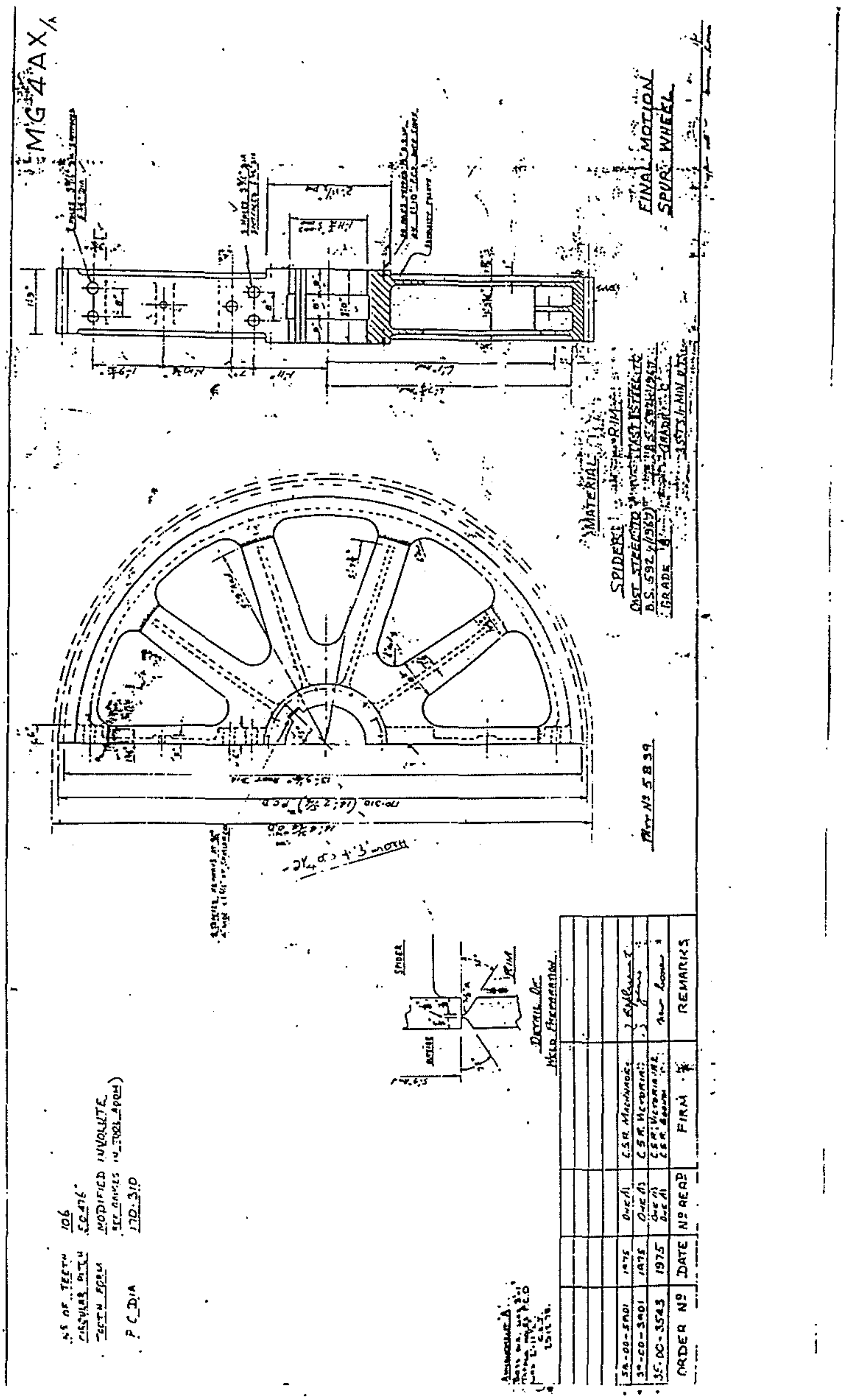
MG 4AX
FINAL MOTION
SPUR WHEEL
MATERIAL
SPIDERS
REMARKS
FIRM
DATE
ORDER Nº

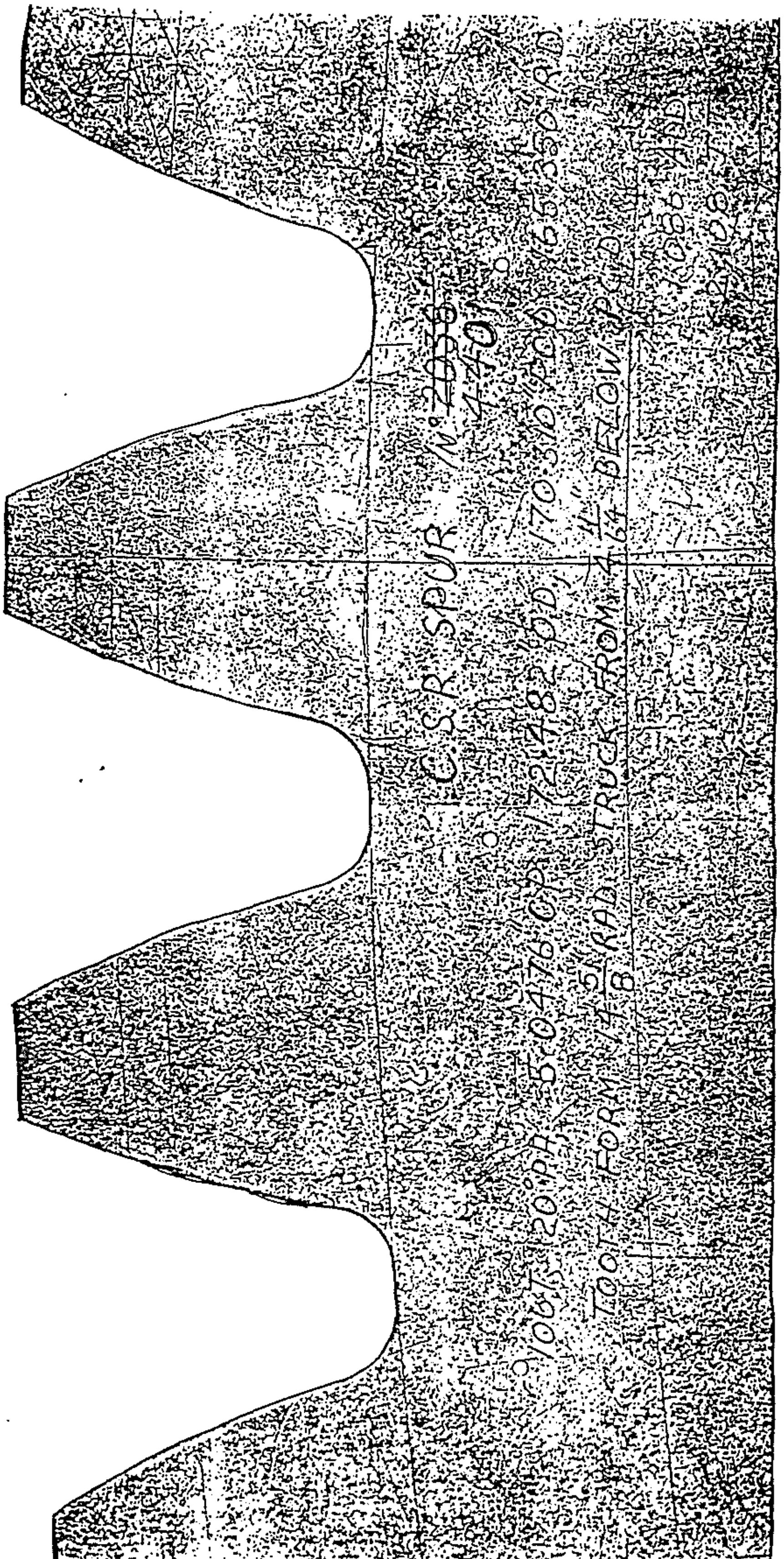
C.S.R. SPUR
TOOTH FORM
STRUCK FROM
BELOW

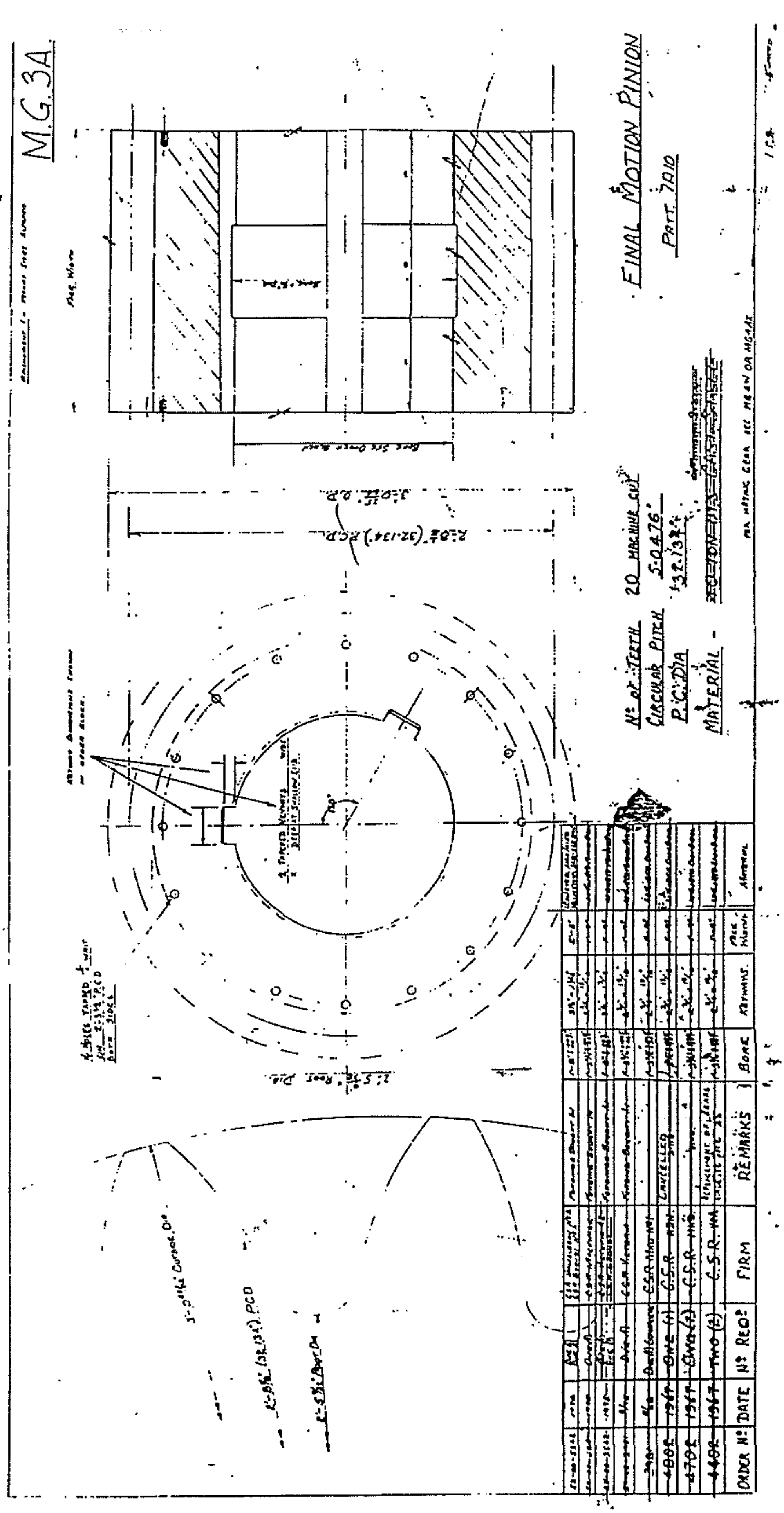
M.G.3A
FINAL MOTION PINION
PART 7010
No OF TEETH 20 MACHINE CUT
CIRCULAR PITCH 5.0476"
P.C.DIA
MATERIAL -
ORDER No
DATE
No REQD
FIRM
REMARKS
BORE
KEYWAYS
MATERIAL

(2)

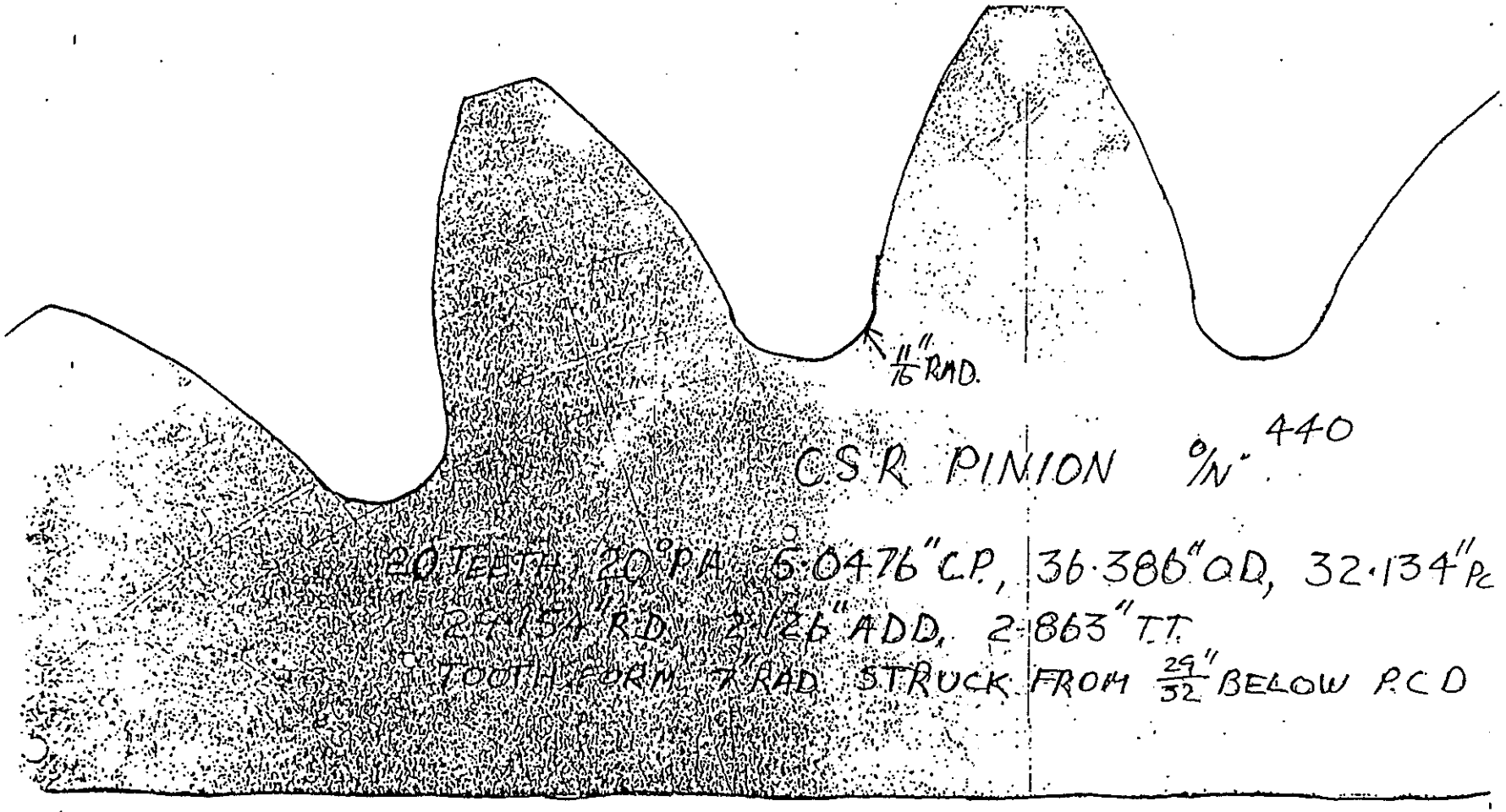

REDUCED SCALE

Appendix A3

Modified input deck for triple teeth model (Fine Mesh) with comments.

```
*HEADING
                    ---------- node creation ----------
*NODE
1,        0.,       0.
2,        0.,       2571.04
      .
      .
3723,     35.7484,  460.776
3724,     38.401,   460.563
                    ---------- plane strain element creation ----------
*ELEMENT, TYPE=CPE8, ELSET=PLANIES
1,    3,    5,    10,   8,
      4,    7,    9,    6
2,    8,    10,   15,   13,
      9,    12,   14,   11
      .
      .
1111,     3713,     3711,     3723,     3721,
          3712,     3718,     3722,     3717
1112,     3711,     3525,     3538,     3723,
          3710,     3532,     3724,     3718
    ---------- contact element creation (μ=0.1) for 1st pinion tooth ----------
*ELEMENT, TYPE=ISL21, ELSET=CONTA_1
1113,     2480,          3547
1114,     3547,          3553
      .
      .
1151,     3715,          3716
1152,     3716,          3719
*INTERFACE, ELSET=CONTA_1
 0.,
*FRICTION, TAUMAX=0.
0.1,      0.
    ---------- contact element creation (μ=0.1) for 2nd pinion tooth ----------
*ELEMENT, TYPE=ISL21, ELSET=CONTB_1
1153,     2228,          3147
1154,     3147,          3153
      .
      .
1191,     3315,          3316
1192,     3316,          3319
```

```
*INTERFACE, ELSET=CONTB_1
0.,

*FRICTION, TAUMAX=0.
0.1,        0.
```

---------- *contact element creation* (μ=0.1) for 3rd pinion tooth ----------

```
*ELEMENT, TYPE=ISL21, ELSET=CONTC_1
1193,       2563,       2747
1194,       2747,       2753
      .
      .
1231,       2915,       2916
1232,       2916,       2919

*INTERFACE, ELSET=CONTC_1
0.,

*FRICTION, TAUMAX=0.
0.1,        0.
```

---------- *slide line definition* for 1st spur tooth ----------

```
*SLIDE LINE, ELSET=CONTA_1, TYPE=LINEAR, SMOOTH=0.4
344,  2059,     2047,     2040,  2030,  2025,  2015,  2010,
2000,  1995, 1985,  1980,  1970,  1965,  1955,  1950,
1940,  1935, 1925,  1920,  1910,  1905,  1895,  1890,
1880,  1875, 1865,
```

---------- *slide line definition* for 2nd spur tooth ----------

```
*SLIDE LINE, ELSET=CONTB_1, TYPE=LINEAR, SMOOTH=0.4
578,  1834,     1822,     1815,     1805,     1800,     1790,  1785,
1775,     1770,     1760,     1755,     1745,     1740,     1730,  1725,
1715,     1710,     1700,     1695,     1685,     1680,     1670,  1665,
1655,     1650,     1618,
```

---------- *slide line definition* for 3rd spur tooth ----------

```
*SLIDE LINE, ELSET=CONTC_1, TYPE=LINEAR, SMOOTH=0.4
792,  1609,     1597,     1590,     1580,     1575,     1565,  1560,
1550,     1545,     1535,     1530,     1520,     1515,     1505,  1500,
1490,     1485,     1475,     1470,     1460,     1455,     1445,  1440,
1430,     1425,     1393,
```

---------- *multi point constraint definition* ----------

```
*MPC
BEAM ,  2060, 1
BEAM ,  2063, 1
      .
      .
BEAM ,  2513, 1
BEAM ,  2515, 1
```

```
BEAM,     3,  2
BEAM,     6,  2
    .
    .
BEAM,   933,  2
BEAM,   934,  2
```

---------- *material property for gear steel* ----------

```
*MATERIAL, NAME=STEEL

*DENSITY
7.82E-6,

*ELASTIC, TYPE=ISO
207000.,  0.29

*DAMPING, ALPHA=1., BETA=0., COMPOSITE=0.
```

---------- *thickness specified for plane strain elements* ----------

```
*SOLID SECTION, ELSET=PLANES, MATERIAL=STEEL
535.,

*RESTART, WRITE, FREQUENCY=1
```

---------- *definition for loading application* ----------

```
*AMPLITUDE,NAME=SCOTT,DEFINITION=TABULAR 0,0,0.15,1,0.3,1
```

---------- *STEP 1 (time = 0.3 s)* ----------

```
*STEP, AMPLITUDE=STEP, INC=200, NLGEOM

*DYNAMIC, HAFTOL=1.E+7
0.01,0.3,1E-10

*BOUNDARY, OP=NEW
1, 1,6,    0.
2, 1,5,    0.

*CLOAD, OP=NEW,AMPLITUDE=SCOTT
2, 6,    1.E+9

*FILE FORMAT, ASCII

*CONTROLS,PARAMETERS=TIME INCREMENTATION 8,10,,,,,,14

*CONTROLS,PARAMETERS=LINE SEARCH
4

*END STEP
```

---------- *STEP 2 (time = 0.21 s)* ----------

```
*STEP, AMPLITUDE=RAMP, INC=200, NLGEOM

*STATIC
0.005,0.21,,0.005
```

```
*BOUNDARY, OP=NEW
1, 1,5,       0.
1, 6,, 0.7
2, 1,5,       0.

*FILE FORMAT, ASCII

*NODE FILE, FREQ=1
U

*EL FILE, POSITION=INTEGRATION POINT, FREQ=1
S
E
*CONTROLS,PARAMETERS=TIME INCREMENTATION 8,10,,,,,,14

*CONTROLS,PARAMETERS=LINE SEARCH
4

*END STEP
```

---------- *end of input deck* ----------

Modified status file for triple teeth model (Fine Mesh) solution with comments.

STEP NUMBER	INCREMENT NUMBER	TOTAL TIME	STEP TIME
1	1	0.007	0.007
1	2	0.007	0.007
1	3	0.017	0.017
1	4	0.027	0.027
1	5	0.037	0.037
1	6	0.050	0.050
1	7	0.066	0.066
1	8	0.085	0.085
1	9	0.105	0.105
1	10	0.124	0.124
1	11	0.144	0.144
1	12	0.166	0.166
1	13	0.189	0.189
1	14	0.212	0.212
1	15	0.234	0.234
1	16	0.257	0.257
1	17	0.285	0.285
1	18	0.300	0.300
2	1	0.305	0.050
2	2	0.310	0.100
2	3	0.315	0.150
2	4	0.320	0.200
2	5	0.325	0.250
2	6	0.330	0.300
2	7	0.335	0.350
2	8	0.340	0.400
2	9	0.345	0.450
2	10	0.350	0.500
2	11	0.355	0.550
2	12	0.360	0.600
2	13	0.365	0.650
2	14	0.370	0.700
2	15	0.375	0.750
2	16	0.380	0.800
2	17	0.385	0.850
2	18	0.390	0.900
2	19	0.395	0.950
2	20	0.400	0.100
2	21	0.405	0.105
2	22	0.410	0.110
2	23	0.415	0.115
2	24	0.420	0.120
2	25	0.425	0.125
2	26	0.430	0.130
2	27	0.435	0.135
2	28	0.440	0.140
2	29	0.445	0.145
2	30	0.450	0.150
2	31	0.455	0.155
2	32	0.460	0.160
2	33	0.465	0.165
2	34	0.470	0.170
2	35	0.475	0.175
2	36	0.480	0.180
2	37	0.485	0.185
2	38	0.490	0.190
2	39	0.495	0.195
2	40	0.500	0.200
2	41	0.505	0.205
2	42	0.510	0.210

Appendix A4

Modified input deck for cracked spur tooth model (50 mm) with comments.

```
*HEADING
                    ---------- node creation ----------
*NODE
1,    -274.737,    404.964
2,    -270.012,    406.391
      .
      .
2980,      -182.655,    446.722
2981,      -182.655,    446.722
                ---------- plane strain element creation ----------
*ELEMENT, TYPE=CPE8, ELSET=PLAINIES
1,    1,    3,    23,   21,
      2,    15,   22,   14
2,    3,    5,    25,   23,
      4,    16,   24,   15
      .
      .
931, 2832,     2828,     2840,     2936,
      2833,   2973, 2938,  2980
932, 2830,     2829,     2890,     2900,
      2831,   2981,  902,   2970
              ---------- node set creation for crack tip nodes ----------
*NSET, NSET=CNOD
2869,     2870,     2871,     2872,   2873,   2874,   2875,   2876,
2877,     2928,     2929,     2930,   2931,   2932,   2933,   2934,
2935
              ---------- node set creation for restrained nodes ----------
*NSET, NSET=LOCKIES
1,    14,    21,   34,    41,    54,    61,    74,
81,   94,    101,  114,   121,   134,   141,   154,
      .
      .
831,  832, 2417,     2418,   2419,   2420,   2421,   2422,
2423,      2424,     2425,     2426,   2427,   2428,   2429,   2430,
2431,      2432,     2433,     2434,   2435
              ---------- material property for cracked tooth ----------
*MATERIAL, NAME=STEEL

*DENSITY
7.8E-6,

*ELASTIC, TYPE=ISO
207000.,  0.29
```

```
---------- thickness specified for plane strain elements ----------

*SOLID SECTION, ELSET=PLANIES, MATERIAL=STEEL
535.,

*RESTART, WRITE, FREQUENCY=1

---------- STEP 1 ----------

*STEP

*STATIC

*BOUNDARY, OP=NEW
LOCKIES, 1,2,  0.

*CLOAD, OP=NEW
1263, 1,   -246003.
1273, 1,   -123002.
1793, 1,   -123002.

---------- J-Integral definiton ----------

*J-INTEGRAL,FREQ=1,CONTOURS=4,OUTPUT=BOTH
-0.35429,0.93514
CNOD

*FILE FORMAT, ASCII

*NODE PRINT, FREQ=1
U

*NODE FILE, FREQ=1
U

*EL FILE, POSITION=INTEGRATION POINT, FREQ=1
S
E

*PRINT, FREQ=1

*END STEP

---------- end of input deck ----------
```

Section of dat file for cracked spur tooth model (50 mm) showing J-Integral solution.

---------- *J-Integral estimates for the four complete integral paths (N/mm)* ----------

J-INTEGRAL ESTIMATES

CRACK NUMBER	CRACKFRONT NODE SET	CONTOURS 1	2	3	4
1	CNOD	0.7318	0.7344	0.7349	0.7345

---------- *largest J-Integral estimate used for geometry function calculation* ----------

Appendix A5

001

Sugar Mills

Herbert River Mills
Victoria Mill
CSR Limited
A.C.N. 000 001 276
PMB
Ingham QLD 4850
Australia

Facsimile (077) 76 1958

Telephone (077) 76 4211

FACSIMILE Date: 16/9/94

To: SCOTT ANDERSON

From: DANNY McGRATH

No of pages including this sheet (2) Please advise promptly if all pages not rec'd

SCOTT,

HERE IS THE RELATIONSHIP CHEST PRESSURE TO TORQUE. BE IT IS HELPFUL.

DANNY McGRATH.

P.S. I'VE SEEN ROB PIERCE ABOUT THE DATA AND HE SHOULD SEND SOON SOON.

Section of dat file for cracked spur tooth model (50 mm) showing

J-Integral estimates for the four complete integration paths (N/mm)

J-INTEGRAL ESTIMATES

CRACK NUMBER	CRACKFRONT CONTOURS NODE SET	1	2	3	4
1	CNOD	0.7318	0.7344	0.7349	0.7345

largest J-Integral estimate used for geometry function calculation